Site U1362[1]

Expedition 327 Scientists[2]

Chapter contents

[1] Expedition 327 Scientists, 2011. Site U1362. *In* Fisher, A.T., Tsuji, T., Petronotis, K., and the Expedition 327 Scientists, *Proc. IODP,* 327: Tokyo (Integrated Ocean Drilling Program Management International, Inc.). doi:10.2204/iodp.proc.327.103.2011
[2] Expedition 327 Scientists' addresses.

Site summary

Integrated Ocean Drilling Program (IODP) Hole U1362A was drilled and cored to 528 meters below seafloor (mbsf; 292 meters subbasement [msb]), geophysically logged and hydrologically tested, and instrumented with a multilevel subseafloor borehole observatory ("CORK") (see Tables **T1, T2, T3** in the "Expedition 327 summary" chapter). Hole U1362B was drilled to 359 mbsf (117 msb), tested with a 24 h pumping and tracer injection experiment, and instrumented with a single-level CORK observatory.

Basement in Hole U1362A was cored from 346.0 to 496.0 mbsf (110–260 msb) with 44.4 m of core recovered (30% recovery). The recovered core consisted of (1) aphyric to moderately phyric pillow basalt, (2) aphyric to sparsely phyric sheet flows, and (3) sparsely to highly phyric basalt flows. The above lithologies were divided into eight units on the basis of changes in lava morphology, rock texture, and phenocryst occurrence. Pillow lava units (Units 1, 3, and 5) were divided according to changes in phenocryst abundance and mineralogy. Sheet flow units (Units 4, 6, and 8) were divided on the basis of the presence of chilled margins and variations in phenocryst mineralogy. No breccia units were recovered (only two centimeter-sized breccia pieces were recovered in total).

Pillow basalt is the most abundant flow morphology of Hole U1362A, with Units 1, 3, and 5 accounting for 78.85 m of the stratigraphy. Pillow basalt was primarily identified by the occurrence of curved glassy chilled margins with perpendicular radial cooling cracks. The basalt is sparsely to highly phyric with olivine, clinopyroxene, and plagioclase phenocrysts having spherulitic, hyalophitic, intersertal, and glomeroporphyritic textures. Pillow basalt ranges from sparsely to moderately vesicular, with a range of secondary minerals filling the vesicles. Alteration in the pillows is variable and ranges from slight to high.

Sheet flows are the second most common lava morphology in Hole U1362A, and these were classified on the basis of continuous sections of the same lithology that increase in grain size downhole through the unit. Curated core recovery in these units averaged 43% and was as high as 112% in Core 327-U1362A-17R (hard rock recovery >100% occurs in part because of tides, as discussed in text and in Fig. **F9** in the "Expedition 327 summary" chapter). Two near-continuous sheet flows recovered in Cores 17R and 18R were divided into two subunits on the basis of a change

doi:10.2204/iodp.proc.327.103.2011

in phenocryst mineralogy. The primary mineralogy of the sheet flows is very similar to that of the pillow basalt, comprising a range of aphyric to moderately phyric basalt with olivine, clinopyroxene, and plagioclase phenocrysts. Grain size within the sheet flows ranges from cryptocrystalline to fine grained, and textures vary from intersertal to intergranular. The sheet flows are nonvesicular to highly vesicular, with some flows exhibiting a similar abundance throughout and others having high variability within a single flow. Alteration within the sheet flows varies from slight to complete. Fracture and vein intensity within the sheet flows is lower than in the pillow basalt and resulted in improved core recovery and larger individual pieces.

The third lithologic type of basalt flow was classified on the basis of the absence of definitive morphological features associated with either pillow lava or sheet flows, allowing only a general "basalt flow" interpretation to be made. These units are aphyric to moderately phyric crypto- to microcrystalline basalt with the same primary mineralogy as basalt from Hole U1362A. The basalt is generally sparsely vesicular with secondary minerals filling vesicles, and textures vary from hyalophitic to variolitic. Alteration is moderate to high and is present as groundmass replacement (mesostasis and phenocrysts), vesicle fill, vein formation, and halos.

Two individual pieces of breccia were recovered: a hyaloclastite sample in Core 327-U1362A-13R and a cataclastic zone in Core 9R. The hyaloclastite is characterized by moderately to highly altered angular clasts in a saponite and altered glass matrix. The cataclastic zone is formed of subangular clasts with moderate alteration similar to the host rock and exhibits evidence of clast rotation and separation with a matrix of highly altered ground basalt.

The lithostratigraphy developed for Hole U1362A is somewhat different from that developed for Hole U1301B, located only 800 m to the south (see Fig. **F10** in the "Expedition 327 summary" chapter). Compared with Hole U1301B, core from Hole U1362A contains considerably greater fractions of sheet flows and basalt flows (called "massive basalt" and "basalt lava," respectively, in Hole U1301B) and evidence for more extensive and higher temperature hydrothermal alteration. Hole U1362A also contains less hyaloclastite breccia; however, only five coherent pieces of this rock type were recovered from Hole U1301B, and it seems likely that much more of this fragile rock type was present but not recovered from the formation in both locations.

Geochemical analyses of basalt samples indicate that they are all normal depleted mid-ocean-ridge basalt (N-MORB) and are inferred to all have the same magmatic source on the basis of cross-plots of TiO_2 vs. Zr. Hydrothermal alteration of basement varying from slight to complete was observed in all basalt from Hole U1362A, with the majority moderately altered. Alteration of the rocks manifests in four ways: (1) replacement of phenocrysts, (2) replacement of groundmass (mostly mesostasis), (3) filling of veins and adjacent alteration halos, and (4) lining and filling of vesicles. In thin section, alteration was observed to range from 8% to 91%. Away from vesicles and veins, background alteration is generally moderate to high in pillow lava and predominantly moderate in sheet and basalt flows and is dominated by saponitic background alteration. Olivine is present only as completely replaced pseudomorphs.

The secondary mineralogy is dominated by clay minerals that are present in all four types of alteration. Saponite is the most abundant of the clay minerals and is present as black, dark green, greenish-brown, and pale blue colors and in thin section is characterized by a pale brown color and mottled or fibrous form. Celadonite is also present in all four types of alteration but is less abundant than saponite. In thin section, celadonite is bright green, and within some vesicles the color varies in intensity, reflecting a mix of saponite and celadonite. Iron oxyhydroxide is the second most abundant secondary phase, occurring both alone as iron oxyhydroxides and mixed with saponite and other clay phases to form iddingsite. Iron oxyhydroxides are identifiable by a bright orange to red color and often stain other phases present. Zeolite phillipsite was identified by X-ray diffraction (XRD) analysis of mixed veins and altered chilled margins in addition to montmorillonite (smectite group) from veins. Carbonate is present as vesicle fill, in veins, and within chilled margins and predominantly occurs mixed with clays and occasionally sulfides. Anhydrite is rarely present in veins from Subunit 6B.

A total of 1230 veins were logged, with an average frequency of 27 veins per meter of recovered core. Vein width ranges from <0.1 to 4 mm, and vein morphology is variable. Saponite is the most abundant vein fill and is present in 76% of the veins, with unidentified clay minerals filling 50% of veins. The next most abundant vein fill is iron oxyhydroxides, which fill 32% of veins. Carbonate and pyrite are present in 10% of veins but are only occasionally the dominant components. Celadonite occurs in 2% of veins and is a larger component of the background alteration. Rare anhydrite veins are present within Subunit 6B. Alteration halos flank 15% of hydrothermal veins and are otherwise found flanking rock edges or apparently unassociated from structural features. Halos range from single-color black, green, or

orange halos to complex multihalos with mixed colors.

The dips of 519 veins and fractures were measured, and three types of fractures were distinguished: (1) veins flanked by alteration halos (haloed veins), (2) veins not flanked by alteration halos but filled with secondary minerals (nonhaloed veins), and (3) joints sometimes flanked by alteration halos but not filled with minerals. Nonhaloed veins were the most frequently observed structures. Nonhaloed veins were identified mainly in massive lava and in some pillow lava pieces. No faults or shear veins with any evidence of displacement were found.

In addition to cores recovered from Hole U1362A, small millimeter- to centimeter-sized chips were recovered from the drill bit in Holes U1362A and U1362B. In both cases the drill bit penetrated only a few meters below the sediment/basalt interface before being pulled to the rig floor, where the drill cuttings were removed. The source of the drill cuttings can be constrained to a short interval at this interface and represents the only recovery of basement material at the sediment/basalt interface at Site U1362. Basalt exhibiting a wide variety of hydrothermal alteration was recovered in these chips, and similar compositions were recovered in both Holes U1362A and U1362B. Alteration types included pervasive green and red alteration, iron oxyhydroxides, pale gray sulfide-bearing mud, and basalt chips with epidote crystals. The occurrence of epidote with pyrite at the seafloor, combined with anhydrite at depth, may indicate that Hole U1362A was formerly a location of hydrothermal upflow.

Whole-round basalt core sections were run through the Whole-Round Multisensor Logger (WRMSL) and Natural Gamma Radiation Logger (NGRL) prior to splitting. Gamma ray attenuation (GRA) density data vary widely as a result of unfilled core liners in sections with poor recovery. Despite this, peak bulk density values are consistent at ~2.5 g/cm^3 for much of the core recovered. For the more cohesive, massive sections recovered in deeper cores, GRA results are slightly higher than 2.5 g/cm^3. Magnetic susceptibility measurements also vary widely, ranging from 0 to 3300 × 10^{-6} SI. Total counts from the NGRL are generally low (1–5 counts/s). For all measurements the highest values were found in massive sections, with other lithologies, namely pillow lava and basalt flows, generally yielding much lower values.

Thermal conductivity was determined in three samples from the uppermost section of pillow basalt, yielding values of 1.63, 1.67, and 1.72 W/(m·K) at depths of 349, 354, and 355 mbsf, respectively. These values compare well with data collected at similar depths in nearby Hole U1301B (1.70 ± 0.09 W/[m·K]). Problems with the thermal conductivity half-space system prevented additional measurements.

P-wave velocities were measured on 70 discrete samples. *P*-wave velocity values determined by manual picking of the first arrival range from 4.5 to 6.0 km/s, with an average of ~5.4 km/s. The average value is greater than values obtained from Hole U1301B. The lowest velocity was measured on a heavily altered sample (327-U1362A-14R-1, 11–13 cm). A test of nearby unaltered material yielded much higher velocity, which demonstrates the influence of rock alteration on *P*-wave velocity. We found no statistically significant overall velocity trend with depth or overall velocity anisotropy depending on sample direction.

Moisture and density properties were determined on 73 discrete samples from Hole U1362A. Bulk density values range from 2.2 to 2.9 g/cm^3, with an average of ~2.7 g/cm^3. Grain density values range from 2.4 to 3.0 g/cm^3, with a mean of ~2.9 g/cm^3. Porosity values range from 2.8% to 15.0%, with a mean of 7.9%. The highest value of porosity was obtained from a highly altered sample that also had the lowest velocity. *P*-wave velocity and porosity are inversely correlated.

Twenty-five whole-round samples (4–20 cm long) were collected for microbiological analysis. Samples were preserved for shore-based DNA analysis, fluorescent in situ hybridization (FISH) and cell counting analysis, and fluorescent microsphere analysis. One sample was also collected for shore-based analysis of particulate organic carbon and nitrogen and carbon and nitrogen isotopes. Hard rock samples span a range of lithologic units, alteration states, and presence of chilled margins, and most contain at least one vein or fracture. Additionally, a few recovered plastic bags that held fluorescent microspheres were collected as a contamination check for DNA analysis. Colonization experiments were assembled for the Hole U1362A and U1362B CORK instrument strings. Fluid samples were collected for shore-based microbiological analysis during the 24 h tracer injection experiment in Hole U1362B.

Remanent magnetization measurements were made on 79 discrete pieces and on portions of 23 core sections. Samples were demagnetized at 5 or 10 mT steps from 0 to 50 mT using the cryogenic magnetometer's inline alternating-field (AF) coils. Most samples display simple magnetization behavior. Principal component analyses were performed on select samples. The majority of samples have positive inclinations, indicating that magnetization was ac-

quired during a normal polarity period, consistent with the age of the crust at this location. Some samples have steep positive inclinations that might be influenced by a drilling overprint. A few samples have reverse magnetizations, which are most likely the result of alteration. Inclinations are scattered around 460–470 mbsf in Unit 6.

A single wireline logging string was deployed in Hole U1362A to resolve physical and hydrological properties and identify suitable intervals for packer installation. The logging string consisted of a qualitative spontaneous potential electrode and sensors for measuring natural spectral gamma ray, bulk density, borehole fluid temperature, tool orientation, tool motion, ultrasonic borehole images, and hole diameter. Two passes were run over the entire open hole section, and a third pass was run over two intervals of particular interest. Seven logging units were identified on the basis of petrophysical log response and borehole conditions.

Both the mechanical and ultrasonic calipers revealed a borehole that was highly enlarged over most of the open hole section. Notable near-gauge sections were identified at 417 and 447 mbsf. Good conditions were expected in these sections on the basis of rotary core barrel (RCB) recovery and by the apparent coring and drilling rates of penetration. Low recovery and higher rates of penetration correlate well with an enlarged borehole. Where the ultrasonic caliper values appear meaningful, they indicate a nearly circular borehole through the near-gauge intervals.

A comparison of caliper logs and apparent penetration rates from Holes U1362A, U1362B, and U1301B suggests that there is some along-strike, lateral continuity in major basement units (see Fig. **F11** in the "Expedition 327 summary" chapter). The uppermost 100 m of basement in all holes at Sites U1301 and U1362 was drilled without coring using a 14¾ inch drill bit, and the lower parts of Holes U1362A and U1362B were drilled with a 9⅞ inch drill bit rather than a coring bit, so quantitative comparison of penetration rates in individual holes can be difficult. Nevertheless, the rapid penetration rate achieved in the uppermost 100 m of basement at Sites U1301 and U1362 is consistent with the rubbly and oversized character of the resulting boreholes and difficulties encountered when deploying 10¾ inch casing.

The ultrasonic borehole images are marred by rotational and heave-induced tool motion. In addition, the ultrasonic tool's sonde head is undersized for these borehole diameters, and no meaningful images can be expected where Hole U1362A is enlarged. Certain fractures and other features were observed in the 447 mbsf near-gauge section, particularly during the third imaging pass made at the highest vertical resolution.

The density readings were impaired by poor borehole conditions in many intervals. Where hole condition was good, logged density compares favorably with density measurements on discrete core samples.

Gamma ray measurements in the basaltic crust are driven by potassium content and were repeatable over the three passes. Where increases in gamma ray values correspond with enlarged borehole intervals, such as the one at 470 mbsf, they may represent zones of greater alteration. A pronounced gamma ray deflection was observed at and above the 10¾ inch casing shoe, likely a measure of trace uranium and thorium in the cement used to isolate the borehole.

Borehole fluid temperature data were acquired while running into the hole and during the three upward logging passes. The borehole temperature gradient increases steeply at the top of the 447 mbsf near-gauge interval, and a 0.5°C temperature anomaly was observed 8 m below the 10¾ inch casing shoe, near 317 mbsf.

Packer experiments were completed in Hole U1362A to assess the permeability of the formation, with the packer set at depth in the open hole. The sealed-hole pressure baseline was recorded for 1 h, and two 1 h long injection tests were conducted, each followed by 1 h to allow the pressure to recover to baseline conditions. Preliminary data analysis indicates a bulk permeability consistent with that in nearby Hole U1301B (Becker and Fisher, 2008).

A 24 h pumping and tracer injection experiment was conducted prior to the CORK deployment in Hole U1362B (**Fisher, Cowen, et al.**). OsmoSamplers and pressure gauges were deployed in a specially designed stinger sub just below the casing shoe in the open hole. After waiting 1 h to allow the hole to equilibrate, seawater was pumped into the formation at a rate of 20 strokes per minute (~7 L/s). At 1 and 20 h into the experiment, freshwater instead of seawater was pumped into the formation for 1 h. The tracers injected included SF_6 gas (for ~22 h), CsCl and $ErCl_3$ salts (at 3 h), CsCl and $HoCl_3$ salts (at 19 h), fluorescent microspheres (at 20 h), and stained bacteria (at 21 h) extracted from sea-surface water. Pumping ceased during the last hour of the experiment so that the hole could equilibrate again. The pressure record will require considerable processing to account for tides and changes in fluid density associated with switching from freshwater to saltwater and with the injection of salts as part of the tracer experiment. Rig floor and stinger fluid samples were collected during tracer injection, and shore-based analysis will be required to develop a detailed

history of injectate chemistry and particle concentration during the test. Pressure data and chemical samples will be collected from CORKs in this area in summer 2011, which will provide the first information from scientific ocean drilling on hole-to-hole solute and particle velocities.

The CORKs deployed during Expedition 327 are modified from the CORK-II design prepared for IODP Expedition 301. The Hole U1362A CORK monitors two basement intervals: a shallow interval extending from the base of the 10¾ inch casing to the top of the deepest set of swellable packers (307.5–417.5 mbsf) and a deeper interval extending from the base of the deepest inflatable packer to the bottom of the hole (429.2–528.0 mbsf). Pressure in both intervals is monitored through ¼ inch stainless steel tubing connected to miniscreens installed just below the inflatable packers at the top of the isolated intervals. Three ½ inch stainless steel fluid sampling lines terminated at two depths (two below packers in the upper interval and one below packers in the lower interval). A single ½ inch polytetrafluoroethylene (PTFE) microbiology sampling line ends in a titanium miniscreen that rests on perforated and coated 5½ inch casing, 7 m below the base of the deepest inflatable packer, just above the perforated collars. The downhole instrument string includes 6 OsmoSamplers and microbial growth incubators positioned within the coated perforated 5½ inch casing and collars, 11 autonomous temperature probes, a 200 lb sinker bar, and a plug to seal the hole near the seafloor.

The Hole U1362B CORK monitors a single basement interval that extends from a single set of swellable and inflatable packers positioned just inside the base of the 10¾ inch casing to the bottom of the hole (272–359 mbsf). Pressure in this interval is monitored via a ¼ inch stainless steel tube connected to a miniscreen installed just below the inflatable packers. The intakes of the three ½ inch stainless steel fluid sampling lines are located on perforated and coated 5½ inch casing, about 3 m below the packers, providing sampling redundancy. A single ½ inch PTFE microbiology sampling line ends in a titanium miniscreen that rests on perforated and coated 5½ inch casing, 7 m below the base of the deepest inflatable packer, just above the perforated collars. The downhole instrument string comprises six OsmoSamplers and microbial growth incubators, eight autonomous temperature probes, a 200 lb sinker bar, and a plug to seal the hole near the seafloor.

Both CORKs include a large-diameter ball valve in the wellhead that can be opened to allow fluids to bypass the top plug through a "lateral" pipe that extends from the main CORK tubing above the seafloor seal ("CORK" design). Researchers will initiate a long-term flow experiment in summer 2011 by deploying a flow meter and opening the ball valve on one of the Site U1362 CORKs using the ROV *Jason*. Flow will continue for at least 1 y, allowing testing of a much larger volume of crust than has been tested during previous scientific ocean drilling experiments.

Background and objectives

Site U1362 (prospectus Site SR-2) is located at the eastern end of the Ocean Drilling Program (ODP) Leg 168 drilling and observatory transect and in the same area where work was completed during Expedition 301 (Davis, Fisher, Firth, et al., 1997; Fisher, Urabe, Klaus, and the Expedition 301 Scientists, 2005). Site U1362 is positioned above a basement high covered by ~240 m of turbidites and hemipelagic mud, south-southwest of Hole 1026B and north-northeast of Holes U1301A and U1301B (Fig. **F1**). Hole U1362A (prospectus Hole SR-2A), the deepest of the two new holes, was intended to be drilled and cased through the sedimentary section and the uppermost 100 m of basement, with coring and sampling planned for ~100–260 m into basement and final hole depth to be determined by hole conditions and available time. The operations plan included wireline logging with a single string (to assess lithologic layering and properties and identify suitable locations for setting packers), testing for permeability using the drill string packer, and instrumenting the borehole with a CORK.

Hole U1362B (prospectus Hole SR-2B) was designed to be drilled and cased through sediment and the uppermost ~30 m of basement, followed by ~50 m of basement drilling with no planned coring or logging. A 24 h pumping and tracer injection experiment was to be completed before the borehole was instrumented with a CORK to monitor a single basement interval. Both of the CORKs to be deployed at Site U1362 were designed to include instruments to monitor formation fluid pressure and temperature, sample fluids (using downhole and wellhead OsmoSamplers), and provide growth substrate for microbes inhabiting the basement aquifer.

The original plan was to have these two basement holes separated by only 40–50 m, 200 m south of Hole 1026B and 800 m north of Holes U1301A and U1301B. Shortly before the start of Expedition 327, the position of Hole U1362B was moved ~300 m south of Hole U1362A (Fig. **F1B**) because of conditions in Hole U1301A and consideration of cross-hole experimental goals.

Like the Site U1362 CORKs, the two CORKs installed at Site U1301 have 16 inch casing through the sediment section and 10¾ inch casing across upper basement. The annulus between these two casing strings in Holes U1301A and U1301B was supposed to contain a rubber casing seal near the seafloor to help isolate the underlying formation from the overlying ocean, but the seals were not available for use as intended during Expedition 301. As a result, both holes remained unsealed and functioned as hydrothermal siphons following Expedition 301, with cold bottom water flowing rapidly into upper basement (Fisher et al., 2008). Hole U1301A "turned around" spontaneously in fall 2007, after which it discharged warm shimmering hydrothermal basement fluids at the seafloor (Wheat et al., 2010).

Multiple unsuccessful cementing attempts were made to seal the 10¾ inch casing strings against basement rocks at depth (with the R/V *JOIDES Resolution* during Expedition 301) and to seal Hole U1301B between the 16 and 10¾ inch casing strings at the seafloor (with the *JOIDES Resolution* during Expedition 301 and with the DSRV *Alvin* during expeditions in summer 2006 and 2007). An additional attempt to cement the cones using the *JOIDES Resolution* was scheduled at the start of IODP Expedition 312 in fall 2005, but these operations were canceled because of poor weather. Cementing of both cones was finally accomplished with the *JOIDES Resolution* in summer 2009 during IODP Expedition 321T. However, examination of the reentry cones and wellheads 3 weeks after that operation and collection of borehole pressure data by submersible and remotely operated vehicle (ROV) in summer 2009 and 2010 (just prior to the start of Expedition 327) indicated that only Hole U1301B was sealed. Hole U1301A continued to discharge warm basement fluids as of the start of Expedition 327.

We originally intended to make a final cementing attempt in Hole U1301A during Expedition 327, but just before the expedition we determined that cementing during Expedition 321T may have fouled two of the pressure gauge monitoring lines installed in Hole U1301B (although the shallowest gauge continues to work normally and indicates conditions returning toward an undisturbed state). In addition, we realized that leaving Hole U1301A open and flowing could be advantageous for the cross-hole tracer experiment planned for Expedition 327 because it might induce some of the tracers pumped into Hole U1362B to flow to the south (toward Hole U1301A), a direction opposite to the inferred regional flow direction in basement. Comparison of tracer transport north and south of Hole U1362B could then help researchers assess the net rate of transport in basement through comparison with the flow rate up Hole U1301A. In addition, Hole U1362B will be used for a 1–2 y cross-hole experiment, beginning when a large ball valve in the wellhead is opened during an ROV servicing expedition in summer 2011. Having Hole U1362A offset 300 m from Hole U1362B and completed in uppermost basement will provide an additional monitoring point for this experiment.

Reflection seismic data were collected across locations for Holes U1362A and U1362B as part of the 2000 ImageFlux expedition (Zühlsdorff et al., 2005; Hutnak et al., 2006) (Fig. F2). These seismic lines show features common to others collected in this area: layered sediments, the sediment/basalt interface, and a series of high-angle normal faults that help to define regional abyssal hill topography running subparallel to the active spreading center 100 km to the west. Holes U1362A and U1362B were placed near the peak of the buried basement ridge that underlies this site, just to the east of a high-angle normal fault in the volcanic crust.

Operations

Transit from Victoria, British Columbia (Canada), to Site U1362

Expedition 327 began on 5 July 2010, following the *JOIDES Resolution*'s maintenance in Victoria, British Columbia (Canada). The last line was released at 1212 h (local time) on 9 July, and the vessel was under way on the 196 nmi journey to Site U1362.

Site U1362

We arrived at Site U1362 at 0815 h on 10 July and deployed a positioning beacon at 0922 h. The vessel was positioned 15 m west of the coordinates of Hole U1362B, the bottom-hole assembly (BHA) was assembled, and the drill string was run to the bottom. Seafloor was tagged at 2672 meters below rig floor (mbrf) at 2200 h. A jet-in test was initiated at 2230 h and was completed by 1100 h on 11 July. The drill string was pulled clear of the seafloor, and the vessel was moved ~300 m in dynamic positioning (DP) mode to a position 15 m west of the coordinates of Hole U1362A. The seafloor was tagged again at 2672 mbrf, and a second jet-in test was initiated at 1250 h.

Hole U1362A Stage 1

The first stage of operations in Hole U1362A consisted of deploying a reentry cone with 20 inch conductor casing, drilling a hole a few meters into basement, and then cementing a string of 16 inch casing

to isolate the sediment column above the basement (Table T1; Fig. F3). On the basis of the jet-in test results, a 53 m string of 20 inch casing was made up and latched into a reentry cone. The reentry cone was deployed through the moonpool at 1700 h on 12 July, and Hole U1362A was spudded at 2345 h. The cone reached the seafloor at 1100 h on 13 July. A drilling BHA was assembled using an 18½ inch tricone drill bit and an underreamer set to cut a maximum hole diameter of 21.5 inches. The drill string was lowered to the seafloor, and the hole was reentered at 0245 h. After drilling for 17 h at an average rate of penetration (ROP) of 18 m/h, the hole was terminated at 2913 mbrf or 241 mbsf. The hole was cleaned with repeated mud sweeps, and the drill string was pulled out of the hole at 0920 h on 15 July. The depth of the basement contact was inferred to be at 2908 mbrf (236 mbsf). Frequent referral to the tide tables contributed to keeping the drilling depths consistent, as tidal fluctuation during our time on site resulted in a 3 m change in the sea level reference datum used by the driller. The rig floor was prepared for running casing, and by 1415 h on 15 July ~230 m of 16 inch casing was assembled, with each joint being welded together. Once the casing running tool was attached, the casing was lowered to the seafloor and Hole U1362A was reentered for a second time. The casing hanger was landed at 2315 h with the casing shoe at 230 mbsf, ~6 m above the basement contact. The bottom of the hole was cemented with 42 bbl of cement preblended with Cello Flake lost-circulation material and a 1.6% by volume calcium chloride accelerator. The drill string cleared the rig floor at 0930 h on 16 July, ending the initial stage of operations in Hole U1362A.

Hole U1362B Stage 1

The first stage of operations in Hole U1362B was similar to that in Hole U1362A (Table T2; Fig. F4). An identical 53 m string of 20 inch casing was made up and latched into another reentry cone. Hole U1362B was spudded at 2135 h on 16 July. The cone reached the seafloor at 1005 h on 17 July. The drilling BHA was assembled as before, the drill string was lowered to the seafloor, and the hole was reentered at 0056 h on 18 July. Drilling commenced at 0230 h and continued until 1700 h at an ROP of 25 m/h. The hole was terminated at 2922 mbrf (250 mbsf), with the basement contact inferred at 242 mbsf. The hole was cleaned with repeated mud sweeps, and the drill string trip back to the surface was initiated at 2245 h on 18 July. The bit cleared the rotary table at 0600 h on 19 July, and the rig floor was prepared for running casing. By 1100 h that morning, 18 joints of 16 inch casing (242 m in length) were made up and attached to the casing hanger. Hole U1362B was reentered at 1500 h, and the casing was washed down to 242.0 mbsf. The bottom of the hole was cemented at 1900 h on 19 July with 40 bbl of cement preblended with Cello Flake and a 1.6% by volume calcium chloride accelerator, with the goal of having 30 m of cement inside the casing and between the casing and the borehole wall. The drill string cleared the rig floor at 0330 h on 20 July, ending the initial stage of operations in Hole U1362B.

Hole U1362A Stage 2

The second stage of operations in Hole U1362A consisted of drilling a 14¾ inch hole to 346 mbsf for the 10¾ inch casing string with the goal of casing the upper portion of basement. The 14¾ inch drilling BHA was assembled, and Hole U1362A was reentered for the third time at 1525 h on 20 July. The top of the cement plug was tagged at 2874 mbrf (202 mbsf), which was within 2 m of the theoretical calculated depth of ~200 mbsf. This was a good indication that the cement job had been successful at cementing the lower 30 m of the hole. After drilling out the cement, basement drilling proceeded without incident to 298 mbsf by 1545 h on 21 July, followed by a 1.25 h period during which the drill string was stuck. After the string was freed, several hours were spent washing and reaming the hole, and by 2315 h the hole was relatively stable. Drilling continued until the desired total depth of 3018 mbrf (346 mbsf). By 0100 h on 24 July, after the hole had been conditioned further, the hole was deemed acceptable for running casing. Assembly of the 10¾ inch casing string began at 0930 h. Twenty-four joints of 10¾ inch casing were made up, followed by a TAM Freecap swellable packer joint. The packer was deployed for the first time during IODP operations and was designed to provide an additional seal to supplement the cement job and the casing hanger seal ring. The swellable packer is designed to absorb water and expand, sealing off the space between the 10¾ and 16 inch casing strings.

The drill string trip began at 1500 h on 24 July. Hole U1362A was reentered for the fourth time at 1900 h. The casing was washed to 2991 mbrf (319 mbsf) before becoming tightly stuck around midnight. After the pipe was worked for 4.5 h, the casing was eventually freed at 0430 h on 25 July. Multiple attempts to advance the casing past 2983 mbrf (311 mbsf) failed, and at 1000 h the decision was made to shorten the casing string. The casing string was tripped back to the surface by 1530 h. The swellable packer was inspected and determined to be undamaged and to gauge, so the 10¾ inch casing hanger and packer were laid out together as a unit. Two

joints of casing were removed, reducing the length of the casing string by 27.5 m to an overall length of 308.5 m. The swellable packer assembly was made up once again to the remaining casing string. Hole U1362A was reentered for the fifth time at 2310 h on 25 July. A few problems were encountered in advancing the casing string past the sediment/basalt interface, but after this point the installation went smoothly and the casing hanger landed at 0530 h. The bottom of the hole was cemented with 40 bbl of cement preblended with Cello Flake and a 1.6% by volume calcium chloride accelerator, designed to fill the bottom ~60 m of the hole. The volume pumped was double the required amount to allow for potentially significant loss of cement into the highly fractured formation. At 0730 h on 26 July the drill string was tripped back to the surface, and the ship was offset back to Hole U1362B.

Hole U1362B Stage 2

The second stage of operations in Hole U1362B consisted of drilling a 14¾ inch hole to 282 mbsf for the 10¾ inch casing string with the goal of casing the upper portion of basement. The BHA was assembled for drilling out the cement inside the 16 inch casing and deepening the hole. The drill string was tripped to the bottom, and Hole U1362B was reentered for the third time at 2030 h on 26 July. The bit tagged the top of the cement plug at 213 mbsf. By 0100 h the following morning the cement was drilled out, and by 0600 h the hole had been cleaned out to the original depth of 250 mbsf. Drilling of the 14¾ inch diameter hole to 282 mbsf was completed at 1645 h on 27 July. This left a 10 m rat hole below the projected 10¾ inch casing shoe depth of 272 mbsf. A significant amount of time was spent on hole conditioning, including multiple wiper trips and mud sweeps. By 2130 h on 27 July the hole was considered to be in acceptable condition and the drill string was recovered back to the surface. The bit cleared the rotary table at 0215 h on 28 July, and preparations began on the 10¾ inch casing string. The BHA included a 10¾ inch casing hanger with a TAM Freecap 10¾ inch × 14¾ inch expandable packer designed to seal the annulus between the 10¾ and 16 inch casings. The string was terminated with a conventional Texas-pattern casing shoe and contained enough casing to place the casing shoe at 272 mbsf. All casing collars were welded with four 2 inch long tack-welds to ensure that none of the joints backed off during subsequent drilling. A caliper measurement of the swellable packer confirmed a 14¾ inch outer diameter, and the assembly was ready for deployment by 0830 h on 28 July. The hole was reentered for the fourth time at 1150 h. The casing was deployed without incident, and at 1330 h the hanger was landed, and latch-in was verified with 15,000 lb of overpull. As before, the bottom of the hole was cemented with 40 bbl of cement preblended with Cello Flake and a 1.6% by volume calcium chloride accelerator. Because of an earlier-than-expected pressure spike, suspicions were that the cement either hardened too quickly while still inside the casing or that the formation was sealed with cement, preventing any further flow out into the formation. To verify the location of the top of the cement plug we decided to reenter Hole U1362B with the tricone drilling assembly before offsetting the ship back to Hole U1362A.

The drilling assembly was tripped to the seafloor, and Hole U1362B was reentered for the fourth time at 0320 h on 29 July. The bit tagged cement at 173 mbsf, suggesting that ~32 bbl (98 m) of cement was inside the casing and 8 bbl (27 m) had exited the casing shoe. The hope was that this cement had gone up the annulus ~27 m, or nearly back to the 16 inch casing shoe at the sediment/basalt interface. Because this was a significant amount of cement, we decided to drill out the cement inside the casing before it hardened any further. This turned out to be a good decision because another 13.25 h was required to drill out 89 m of fresh cement at an average ROP of 6.7 m/h. Drilling was halted 10 m above the casing shoe because the science party did not want to open Hole U1362B to seawater circulation this early in the expedition. The drilling assembly was pulled clear of the seafloor at 1905 h on 29 July, ending the second stage of operations in Hole U1362B.

Hole U1362A Stage 3

Hole U1362A was reentered for the sixth time at 0050 h on 30 July. The drill bit was lowered to 282 mbsf before contacting cement, which was within 2 m of the calculated displacement depth, placing the cement exactly where desired. Drilling of the cement plug began at 0230 h on 30 July, and at 0730 h the bit broke through the last of the cement at 309 mbsf, ~1 m below the 10¾ inch casing shoe. Cleaning up the rat hole below the casing shoe to 346 mbsf proved difficult. Once again, a significant amount of time was required to clean and condition the hole, which included multiple wiper trips, mud sweeps, and aggressive reaming of several trouble spots. The hole was believed to be in good enough condition for coring by 0200 h on 31 July, after 18.5 h of struggling through the same 38 m section. The drilling BHA cleared the rig floor by 0900 h, and preparations began for rotary core barrel (RCB) coring.

An RCB roller cone bit with a C-7 cutting structure was made up to a standard bit sub. Three additional drill collars were picked up, allowing a five-stand BHA to be assembled. The total length of drill collars in the BHA was 158.7 m, which allowed the BHA to extend ~21 m inside the 10¾ inch casing when the bit was at total depth. Thus, only slick pipe was in the open borehole, with the only upset located right at the bit. This technique was successfully used during Expedition 301 to minimize the potential for a stuck drill string.

Hole U1362A was reentered for the seventh time at 1715 h on 31 July, and the first RCB core barrel was deployed at 2215 h. The preliminary drilling needed to install the casing was designated as a drilled interval, dictating the first RCB core be identified as Core 327-U1362A-2R (Table T3). This core advanced 6.6 m to 352.6 mbsf per drill pipe measurements and was on deck at 0535 h on 1 August. Recovery was 1.99 m, for an official recovery of 30.2%. Because of tidal influences the actual advance was closer to 5.5 m, which yielded an unofficial recovery of 36.2%. Cores 3R, 4R, and 5R advanced to 362.2, 364.7, and 370.2 mbsf, respectively. Challenges were encountered throughout the coring process. Effective hole cleaning was a constant problem, requiring successively larger and more frequent high-viscosity mud sweeps as well as the use of higher pump strokes while cutting the core. Penetration rates were variable, ranging from ~1 m/h in the more massive altered rock to >4 m/h in the more friable material. Recovery was variable as well, with an average of 27.1%.

Coring continued and the formation alternated between massive and highly fractured zones, with rapid penetration rates associated with high drill string torque and circulation pressures. These conditions almost always led to the pipe getting stuck with a loss of rotation and circulation. The highest vulnerability seemed to be when making drill pipe connections after completing a cored interval. Ultimately, what seemed to work best was the use of more frequent and larger mud sweeps (35–50 bbl each) and spotting heavy mud pills in the pipe just prior to making a connection. Coring continued at an average pace of ~23 m per day, which included many hours of lost time getting unstuck and making impromptu wiper trips to get coring parameters back to normal.

Cores 327-U1362A-6R through 14R advanced to 3120.6 mbrf (448.6 mbsf). The drill string was recovered for a bit change and to extend the length of the BHA. We believe that the only reason coring was maintained in this hole is because only slick pipe (i.e., 8¼ inch drill collars) extended into the open hole below the 10¾ inch casing shoe. Having the collars in the hole with no external upsets allowed the pipe to be pulled back up the hole when required to reestablish rotation and circulation. As a result, when the drill string was tripped to the surface to change the core bit to a new C-7 RCB bit, nine additional drill collars were added to the drill string. Severe damage was noted on the upward-pointed shoulder of the used bit because of the backreaming required by the multiple incidents of stuck pipe. The BHA was heavily sandblasted/polished on all joints that extended below the reentry cone.

The pipe was tripped to the bottom once again, and in <15 min Hole U1362A was reentered for the eighth time at 2335 h on 5 August. After the top drive was picked up the bit was washed/reamed to within 1 m of the total depth without any major issues. At that point, however, the drill string became stuck and an additional 6 h was required to work the drill string free and condition the hole before coring could resume. RCB coring continued with Core 327-U1362A-15R, starting at 448.6 mbsf, and continued through Core 21R to a total depth of 3168 mbrf (496.0 mbsf). Core 21R was on deck at 1255 h on 8 August. Cores 15R through 18R were cut with very slow ROPs of 1–2 m/h or less in a much more massive and less fractured formation. Recovery through this interval was excellent, averaging >75%. Cores 19R through 21R, however, were recovered from highly fractured material with ROPs in the 4–5 m/h range, and recovery dropped to 24.3%. The last core (21R) was cut with elevated drill string torque indicative of potential hole problems to come. The use of significantly larger mud sweeps (65–150 bbl each) resulted in more effective hole cleaning and fewer stuck-pipe incidents.

The coring cycle was followed by three wiper trips to the 10¾ inch casing shoe and back to total depth. Hole conditions improved with each cycle but not to an acceptable level for wireline logging, packer testing, and ultimately the CORK deployment. The first wiper trip required 7 h of washing/reaming and had 54 m of fill to remove from the bottom of the hole. The second wiper trip required 4.5 h of washing/reaming and had 46 m of bottom fill. The third wiper trip required only 3.5 h of washing/reaming and had 28 m of fill. Further wiper trips were abandoned in favor of deepening the hole by drilling, and at 0700 h on 9 August the pipe trip began back to the surface.

The RCB assembly was switched to a 9⅞ inch tricone drilling assembly. The tricone bit is equipped with bigger cutters and bearings that are better suited to rough drilling conditions and is also capable of handling the higher flow rates necessary for effective

hole cleaning. At 0700 h on 9 August the pipe round-trip began, and at 1935 h that same evening Hole U1362A was reentered for the ninth time. The bit was run to 476 mbsf without rotation or circulation. The hole was washed and reamed through 20 m of soft fill to total depth, and a 50 bbl high-viscosity mud sweep was circulated. Another 17 h was required to deepen the hole by 32 m to a final total depth of 528 mbsf. Two 75 bbl high-viscosity mud sweeps were pumped, and at 1800 h on 10 August a series of three wiper trips was initiated to clean up and condition the hole. This required 11 h to complete, including the requisite mud sweeps. After the third wiper trip the pipe was lowered without rotation or circulation to 515 mbsf. After some resistance at that depth the pipe broke through the plug easily and the hole was found to be open to total depth. At 0500 h on 11 August the pipe was tripped back to the casing shoe, and 3.5 h was spent on standby waiting for the hole to equilibrate and to allow any remaining cuttings to fall to the bottom. During that time general rig maintenance was conducted, as was a pressure test of the rig circulation system in preparation for the packer flow test. At 0930 h on 11 August the drill string was lowered into the hole without rotation or circulation, reaching 512 mbsf. A 75 bbl high-viscosity mud sweep was circulated, and the drill string was recovered back to the surface.

Hole U1362A wireline logging and packer pumping test

The wireline logging/packer BHA was assembled, the drill string was tripped to the seafloor once again, and at 0211 h on 12 August Hole U1362A was reentered for the tenth time. The pipe was spaced out to 264 mbsf (still inside the 10¾ inch casing), and preparations began for wireline logging. At 0545 h on 12 August a single suite of logging tools was run in the hole (see **"Downhole measurements"**). The logging string reached 507 mbsf without any resistance. Two full passes were made from 507 mbsf to the casing shoe at 308 mbsf. A third partial pass was made from 508 to 373 mbsf across the area of interest for setting the lower packer. Wireline logging was completed and the tools were rigged down by 1615 h on 12 August.

The drill string was lowered to 519 mbsf without rotation or circulation for another depth check. The end of the pipe was raised to 436 mbsf, positioning the TAM packer assembly at the desired depth of 424.5 mbsf. After some difficulty setting the packer in open hole (attributed to the >2 m of vessel heave), the first flow test was completed by 0430 h on 13 August. The drill string was raised up into the 10¾ inch casing for the second and final flow test. This test was canceled when the packer repeatedly failed to lock in pressure. It was possible to pressure up the packer, but the pressure could not be locked in the element to set the packer. At 1000 h on 13 August the drill string was tripped to the surface, and the end of the pipe cleared the rotary table at 1800 h. Upon recovery, inspection of the packer showed evidence of extensive damage, and water was seen leaking from a bad gouge near the lower end, explaining why the packer failed to hold pressure.

Hole U1362A CORK wellhead and casing deployment

Assembly of the CORK began at 1845 h on 13 August. The CORK running tool was made up to a 2 m drill collar joint and laid out on the rig floor for later use. The bullnose was made up with three perforated and coated 8¼ inch drill collars. A single joint of perforated and coated 5½ inch casing, along with the required crossover subs, was made up and lowered into the moonpool area. The coated collars and casing joint were wiped clean with isopropyl alcohol and held off the steel penetrator in the moonpool floor. A microbiology miniscreen was installed on the lower end of the 5½ inch casing joint and its umbilical was attached. A chemistry miniscreen was attached in the upper third of the 5½ inch casing joint along with its umbilical. At 2130 h the first inflatable packer was installed, followed by a landing collar and the first swellable packer assembly. A pressure miniscreen was installed on the 4½ inch casing mandrel below the inflatable packer along with the umbilical connection.

When the first swellable packer sub was picked up on the rig floor, it was determined that the swellable element was >9¾ inches in places, considerably larger than the 8½ inch diameter that was expected and too large to be run in an irregular open hole drilled with a 9⅞ inch drill bit. The swellable packer subs to be used at depth below the CORK wellheads comprised two separate packer elements, each with 30 inch sealing length, built around the same 4½ inch casing used for most of the rest of the CORK casing. The two swellable elements were intended to be deployed in pairs. Each element was split longitudinally, with molded channels on the inside to accommodate the umbilical lines. The halves are bolted together over the umbilicals, and the design is such that the packer will swell into and seal against the casing or borehole wall over time. This process is supposed to take several weeks to complete once the element is submerged in seawater. Because there were concerns about getting a >9¾ inch diameter into the open hole, we decided that the packer ele-

ments should be machined down to 8½ inches. Although time consuming (almost 24 h for both swellable packer elements), this was considered better than running the packers with too large a diameter or omitting them entirely.

The first pair of swellable packer elements having a reduced diameter was ready for installation at 1100 h on 14 August, allowing work to proceed in the moonpool with umbilical connections and miniscreen installations. Installation of the second swellable packer pair began at 1830 h that evening. By 2200 h, eight additional joints of 4½ inch casing were run, and the second set of inflatable and swellable packers was installed, including additional chemistry and pressure miniscreens. This packer set did not have to be reduced in diameter because it was to run inside 10¾ inch casing rather than open hole. Another 22 joints of 4½ inch casing were run by 0845 h on 15 August. At that point the CORK head was picked up, the CORK running tool was made up to the CORK head, and the head was made up to the top 4½ inch casing joint, all within 30 min. The final umbilical terminations were made, including all strapping and securing. Only a few casing centralizers were installed on the CORK stinger to minimize the potential for getting stuck in the open hole during deployment. A single 5½ inch centralizer was used to protect the lowermost chemistry miniscreen. A 4½ inch centralizer was used next to the lowermost pressure screen, above the first swellable packer and below the second inflatable packer. A pair of 4½ inch centralizers was installed on all 4½ inch casing joints that were to remain inside the 10¾ inch casing. The packer inflation hose was installed between the running tool and the CORK head, the valves were opened, and after picking up a single stand of drill collars, the CORK was lowered into the water. The CORK was pulled back up after 5 min to close the valves and secure the valve handles with rubber bands. The fit of the vibration-isolated television (VIT)/subsea TV frame over the CORK head was verified. The pipe trip to the seafloor with the CORK assembly was initiated at 1300 h on 15 August.

Hole U1362A CORK instrument string deployment

At 1630 h on 15 August the drill string was positioned just above the seafloor and preparations began for instrument string deployment. A 200 lb sinker bar was assembled below six OsmoSampler sections. When the OsmoSamplers were suspended in the pipe, deployment of the Spectra cable and temperature loggers began. The deployment of the 464 m long instrument string proceeded rapidly because the string had lifting eyes prespliced into the Spectra cable at 25 m increments, saving hours of rig time. The instrument string was slowly lowered to the bottom at 1815 h, and by 1945 h the string had landed and latch-in had been verified with 400 lb of overpull. Within minutes the weakened shear pin was sheared off and the wireline was recovered. By 2230 h the drill string was spaced out for reentry and the VIT/subsea TV reached the end of the pipe. The attempted reentry was suspended at this point when it became apparent that the instrument string was protruding beyond the end of the CORK bullnose. The wireline sinker bar and first OsmoSampler section were visible beyond the CORK stinger. An attempt at reentry and deployment in the open hole was not considered advisable because this would most likely result in damage to the instrument string and possibly in loss of the hole. Unfortunately, we did not have the small RS fishing tool needed to unlatch the top plug from the CORK, so we had no way to recover the instrument string without recovering the CORK wellhead. We decided to bring the drill string back to the surface, and at 0200 h on 16 August the CORK was hung off in the moonpool. The instrument string was released using the screws built into the top of the wellhead for future removal by a submersible should the RS fishing tool fail to release the plug. The top plug was lifted, and part of the Spectra cable was pulled from the hole, shortened and spliced, and reinserted into the CORK. The top plug was latched into place while the wellhead was at the surface, rather than waiting until it was at the seafloor.

At 0600 h the drill string was once again tripped to the seafloor. The trip took longer than the initial attempted deployment because the pipe had to be filled from a water hose after each stand was assembled. The water was needed to prevent a differential pressure from building up and overloading the latch system on the instrument string. Hole U1362A was reentered for the eleventh time at 1150 h. The CORK was landed without incident, and the inflatable packer assemblies were inflated with 1500 psi pressure over a period of 30 min. The VIT/subsea TV was recovered, and at 1600 h preparations began for deploying the CORK platform.

The platform halves were maneuvered onto the moonpool doors and bolted together. Another 2 h was spent assembling the platform deployment vehicle with the VIT sleeve and rigging the various required slings. At 1800 h the platform began its trip to the seafloor, but at 2007 h the subsea TV camera went black. After some initial troubleshooting by an Overseas Drilling Limited (ODL) electronics technician, the VIT/subsea TV with the suspended CORK

platform was recovered back to the ship. A faulty connector was replaced, and the VIT was once again run to the bottom. Upon initial landing at 0230 h on 17 August the platform reached the CORK running tool but failed to release. After being worked up and down for ~1 h, the platform eventually released. The VIT was recovered back to the ship, and the deployment tool was removed along with all platform deployment slings so that they would not become entangled with the CORK installation. The VIT/subsea TV was deployed back to the bottom, confirming that the platform had not released correctly and was hanging at an angle off the CORK running tool. The VIT sleeve was set down on the platform multiple times before the platform was jarred off and fell into position on the rim of the reentry cone. The running tool was released from the CORK head at 0600 h on 17 August, successfully completing the installation of the Hole U1362A CORK. The drill string was tripped back to the surface, and the recovery tool cleared the rig floor at 1045 h, ending operations in Hole U1362A. Close inspection of the platform deployment tool indicated that one of its arms was bent from impact with the bolt screwed into the CORK running tool to protect the packer inflation hose fitting. As a result, only two of the three arms released initially, causing the platform to hang on the third arm and resulting in the cocked attitude of the platform on the CORK head. A shorter bolt that would not interfere with the platform deployment was installed for the next deployment.

Hole U1362B Stage 3

The drill string was recovered following operations in Hole 1027C (see **"Operations"** in the "Site 1027" chapter). The BHA was changed to a drilling BHA, and a new 9⅞ inch tricone drill bit was deployed. Hole U1362B was reentered for the sixth time at 0423 h on 21 August. The bit was advanced to the bottom, taking weight at 172 mbsf. The top drive was picked up, and the hole was washed/reamed to 262 mbsf, where the top of the undrilled cement was contacted. The cement was drilled out, and the hole was cleaned to the bottom of the 14¾ inch hole at 282 mbsf. The hole was deepened another 57 m to 339 mbsf, 3 m short of the original target depth of 342 mbsf. A 50 bbl sweep of high-viscosity mud was circulated, and two successive wiper trips were conducted from the 10¾ inch casing shoe to total depth. On the last wiper trip the driller noted some resistance at 310 mbsf, but this was easily passed, and 6 m of hard fill was noted at the bottom. Another 50 bbl mud sweep was circulated, and at 1630 h on 22 August the drill string was tripped back to the surface, clearing the seafloor at 1745 h.

Hole U1362B pumping test and tracer injection experiment

Assembly of the injection/flow test BHA began at 2200 h on 22 August. This BHA included a specially made injection sub that had axial circulation slots in the sides and functioned as a carrier for downhole pressure gauges and for osmotic samplers, which would be used to sample the injectate downhole. The assembled BHA initially had the bottom of the injection pipe extending 13.4 m below the 10¾ inch casing shoe into open hole. The drill string was tripped to the seafloor, and at 0330 h on 23 August a preinjection exercise was conducted to ensure that all parties involved (drill crew, gas injection crew, cementer, and rig floor sampling crew) understood their respective roles and that all equipment was set up properly. Hole U1362B was reentered for the seventh time at 0715 h. The drill string was run in the hole and began taking weight ~3 m before landing the Dril-Quip running tool in the 10¾ inch casing hanger. The pipe was eventually worked down, and the running tool was landed. After waiting 1 h for the hole to equilibrate and establish a baseline starting point, the rig pumps were engaged at a circulation rate of 20 strokes per minute (spm). When pump pressure rose quickly it became apparent that the system was clogged. The drill string was tripped back to the surface, clearing the rig floor at 1700 h. Upon recovery, the end of the stinger was found to be packed with drill cuttings, ground up cement, and drilling mud. Not only did this inhibit the injection of fluid into the borehole, it was an indication that the hole was likely packed off and would have to be opened up before a viable injection test could be conducted. The same bit and drilling BHA used previously was reassembled and deployed to the seafloor. Hole U1362B was reentered for the eighth time at 0125 h on 24 August. The drilling assembly was run to the bottom without rotation or circulation, taking weight at 308 mbsf. No sign of what was plugging the hole was detected. The hole was repeatedly washed, reamed, and swept with high-viscosity mud. Once the hole was deemed to be in acceptable condition, the drill string was pulled back into the 10¾ inch casing string at 1015 h to begin a 1 h waiting period to allow the hole to stabilize. This period was followed by another round of wiper trips and hole conditioning because there continued to be spots in the hole that could not be passed without using circulation and/or rotation. The most troublesome spots seemed to be at 353 and 359 mbsf. Ultimately, these spots were cleared, and the drilling assembly was recovered back to the surface. At 2100 h on 25 August the injection BHA was reassembled. This time the space-out was changed to position the

lower end of the injection stinger only 3.76 m beyond the 10¾ inch casing shoe. The assembly was redeployed to the seafloor, and prior to reentry a series of pressure readings was taken at slow circulation rates to provide baseline pressures. Hole U1362B was reentered for the ninth time at 0642 h on 26 August. This time the injection assembly landed without incident. Once again a 1 h waiting period was begun to provide a baseline for the start of the 24 h injection test. At 0900 h the injection test started with 20 spm on the rig circulating pumps, using seawater as the injected medium. The VIT/subsea TV camera was lowered to provide assurance that no fluid was leaking from the hole. The 24 h injection test was successfully completed by 0900 h on 27 August, followed by a 1 h waiting period to allow the hole to equilibrate. The injection BHA was recovered back to the ship, and the osmotic samplers and downhole pressure data loggers were removed from the injection sub carrier. The injection schedule, tracers used, and other information concerning this experiment are presented in **Fisher, Cowen, et al.**

Hole U1362B CORK wellhead and casing deployment

Because having enough open hole was critical to the successful deployment of the CORK, a final depth check was conducted using a drilling BHA prior to CORK assembly and deployment. At 2130 h on 27 August Hole U1362B was reentered for the tenth time. The drill string was lowered to 261 mbsf (inside the 10¾ inch casing), and the top drive was picked up in case it became necessary to wash or ream the hole to the bottom. The bit was lowered without rotation or circulation to 348 mbsf, or just 11 m above the total depth of the hole at 359 mbsf (below the CORK stinger space-out depth of 312 mbsf), and the drilling assembly was recovered back to the surface.

At 0530 h on 28 August, preparations were begun for assembling and deploying the CORK in Hole U1362B. The running tool was made up to a 2 m drill collar pup joint and laid out on the rig floor for later use. The bullnose was made up with three 8¼ inch perforated and coated drill collars and a single joint of perforated and coated 5½ inch casing, along with the required crossover subs. The coated collars and casing joint were wiped clean with isopropyl alcohol and held off the steel penetrator in the moonpool floor. A microbiology miniscreen was installed on the lower end of the 5½ inch casing joint, and the umbilical was attached. Three chemistry miniscreens and their respective umbilical lines were attached to the upper part of the 5½ inch casing joint, followed by an inflatable packer, a landing collar (for a future internal instrument string having a bottom plug), and a swellable packer set. The single pressure miniscreen was installed on the 4½ inch casing mandrel below the inflatable packer and was connected to the final umbilical. Nineteen joints of 4½ inch casing were made up, and the umbilical lines were strapped and secured to the casing using bands. The CORK running tool was made up to the CORK head, the head was made up to the top 4½ inch casing joint, and the umbilicals were terminated. Only a few casing centralizers were installed on the CORK stinger to minimize the potential for hanging up in open hole during deployment. A single 5½ inch centralizer was used to protect the chemistry miniscreens. A single 4½ inch centralizer was installed near the base of the 4½ inch packer mandrel. Two 4½ inch casing centralizers were installed on each 4½ inch casing joint that would remain inside the 10¾ inch casing string. The packer inflation hose was installed between the running tool and the CORK head, the valves were opened, and after picking up a single transition stand of drill collars the CORK was lowered into the water. The CORK was pulled back to close the valves and secure the valve handles with rubber bands. The CORK assembly trip to the seafloor began at 2315 h on 28 August.

Hole U1362B CORK instrument string deployment

At 0200 h on 29 August the drill string was positioned just above the seafloor, and preparations began for deploying the instrument string. A ~200 lb sinker bar (wet weight) was assembled with the osmotic sampler sections, temperature data loggers, Spectra cable, and the landing sub. This process, including the trip to the seafloor, required ~4 h. The wireline trip was made at a very slow speed (15–20 m/min). A Spectra stretch test using the traveling block on the rig (completed prior to string deployment) indicated that scientists needed to allow for 2% stretch rather than the 1% indicated by the manufacturer, so the cable was terminated accordingly. To avoid the problem experienced in Hole U1362A of the instrument string extending beyond the end of the CORK stinger, the last 20 m of deployment was made very slowly while monitoring the end of the CORK with the VIT camera, allowing us to stop the winch operator quickly should the string be seen to protrude beyond the end of the CORK stinger. In such a case, the instrument string could have been recovered before latching in, thus avoiding a drill pipe trip with the CORK. This time the space-out on the Spectra cable was fine (having been adjusted for greater anticipated cable stretch), and the instrument string landed without extending past the bullnose on the CORK stinger. The perceived latch-in

was verified with several hundred pounds of overpull, and the GS overshot, equipped with a weakened shear pin, was jarred off after four attempts. The sinker bar string was recovered back to the surface, and at 0648 h Hole U1362B was reentered for the eleventh time. At this point water was observed to be flowing from the drill pipe onto the rig floor, associated with ship heave. This suggested that the landing sub might not be seated. The CORK string was pulled clear of the reentry cone, and the sinker bars were deployed once again to engage the pulling neck on the instrument string to verify latching. Again, after applying several hundred pounds of overpull it appeared that the string was properly latched. However, during the jar-off attempt the wireline gained the weight of the instrument string. Either the string was latched and the jarring caused the latching mechanism to fail, or the string had not been fully latched in originally. The instrument string was recovered back to the surface and inspected. No problems were noted with the latch or the Spectra cable. The landing/latch assembly was changed out in the event there was a tolerance problem or something was imperceptibly wrong with the latch.

At 1030 h on 29 August, the string was redeployed. This time, however, it was difficult to achieve any overpull after landing the top plug in the CORK wellhead. The GS overshot was jarred off once again, and the sinker bars were recovered. Subsequent discussions regarding the water pumping action centered on the possibility that sufficient clearance in the latch-down mechanism allowed the sub to lift off the seat because of heave-induced pipe surge, which in turn allowed water to flow past the small-diameter O-ring seal. In fact, latching the top plug is not required to seal the CORK; the latch is intended mainly as a means of checking that the plug is landed, and that the overshot can be jarred loose, but sealing is provided by an O-ring on a tapered seal surface, held down by the weight of the instrument string. At 1330 h Hole U1362B was reentered for the twelfth time. The CORK assembly was run in the hole without incident, and at 1515 h the CORK head landed in the 10¾ inch casing hanger at the correct drill string depth measurement. Visual observation confirmed the CORK head was in the correct position, and the VIT/subsea TV was recovered back to the surface. The inflatable packers on the CORK string were inflated to 1000 psi for 30 min. The VIT/lunar lander and CORK platform were assembled in the moonpool area, and at 1800 h the platform was deployed through the moonpool. The CORK platform was successfully released at 1930 h, the VIT was recovered, and the deployment slings and tool were rigged down. The VIT frame was redeployed at 2200 h, and visual confirmation was received that the platform was resting properly on the reentry cone. At 2217 h on 29 August the running tool was released, completing the Hole U1362B CORK installation.

The VIT frame was run back to the seafloor with a grappling hook to recover a beacon that had not surfaced. The beacon was grabbed at 0146 h and was on deck by 0255 h. The beacon did not release properly because it had a tangled tether, which kept the weight attached. VIT footage of a subset of operations is included in MOVIES in **"Supplementary material."** The drill string was pulled up by 0815 h, and the rig was secured for transit by 1300 h. The thrusters were raised at 1315 h, and the ship was under way for Grizzly Bare Site U1363 (prospectus Site GRB-1A).

Petrology, hard rock geochemistry, and structural geology

Basement was cored from 346.0 to 496.0 mbsf (110–260 msb) in Hole U1362A with 45.27 m of core recovered (30%). The recovered core consisted of (1) aphyric to moderately phyric pillow basalt, (2) aphyric to sparsely phyric sheet flows, and (3) sparsely to highly phyric basalt flows. These lithologies were divided into eight units on the basis of changes in lava morphology, rock texture, and phenocryst occurrence (Fig. **F5;** Table **T4;** see Site U1362 visual core descriptions in **"Core descriptions"**). Pillow lava units (Units 1, 3, and 5) were divided according to changes in phenocryst abundance and mineralogy. Sheet flow units (Units 4, 6, and 8) were divided on the basis of the presence of chilled margins and variations in phenocryst mineralogy. In this hole breccia recovery is limited to one 7 cm piece of a magmatic breccia and a single centimeter-sized cataclastic zone, neither of which is defined as an individual unit.

In addition to cores recovered from Hole U1362A, small millimeter- to centimeter-sized chips were recovered from the drill bit in Holes U1362A and U1362B. In both cases the drill bit only penetrated a few meters below the sediment/basalt interface before being pulled to the rig floor, where the drill cuttings were removed. The source of the drill cuttings can be constrained to a short interval at this interface and represents the only recovery of basement material at the sediment/basalt interface at Site U1362. The cuttings were rinsed and separated on the basis of color or mineralogy, where possible. A

range of variably altered clinopyroxene plagioclase phyric microcrystalline basalt was recovered (see "Basement alteration"). A chilled margin 3 cm long was also recovered from the bit in Hole U1362B. No basement units were assigned because of the limited recovery of chips from the drill bits.

Lithologic units

Pillow basalt (Units 1, 3, and 5)

Pillow basalt forms the most abundant flow morphology of Hole U1362A, with Units 1, 3, and 5 accounting for 78.85 m of the stratigraphy. Pillow basalt was primarily identified by the occurrence of curved glassy chilled margins. In larger pieces perpendicular radial cooling cracks were present (Fig. F6), but often the pieces recovered with glassy chilled margins were too small to determine if the cracks were radial. The largest piece of pillow basalt recovered was 45 cm in length. The pillow basalt core with the highest recovery had 35% recovery for a 5.5 m advance and contained nine chilled margins (Core 327-U1362A-5R). The sizes of individual pillow lava pieces can be inferred to be between 45 and 61 cm in diameter. The pillow basalt is dominantly hyalophitic and glomeroporphyritic in texture and varies between cryptocrystalline and microcrystalline in groundmass grain size. It is sparsely to highly phyric, with olivine, clinopyroxene, and plagioclase phenocrysts present. Thin section observations identified spherulitic, hyalophitic, intersertal, and glomeroporphyritic igneous textures. Pillow basalt ranges from sparsely to moderately vesicular, with a range of secondary minerals filling the vesicles. Alteration in the pillows is variable and ranges from slight to high, manifesting as replacement of mesostasis and phenocrysts, vesicle filling, glassy margin replacement, and vein formation with adjacent alteration halos.

Sheet flows (Units 4, 6, and 8)

Sheet flows are the second most common lava morphology in Hole U1362A and were classified on the basis of continuous sections of the same lithology with increasing grain size downhole from the top of the flow and fewer chilled margins. Core recovery in these units averaged 43% and was as high as 112%. Recovery of >100% in Core 327-U1362A-17R is an artifact of tidal fluctuations during coring, which resulted in the depth penetrated appearing to be smaller than the recovered core length. Two nearly continuous sheet flows recovered in Cores 17R and 18R were divided into two subunits on the basis of a change in phenocryst mineralogy.

Primary mineralogy of the sheet flows is very similar to that of the pillow basalt, with a range from aphyric to moderately phyric basalt with olivine, clinopyroxene, and plagioclase as phenocryst phases and forming the groundmass. Grain size within the sheet flows is variable, ranging from cryptocrystalline to fine grained in Subunit 4C, and textures vary from intersertal to intergranular. The sheet flows range from nonvesicular to highly vesicular, with some flows exhibiting similar abundance throughout (e.g., Subunits 6A and 6B); others are highly variable within the flow (e.g., Subunit 4C). Alteration within the sheet flows varies from slight to high and is associated with groundmass replacement, vesicle fill, vein formation, and alteration halos. Alteration halos within the sheet flows are highly variable and not always clearly associated with a recovered vein (see "Basement alteration"). The lower fracture and vein intensity in the sheet flows compared to in the pillow basalt resulted in improved core recovery and larger individual pieces (maximum piece length of 140 cm in Section 327-U1362A-17R-1).

Basalt flows (Units 2 and 7)

Classification of basalt flow units is based on the absence of definitive morphological features associated with either pillow lava or sheet flows, allowing only a general "basalt flow" interpretation to be made. When present, glassy chilled margins lack definitive pillow structure and could represent either a pillow margin or the margins of a thin sheet flow. These basalt units are aphyric to moderately phyric crypto- to microcrystalline with the same primary mineralogy as basalt from Hole U1362A. The basalt flows are generally sparsely vesicular, with secondary minerals filling vesicles and textures varying from hyalophitic to variolitic. Alteration is moderate to high and is present as groundmass replacement (mesostasis and phenocrysts), vesicle fill, vein formation, and halos.

Igneous petrology

The basaltic rocks recovered from Hole U1362A are divided into three types, as described above (pillow lava, sheet flows, and thin basalt flows), and 27 samples were selected for petrographic analysis (see Site U1362 thin sections in "Core descriptions").

Pillow lava (sparsely to highly phyric basalt)

The pillow lava from Hole U1362A varies from sparsely to highly phyric basalt. Subunit 5B is sparsely phyric basalt with glassy to fine-grained groundmass and <4% phenocrysts. Unit 1 and Subunit 5A are moderately to highly phyric basalt with glassy to microcrystalline grain size and ~6%–15%

phenocrysts. Plagioclase is the most abundant phenocryst phase (~3%–11%), with clinopyroxene (~1%–10%) and olivine pseudomorphs (<5%) also present in most of the phyric samples.

This lava is predominantly hyalophitic and glomeroporphyritic to subophitic (partial inclusion of plagioclase in clinopyroxene) with frequent examples of intersertal and spherulitic texture. A glassy chilled margin sample (327-U1362A-2R-1, 121–126 cm; Fig. F7) displays a transition from holohyaline to spherulitic texture in which spheroidally arranged aggregates of acicular microcrystals become increasingly abundant away from fresh amber glass. Several textures were frequently observed across a single thin section (Fig. F8C–F8E) and also within a single (sub)unit.

Sheet flows

The sheet flows of Units 4, 6, and 8 vary from aphyric to moderately phyric basalt. Subunit 4C is aphyric fine-grained basalt with <2% phenocrysts, and Units 6 and 8 and Subunits 4A, 4B, and 4D are sparsely to moderately phyric microcrystalline basalt with 1%–7% phenocrysts. Overall, plagioclase is the most abundant phenocryst phase (<5%), with clinopyroxene (<3%) and olivine pseudomorphs (<2%) also present. Almost all sheet flow interiors display intersertal texture with frequent glomeroporphyritic clots and infrequent sections of high vesicularity.

Basalt flows

The thin basalt flows of Units 2 and 7 are moderately olivine clinopyroxene phyric (~8% phenocrysts). Samples close to flow margins exhibit cryptocrystalline grain size and variolitic to hyalophitic textures, and samples from flow interior locations are microcrystalline to fine grained and have intersertal to intergranular and seriate textures.

Phenocryst phases

Plagioclase

Plagioclase is the most abundant phenocryst phase and typically makes up <10% of pillow lava and <5% of sheet and basalt flows. Phenocrysts range from 0.2 to 4.1 mm in length and are mostly euhedral in shape. More than 60% of crystals are found in clots with mainly clinopyroxene and in rare cases olivine. Euhedral platy to stubby discrete crystals are present throughout, and rare skeletal or quench plagioclase crystals are found in lower pillow lava units. Simple to oscillatory zoning is uncommon but is present in some crystals (e.g., Sample 327-U1362A-9R-2, 74–75 cm). Glass and clinopyroxene inclusions are occasionally present as blebs and microlites parallel with plagioclase twin planes. Alteration of crystals varies from 0% to 20% and generally manifests as replacement by secondary clays, saponite, iron oxyhydroxides, and oxides along cracks, cleavage planes, or crystal edges (Fig. F9).

Clinopyroxene

Clinopyroxene is present in almost all thin sections and typically makes up <1.5% of pillow lava, <1.0% of sheet flows, and <8.0% of thin basalt flows. Phenocrysts are generally <1.2 mm long (rarely up to 5.5 mm) and are typically anhedral to euhedral, stubby to short prismatic or round crystals and are predominantly intergrown with plagioclase in glomeroporphyritic clots. Solitary subhedral to euhedral crystals are uncommon and tend toward seriate texture. Simple basal twinning is common throughout. Alteration of clinopyroxene varies from 0% to 80% and manifests as replacement by secondary clays, saponite, iron oxyhydroxides, and oxides along cracks, cleavage planes, or crystal edges (Fig. F9).

Olivine

Olivine is only observed in thin sections as a pseudomorph, with an average abundance of 1%–2%. Olivine phenocrysts (0.1–1.7 mm; average width = 0.6 mm) are completely replaced by a variety of secondary phases and are identified by their subhedral crystal morphology and textural relationships with surrounding minerals. Larger olivine crystals (as large as 1.7 mm in diameter) from sheet flow interiors tend to be skeletal and coexist with more equant, smaller crystals. Identified pseudomorphs of olivine are granular saponite, celadonite, iddingsite, and opaque minerals (Fig. F9).

Groundmass

The groundmass of rocks recovered from Hole U1362A varies from hypocrystalline to holocrystalline. Constituent minerals are the same as those present as phenocrysts, but modal abundances vary between samples. The groundmass is composed primarily of plagioclase and clinopyroxene. Plagioclase occurs as microlaths, microlites, and quench crystals and is marginally the more abundant groundmass crystalline phase, composing 2%–43% of pillow lava, 27% of thin basalt flows, and 34%–41% of sheet flow interiors. Clinopyroxene occurs as microlaths, microlites, and aggregates of fibrous or plumose crystals and composes 1%–36% of pillow lava, 31% of thin basalt flows, and 24%–38% of sheet flows. Anhedral to subhedral microcrysts of pseudomorphed olivine are present in low abundances in pillow lava and thin basalt flows (original abundance of 0.5%–8%)

and are slightly more abundant in thick sheet flows (8%–12%). Trace amounts of opaque minerals are also present throughout all units.

Cryptocrystalline mesostasis makes up the remainder of the groundmass in the basalt. Abundances are highly variable in pillow basalt, ranging from 14% to 80%. Sheet flows and thin basalt flows are less variable, with mesostasis abundances of 10%–22% and 28%, respectively. Mesostasis textures are variable within a single sample, but basalt from different units of the same lithology exhibits the same range of textures. Nearly all lithologies display hyalophitic and intersertal textures. Spherulitic and variolitic textures are common in pillow lava and thin basalt flows (Figs. F8, F10). Primary magmatic opaque minerals are disseminated throughout the mesostasis, forming small (<0.1 mm) granular euhedral to subhedral solitary grains. The mesostasis exhibits patchy alteration in which discrete areas of groundmass are more intensely altered than the background replacement of original host rock to secondary hydrothermal clays (saponite and celadonite) and iron oxyhydroxides (Fig. F11).

Almost all units are sparsely to moderately vesicular (3%–9% vesicles in most samples). The majority of these are slightly to moderately spherical and 0.1–9.0 mm in diameter. There is little to distinguish between units except for a large contrast in vesicle abundances between Subunits 4C and 4D, which range between nonvesicular (<0.1%) and highly vesicular (20%). The majority of vesicles are >50% filled by mono- to polymineralic secondary assemblages that include saponite, celadonite, iron oxyhydroxides, pyrite, and mixed clays. The presence of concentrically filled vesicles is related to the overall alteration of the lithology and is described in more detail in **"Basement alteration."**

Basement alteration

All of the basement rocks recovered from Hole U1362A have undergone alteration by interaction with seawater. The extent of alteration varies from slight to completely altered, and most pieces are moderately altered. The rocks manifest four types of alteration: (1) replacement of groundmass, (2) replacement of phenocrysts, (3) hydrothermal veins and alteration halos, and (4) lining and filling vesicles. In thin section, alteration is observed to range from 8% to 91%. Away from vesicles and veins, background alteration is generally moderate to high in pillow lava and predominantly moderate in sheet and basalt flows and is dominated by saponitic background alteration. Olivine is present only as completely replaced pseudomorphs.

Secondary minerals

The identification of secondary minerals was primarily made in hand specimen, with subsequent partial verification by thin section observations and XRD. The distinction of specific secondary clay minerals was made for only a few examples during logging of alteration and veins.

The most abundant secondary minerals in Hole U1362A are clay minerals, which are present in all four types of alteration. Clay minerals were identified primarily by color and were verified where possible by thin section observations. Saponite is the dominant clay mineral and is present throughout all cores. In hand specimen saponite occurs in black, dark green, greenish-brown, and pale blue colors. In thin section it is characterized by pale brown color and mottled or fibrous form. Saponite generally evenly replaces groundmass and phenocrysts, preserving the primary igneous textures. In the case of highly to completely altered samples, saponite replacement is pervasive across mesostasis and groundmass crystals to form continuous mottled replacement, destroying the original textures (Fig. F12). Commonly, saponite lines or fills vesicles, forms a lining along vein edges, and replaces both groundmass and phenocrysts (Fig. F12). Saponite occurs occasionally as pale blue, either as alteration of glassy chilled margins or lining vesicles. In Unit 6 saponite occurs as a dark green waxy coating on most fractures and veins. Celadonite is the only other clay mineral confidently identified in hand specimen and thin section observations and occurs as bright green/blue in hand specimen. Celadonite is also present in all four types of alteration but is less abundant than saponite. In thin section celadonite is bright green, and within some vesicles the intensity of the color varies (see **"Vesicle filling"**).

Iron oxyhydroxide is the next most abundant secondary phase, and it occurs either alone as iron oxyhydroxides or mixed with saponite and other clay phases. Iron oxyhydroxides are easily identified by their bright orange to red color and often stain other phases present. When present as replacement of phenocrysts and groundmass, iron oxyhydroxides are mixed with saponite and clays (iddingsite) and form hyalophitic texture. In veins and lining or filling vesicles, iron oxyhydroxides are bright orange to red-brown and occur with or without intergrown clays. Staining and replacement of phenocrysts with iron oxyhydroxides is a common feature in the dark gray/black halos present throughout the hole.

The zeolite phillipsite was identified by XRD analysis of altered chilled margins (Sample 327-U1362A-3R-1, 22–24 cm) (Table T5). Other veins analyzed by XRD contained montmorillonite (smectite group) and se-

piolite clay phases. The sepiolite is interpreted to be contamination from drilling mud. Carbonate is present as vesicle fill in veins and within chilled margins. XRD analysis of carbonate-bearing samples identified the carbonate as calcite (Samples 327-U1362A-2R-1, 43–45 cm; 14R-2, 53–54 cm; and 16R-2, 56–119 cm). Anhydrite is present in veins from Core 18R, where it occurs as pure white crystals and was identified by bright third-order interference colors in thin section.

In addition to cores recovered from Hole U1362A, small millimeter- to centimeter-sized chips were recovered from the drill bit in Holes U1362A and U1362B. Basalt exhibiting a wide variety of hydrothermal alteration was recovered in these chips, and similar compositions were recovered in both Holes U1362A and U1362B. Alteration types included pervasive green and red alteration, iron oxyhydroxides, pale gray sulfide-bearing mud, and basalt chips with tentatively identified epidote crystals. Spot analysis of the epidote crystals undertaken postcruise at the National Oceanography Centre, Southampton, confirmed epidote to be present within the basalt chips recovered from the sediment/basalt interface in Hole U1362A (Table **T6**). XRD analysis identified saponite, sepiolite, and phillipsite in the green alteration and pyrite with gismondine in the sulfide mud. The sepiolite is interpreted to be a contaminant from the drilling mud. A 3 cm long chilled margin was also recovered from Hole U1362B.

Breccia

Breccia is not common in this hole and is only present as small localized features. No unit-size hyaloclastite breccia was recovered. A single occurrence of magmatic breccia (hyaloclastite) present in Section 327-U1362A-13R-1 (Piece 8) consisted of two large basaltic clasts and multiple small <1–5 mm clasts in a saponite and altered-glass matrix (Fig. **F13**). The large clasts are subangular and as large as 42 mm and form 75% of the piece. Alteration within these clasts is high: black halos dominate the clasts with small 10 mm slightly altered cores. Multiple vein compositions in the clasts formed both before and after brecciation, the latter observed as veins continuing from the matrix into the clast itself. The saponitic matrix (16 mm wide at the broadest point) contains a complete range of smaller clasts that vary from moderately altered to completely replaced and pseudomorphed by secondary phases. These clasts are predominantly replaced by saponite, with clast rims highlighted by pale green clays. Internal structure in these clasts is often preserved; one example shows a filled vesicle still present. The wide range of alteration of the smaller clasts of the same size requires multiple sources of material to form the hyaloclastite. A piece of hyaloclastite from Section 327-U1362A-13R-1 (Subunit 5A, pillow basalt) contains a wide variety of alteration features, including altered chilled margins, black alteration halos, and large iron oxyhydroxide veins with multilayered halos.

A second example of breccia in Hole U1362A is a tectonic breccia vein in Subunit 4A (Section 327-U1362A-9R-2 [Piece 10, 74–87 cm]), interpreted to represent a cataclastic zone. This cataclastic zone forms approximately half of Piece 10, oriented diagonally through the piece (Fig. **F14**). A 2–3 mm dark green vein of saponite and pulverized basalt marks the edge of the cataclastic zone, with subparallel saponite veins and adjacent green-brown alteration halos. The alteration of the host basalt (background and halos) is consistent with the alteration both within Section 327-U1362A-9R-2 and the remainder of the subunit. All of the clasts show <0.1 mm light to dark brown alteration along their edges. The matrix in this breccia is dark green and in thin section appears to be predominantly pulverized hydrothermally altered host rock with no evidence of later cementation by secondary phases.

Glass

Volcanic glass is a common feature throughout the hole and is predominantly found within the pillow lava units on chilled margins. Glassy chilled margins vary from <1 mm to several centimeters and are altered to varying degrees. Of the 61 chilled margins recovered, some have retained fresh glass in addition to replacement by secondary phases (palagonite and saponite), whereas others are completely replaced by saponite. In examples where the alteration of glassy chilled margins is not complete, hydrothermal veins are commonly observed crossing through and along the margin. Compositionally, these veins include both green and pale blue saponite and carbonate. Continuation of these veins into the pillow core perpendicular to the chilled margin was also observed, indicating that the same hydrothermal fluids moved through the pillow core and margin. In thin section, volcanic glass is amber in color and contains microlites of plagioclase and clinopyroxene, multiple subparallel and crosscutting microveins, and aggregates of opaque microcrystals emanating from nuclei. Volcanic glass recovered within the sheet flow and basalt flow units has a similar range of features and differs only in abundance and absence of the characteristic radial cooling cracks observed in the pillow lava examples.

Vesicle filling

Most units from Hole U1362A are sparsely to moderately vesicular, containing 0.1–9.0 mm diameter vesicles. The majority of vesicles are partially to completely filled with one or more secondary minerals, and those observed in thin section are generally filled with >50% secondary phases. Secondary minerals present within vesicles include saponite (pale green, pale brown, or pale blue), celadonite, iron oxyhydroxides, carbonate, unspecified clay, and pyrite. Saponite and iron oxyhydroxides are the most common secondary minerals, and either or both occur in every unit. On both unit and piece scales the variability of vesicle-filling minerals is high, with a typical assemblage for a unit containing seven or more different secondary minerals (Fig. **F15**). The mineralogy and order of filling within the vesicles can be used as a record of changes in fluid chemistry and can be combined with crosscutting vein relationships to document the order of secondary mineral formation. Hand specimen observations of sequential relationships from Hole U1362A vesicles include the following:

- Saponite lining with cores of
  - Iron oxyhydroxides
  - Pyrite
  - Pale green clay
  - Carbonate
  - Celadonite
  - Mixed brown and white (clay + carbonate?)
- Iron oxyhydroxide lining with cores of
  - Saponite
  - Celadonite
  - Pale green clay
- Celadonite lining with cores of
  - Saponite
  - Iron oxyhydroxides

The overlap between saponite, iron oxyhydroxides, and celadonite as lining and filling vesicles (e.g., saponite with celadonite core and celadonite with saponite core) indicates continual evolution of secondary mineral formation. Conclusive relationships can only be made for carbonate and pyrite, which must form later because they are always present within the cores of previously lined vesicles or as monomineralic vesicles.

The continual evolution of the early secondary minerals is highlighted in thin section, where concentrically multilayered vesicles are evident. Figure **F16** shows a multilayered vesicle with bright green celadonite lining and subsequent filling of mixed celadonite with saponite, resulting in varied shades of green.

When vesicles are present within alteration halos the composition of the halo strongly influences the secondary minerals that fill the vesicles. For example, vesicle fill is dominated by iron oxyhydroxides in orange-brown halos.

Veins

A total of 1230 hydrothermal veins were identified and logged in Hole U1362A, with an average frequency of 27 veins per meter of recovered core (see VEINLOG in **"Supplementary material"**). Vein thickness varies from <0.1 to 4.0 mm, and veins recovered include planar, straight, curved, branched, crosscutting, stepped, kinked, and irregular shapes. More than 75% of the veins are <0.1 mm in width. The most prevalent vein mineralogy is saponite, which is present in at least 76% of veins. Clay minerals too fine grained to identify occur in 50% of the total veins (Fig. **F17**). The next most abundant vein mineral is iron oxyhydroxides, with 392 occurrences (32%). Carbonate was identified in 119 veins (~10%) but is present as the main component (>50% abundance) in only 34 of these veins. Pyrite is present in 107 veins and only rarely by itself (7 monomineralic pyrite veins). Celadonite is present in 21 veins (~2%) and is, overall, much more prevalent in the background alteration. Anhydrite is present in at least 2 veins. Of the recovered veins, 40% occur as monomineralic veins, with the remaining 60% of veins filled with two or more secondary minerals. Alteration halos directly associated with an adjacent vein are present in only ~15% of the observed veins (see **"Alteration halos"**).

Multilayered veins can be used to determine the sequence in which secondary minerals formed. In Hole U1362A layered veins are a common feature, and saponite generally forms the outermost lining. Vein core compositions include iron oxyhydroxides, carbonate, and celadonite, although iron oxyhydroxides are also present in the outermost layers in some examples (Fig. **F18**). Crosscutting relationships between different generations of veins were identified in 11 intervals.

Carbonate veins are the fourth most abundant in Hole U1362A, although they predominantly occur with carbonate as a minor phase. Carbonate is commonly found within the altered chilled margins and is mixed with pale green clays. When carbonate is the dominant mineral, it occurs with saponite and pyrite as accessory minerals. An anhydrite vein was identified in one thin section from Sample 327-U1362A-18R-2, 100–102 cm (Fig. **F19**), and on the basis of this calibration at least one other vein was also identified, also in Core 18R. Anhydrite is present as a white vein with good crystal structure and is as-

sociated with saponite as a lining. In addition to pyrite within veins, chalcopyrite was tentatively identified on two exposed vein surfaces.

Alteration halos

In addition to the generally pale to dark gray background alteration exhibited in the basalt of Hole U1362A, alteration halos are also a prevalent feature throughout the hole. The halos are either adjacent to hydrothermal veins, bordering individual rock pieces, or are not visibly associated with any defining hydrothermal or structural feature. Alteration halos flanking veins (15% of the total veins) vary from 0.2 to >35 mm wide and are associated with both monomineralic veins (saponite, clay, and iron oxyhydroxides) and polymineralic veins (celadonite, carbonate, sulfides, and talc). In two places alteration halos are present around predominantly carbonate veins (>50% carbonate).

Classification of halos was based on the color of the halo. When more than one color is present the halo was described as mixed. The dominant single-color halo is dark gray and ranges from 1 to 20 mm in width (Fig. **F20**). Compositionally, these halos represent the alteration of mesostasis and groundmass with comparatively more intense replacement and overprinting by saponite than pervasive background alteration. Additional secondary minerals that may or may not also be present within halo alteration zones include celadonite and unidentified oxides. The distribution of secondary minerals within the halos is similar to the background alteration and replaces mesostasis and phenocrysts. Orange halos are also reasonably abundant and mineralogically represent host rock extensively replaced by iron oxyhydroxides. The dark green halos are the rarest of the single-color halos and are a mix of saponite and celadonite (Fig. **F21**).

Mixed halos are the most abundant halo type and form a wide range of multilayered and patchy halos. We frequently observed orange alteration spots within the dark gray halos where iron oxyhydroxides replaced vesicles and phenocrysts (Fig. **F22**). Orange alteration spots also occur in the dark green and pale gray halos. Distinct bands of colors can be clearly seen in hand specimen in multilayered halos. Color combinations in this type of halo include dark gray and pale gray; pale gray, orange, and dark gray; orange and dark gray; dark gray and pale brown; dark green and light green; dark gray, dark green, and light green; and dark green, orange, pale brown, and dark gray (Fig. **F23**). Mixed halos occur flanking veins and occasionally as piece borders and are the only type where no visible association with veins/structures is present (Fig. **F24**). The nonassociated halos are several centimeters wide, are generally larger than vein-flanking halos, and are abundant within Sections 327-U1362A-9R-1 and 11R-2. The range of colors in the layered halos represents changes in the dominant secondary minerals present. Those with green color contain celadonite, whereas orange-brown halos contain iron oxyhydroxides.

Alteration summary

Low-temperature (<100°C) hydrothermal alteration of basalt from the ocean crust has been documented in numerous boreholes (e.g., ODP Holes 504B and 1256D) and is generally described in terms of two components: open circulation of seawater causing oxidative alteration and restricted circulation causing nonoxidative alteration (Laverne et al., 1996; Teagle et al., 1996; Teagle, Alt, Umino, Miyashita, Banerjee, Wilson, and the Expedition 309/312 Scientists, 2006). Each of these alteration styles can be associated with the formation of different secondary minerals; iron oxyhydroxides and celadonite are typical of oxidative alteration, whereas saponite and sulfides are indicative of nonoxidative alteration.

The range of secondary minerals present in Hole U1362A is consistent with hydrothermal alteration in both oxidative and nonoxidative environments. The extent of hydrothermal alteration is variable on a unit-by-unit scale, but overall comparison of the three types of units identifies a few differences. For example, pillow lava has the same range in total alteration as the sheet flows. However, detailed observations of thin sections demonstrate that the pillow lava is predominantly highly altered, whereas the sheet and basalt flows are moderately altered. Vein density clearly differs by unit type, with ~32–37 veins per meter of recovered core in the basalt flow and pillow lava units and ~17 veins per meter of recovered core in the sheet flows. There are no clear correlations between secondary mineral occurrence in veins and the different unit lithologies, although variations exist. For example, sulfide veins are more prevalent in the lower units (Subunit 5B to Unit 8), and celadonite does not appear deeper than Subunit 6B. It is difficult to reconcile the vein mineral assemblages in each unit to define dominance of oxidative or nonoxidative alteration.

In addition to secondary minerals characteristic of typical hydrothermal alteration of upper oceanic basement, Hole U1362A also contains some secondary minerals that indicate more complex hydrothermal processes. The recovery of epidote at the sediment/basalt interface is unusual. Epidote is a greenschist facies mineral generally associated with high-temperature hydrothermal alteration and has

been recovered from in situ ocean crust in only a few locations (e.g., Holes 1256D [Teagle, Alt, Umino, Miyashita, Banerjee, Wilson, and the Expedition 309/312 Scientists, 2006] and 894G [Shipboard Scientific Party, 1993] and the Tonga forearc [Banerjee et al., 2000]). Epidote has been linked to upflowing hydrothermal fluids in ophiolite studies. The presence of anhydrite veins in Hole U1362A is a new discovery from Juan de Fuca Ridge-flank drilling. Anhydrite has been found in other upper crustal sites and can be related to mixing of hydrothermal fluids and seawater. The occurrence of epidote with pyrite at the seafloor, combined with anhydrite at depth, may indicate that Hole U1362A was formally a location of hydrothermal upflow.

Hard rock geochemistry

Thirty-one representative samples of igneous rocks were analyzed for major and trace elements using a Teledyne-Leeman (model Prodigy) Inductively Coupled Plasma–Atomic Emission Spectrometer (ICP-AES). Sample selection for ICP-AES analysis was targeted toward the freshest material from Hole U1362A in order to obtain a downhole record of primary magmatic compositions. The methods of preparing and analyzing the samples are described in detail in **"Petrology, hard rock geochemistry, and structural geology"** in the "Methods" chapter. The international standard BCR-2 was analyzed nine times over three runs and indicates that the analytical precision was <3% for major elements and <10% for trace elements.

The major and trace element data for the 31 selected samples is shown in Table **T7.** Loss on ignition (LOI) values and calculated Mg number (Mg#) of the samples are also included in the table. All of the samples are characterized as N-MORB. The good linear correlation between TiO_2 (weight percent) and Zr (parts per million) for all 31 samples indicates that the different basalt units of Hole U1362A originated from a similar, if not the same, source (Fig. **F25**).

The samples are grouped into three unit types: basalt flow, pillow, and sheet flow. Plots of major and trace element abundance versus Mg# of the three unit types are shown in Figures **F26** and **F27.** Generally, the samples do not show significant correlations between major or trace elements and Mg#; however, some trends can be distinguished for the different unit types. For example, for all unit types MnO decreases with increasing Mg#. Similarly, for basalt flow and sheet flow units, Na_2O, TiO_2, P_2O_5, Sc, V, and Zr are positively correlated with Mg#.

The variations of major and trace elements and Mg# with depth are shown in Figure **F28.** Although there are some fluctuations, Fe_2O_3 shows a weak increasing trend with depth, MgO slightly decreases, and Mg# decreases. Cu decreases with depth, and Cr decreases with excursions at Unit 5 (pillow lava) and Unit 7 (basalt flow). The vertical variations of TiO_2, V, and Zr are consistent with the rock type; usually the contents from pillow lava samples (Units 1 and 5) are lower than those from basalt flows (Units 2 and 7) and sheet flows (Units 4, 6, and 8).

Structural geology

Basalt from Hole U1362A documents a range of structural features related to different processes. These include fractures formed during eruption, such as the radial cooling cracks of pillow lava; hydrothermal alteration preserved as veins; later tectonic fractures such as any planar features and cataclastic zones; and fractures induced by coring.

The dips of 519 veins and fractures were measured in the recovered cores from Hole U1362A. Three types of veins and fractures were distinguished in the cores: (1) veins flanked by alteration halos (termed "haloed veins"), (2) veins not flanked by alteration halos but filled with secondary minerals (termed "nonhaloed veins"), and (3) joints sometimes flanked by alteration halos but not filled with minerals. Nonhaloed veins were the most frequently observed structures in rocks from Hole U1362A. Nonhaloed veins were identified mainly in the massive lava and some pillow lava pieces. No clear faults or shear veins showing any evidence of displacement were found.

Figure **F29** shows the distribution of measured fracture and vein dips and indicates an overall progressive increase in frequency with increasing dip angle. More than 50% of the measured veins form slight trimodal peaks identified at 40°–50°, 65°–75°, and 80°–90°. Fractures and veins are not uniformly distributed but occur more frequently in the pillow lava units relative to the massive lava units (Fig. **F30**). The deeper pillow lava and massive units (e.g., Units 5 and 6) have similar distributions of vein and fracture dips. However, these similarities may be artifacts of the uneven number of samples in each unit. Histograms of vein/fracture dip for haloed structures compared to those of nonhaloed veins (Fig. **F31**) show that haloed and nonhaloed features have different structural characteristics. Haloed fractures are predominantly steeply dipping, with frequency increasing with dip angle. Nonhaloed veins have peaks at 20°–30°, 40°–45°, 50°–55°, 60°–70°, and 80°–90°. For massive lava, the expected sampling bias during coring is toward horizontal structures that are more likely to be intersected by a vertical hole. The observed predominance of steeply dipping haloed

veins is therefore interpreted to reflect the actual distribution of fracture dips in the basement at Site U1362. Recovery was very high in Core 327-U1362A-18R, where a near-continuous sheet flow was recovered. This whole-round core was imaged multiple times, and the images were stitched together to produce a continuous image of the core exterior (see CORE18R in **"Supplementary material"**; Fig. **F32**).

The cataclastic zone recovered in Subunit 4A (Section 327-U1362A-9R-2 [Piece 10, 74–87 cm]), was classified as tectonic breccia because the matrix is composed of ground up basalt. This cataclastic zone forms approximately half of Piece 10, oriented diagonally through the piece (Fig. **F14**). The cataclastic zone is up to 28 mm long and is composed of subangular pieces of fine-grained host rock as large as 18 mm that were fractured in situ perpendicular to the vein orientation. Open spaces of 1–2 mm are present between the larger clasts, but generally the cataclastic zone is fully consolidated with matrix and clasts. Smaller clasts are also present and exhibit varying degrees of clast rotation and separation. The good fit between adjacent clasts, the examples of clast rotation of the smaller clasts, and the composition of the matrix are evidence for classifying this as a tectonic breccia. The steep angle and presence of alteration halos suggest this feature formed at a similar time as the vertical cracks with alteration halos.

Hand specimen observations support the following sequence of structure formation in rocks from Hole U1362A:

1. Formation of radial cooling cracks perpendicular to pillow margins;
2. Formation of vertical cracks and cataclastic zones with associated hydrothermal alteration halos during normal faulting near the ridge axis;
3. Development of younger fractures without halos; and
4. Formation of planar fractures in massive lava by tectonic stress.

The observed dominance of vertical extensional-related structures is consistent with the location of Site U1362 on an abyssal, normal-faulted basement high.

Microbiology

Microbiological hard rock samples were collected from almost every RCB-cored interval of Hole U1362A, as well as from one bit sample from the sediment/basalt interface cored in Hole U1362B. Roughly 5% of the hard rock core that was recovered from Hole U1362A was taken as whole-round samples from the core splitting room and dedicated to microbiological analysis. The 25 hard rock microbiology samples span a range of lithologic units, alteration states, and chilled margin presences, and most contain at least one vein or fracture. Photographs of the samples are available in MICROBIO in **"Supplementary material."** Shipboard scientists attempted to prepare total cell counts of rock samples fixed in formaldehyde solution and stained with either acridine orange or SYBR Green I DNA stains; however, a lack of antibleaching immersion oil during the expedition prevented stable cell-fluorescence signals and precluded accurate cell-count measurements.

Microspheres were used during all coring operations to help in evaluating core contamination. Microsphere density was evaluated in all samples, generally both before and after the outer surfaces of rocks were flame sterilized prior to being split. Contamination checks (Table **T8**) indicate that microsphere density tends to be high in exterior alteration crusts and within glassy margins, whereas interior rock sections generally have no or low microsphere densities. Additionally, a few recovered plastic bags that held the fluorescent microsphere solutions in the core catcher were collected for contamination checks during shore-based DNA analysis.

Physical properties

Physical property measurements in the basement section of Hole U1362A included whole-round magnetic susceptibility, density, and natural gamma radiation (NGR) emissions measured on every section greater than 50 cm in length; section-half measurements of magnetic susceptibility; and discrete measurements of thermal conductivity, *P*-wave velocity, and moisture and density (MAD) properties (e.g., bulk density, grain density, and porosity) (Figs. **F33, F34;** Table **T9**). Sampling frequency for discrete samples was generally two per section, with extra samples collected where there were visibly significant changes in lithology, alteration, or texture.

Magnetic susceptibility

Whole sections were run through the WRMSL after the core liner was split, with sampling resolution set at 1 cm regardless of section continuity. No effort was made to correct for incomplete filling of the core liner or for discontinuous rock characteristic of this formation or to correct for voids caused by the removal of whole-round sections for microbiological analysis. Magnetic susceptibility is as high as ~3300 × 10^{-6} SI, with the highest values corresponding to massive lava flows recovered in Cores 327-U1362A-17R and 18R at 458 and 463 mbsf, respectively (Fig. **F34C**). Other lithologies (pillow lava and

sheet flows) generally yield values of <1500 × 10^{-6} SI, partly because of highly fractured layers and poor core recovery, both of which reduce magnetic susceptibility.

After sections were split, archive halves were run through the Section Half Multisensor Logger (SHMSL). Point measurements were made at 1 cm intervals. Magnetic susceptibility trends determined through this method are similar to those obtained from the WRMSL; however, the discontinuous nature of the core sections is more apparent in these data (Fig. F34C). Point susceptibility rarely exceeds 1500 × 10^{-6} SI in pillow lava (Unit 3 and Subunits 1A, 1B, 5A, and 5B). Thin sheet flows (Unit 2 and Subunits 7A and 7B) yield similar values, with occasional isolated excursions to higher values in larger pieces. Massive flows (Subunits 6A and 6B) with high recovery, mainly Cores 327-U1362A-17R and 18R, have the highest point susceptibility values, often exceeding 3000 × 10^{-6} SI (Fig. F34C). Among cores with large continuous pieces (Cores 327-U1362A-12R and 16R), point susceptibility values often vary widely from those determined by the WRMSL, sometimes by as much as 500 × 10^{-6} SI. It may be possible to use the point susceptibility records as a filter for the WRMSL susceptibility data; however, no attempt was made to do so during this expedition.

Gamma ray attenuation density

The bulk density of the core is estimated by GRA measured on the WRMSL. Density results differ by as much as 15% between GRA and MAD property samples, with GRA results typically providing a lower bound on true values. In general, the data remain fairly consistent at ~2.5 g/cm^3, dropping only when poor recovery creates gaps that interfere with measurements (Fig. F34A).

Natural gamma radiation

The integrated counts per second (cps) detected by the NGRL serves as a rough estimate of the variability of radioactive elements in the cores. NGRL data are fairly constant with depth (~2–4 cps), typically peaking only in massive lava flow sections where core was more likely to fill core liners (Cores 327-U1362A-17R and 18R, in particular) (Fig. F34D).

An initial attempt was made to correlate integrated NGRL counts with degree of alteration, but no significant correlation was identified. A more detailed analysis making use of the full spectra collected by the NGRL may yield more information regarding relative abundances of radioisotopes.

Thermal conductivity

Thirty individual measurements were made on three basalt samples over the interval of 349–355 mbsf (Fig. F35; Table T9), with samples being chosen on the basis of size, continuity, and the absence of fractures or veins. A minimum length of 8 cm was required to achieve full contact between the sample and the thermal conductivity probe. Although we planned for a much more extensive testing program, only three samples produced reliable data because of the inconsistent performance of the thermal conductivity system, which gave wildly variable (and often unreasonably low or high) values and often would not get beyond the preheating "drift" stage of testing. Some of the difficulty was eventually traced to a corroded connector embedded in the half-space puck, but the acquisition and processing software also contributed to these problems.

The three samples that yielded thermal conductivity data came from the uppermost section of pillow basalt, providing values of 1.63, 1.67, and 1.72 W/(m·K) at depths of 349, 354, and 355 mbsf, respectively. These values compare well with data collected at similar depths into basement in nearby Hole U1301B (1.70 ± 0.09 W/[m·K]) (Fig. F35).

P-wave velocity

Seventy-three discrete samples were collected for measurement of *P*-wave velocity. The samples were carefully cut and polished in order to ensure good contact between the sample and transducers. Forty-five samples were cut from oriented pieces as 2 cm × 2 cm × 2 cm cubes, allowing two horizontal velocities (*x*- and *y*-axes) to be measured in addition to vertical velocity (*z*-axis). From unoriented pieces we extracted cylinder-shaped samples, allowing *P*-wave velocity measurement in one direction. We were unable to measure *P*-wave velocities on 3 cylindrical samples because they cracked or split after extraction, but measurements were made on the remaining 70 samples.

We checked the velocity of the calibration standards after every measurement on saturated samples because the Gantry transducer pairs were unstable, as described in "Physical properties" in the "Methods" chapter. If the calibration value was not within tolerances (2.75 ± 0.25 km/s), we calibrated repeatedly until the values converged. In addition, we measured velocities four times on each axis by rotating in 90° increments and averaging the results. After we finished the overall velocity measurements we remeasured velocities for selected samples. We found that even though we frequently calibrated the measurement device the second set of velocities of-

ten differed from the first set. We decided to resaturate and remeasure all samples with a manual picking method (see "Physical properties" in the "Methods" chapter) in order to check the validity of the velocity data measured with the automated method. We also calculated *P*-wave velocities in dry conditions using both methods.

P-wave velocities of saturated samples measured with the automated method range from a minimum of 4.8 km/s to a maximum of 6.3 km/s, with an average of ~5.6 km/s. *P*-wave velocities of saturated samples determined by manual picking range from a minimum of 4.5 km/s to a maximum of 6.0 km/s, with an average of ~5.45 km/s (Fig. F33). Although calculating *P*-wave velocities determined by manually picking the first arrival were slower than those determined using the automatic picking method, the overall velocity trends derived from the two methods are consistent. Both averages are greater than the values obtained from similar core samples in Holes 1026B, 1027C, and U1301B (Shipboard Scientific Party, 1997; Expedition 301 Scientists, 2005). Furthermore, the average values are faster than regional values determined using seismic reflection techniques (Rohr, 1994) and vertical seismic profile (VSP) experiments (Expedition 301 Scientists, 2005). One might expect regional and VSP values to be slower because of large-scale fractures. The *P*-wave velocities measured in saturated conditions are ~200 m/s faster than those in dry conditions because the rock elastic bulk modulus usually stiffens when air in dry pores is replaced with less compressible seawater.

The lowest velocity (~4.5 km/s) was measured on a heavily altered sample (327-U1362A-14R-1, 8–10 cm). A test of nearby unaltered material yielded much higher velocity, which demonstrates the influence of rock alteration on *P*-wave velocity. The lithology difference (i.e., margin part of pillow, central part of pillow, basalt flow, and sheet flow) generates the local velocity variation. However, we found no statistically significant overall velocity trend with depth or overall velocity anisotropy.

Moisture and density

The same 73 discrete samples collected from Hole U1362A for *P*-wave velocity measurements were used in the determination of MAD properties, including cubic samples and cylindrical samples. Because we had doubts about the vacuum pump saturating samples completely, we measured the wet and dry mass of all samples twice.

Bulk density values range from 2.20 to 2.90 g/cm^3 (mean = ~2.7 g/cm^3). Grain density exhibits a range of 2.41–3.00 g/cm^3 (mean = ~2.9 g/cm^3) (Fig. F34). Porosity values span a range of 2.8%–15.0% (mean = 7.9%) (Fig. F33). The highest porosity value was from a highly altered sample that also had the lowest *P*-wave velocity. This implies that high porosity may be a proxy for increasing rock alteration. The data clearly show *P*-wave velocity and porosity to be inversely correlated (Fig. F36), which may be influenced by several factors: primary porosity, sample cracking, rock alteration, or core disturbance. Although the velocities in Hole U1362A are higher than those in Hole U1301B, the slope of the velocity-porosity relationship is similar (Expedition 301 Scientists, 2005). Because the velocities for constant porosity are significantly influenced by pore geometry as well as crack aspect ratio (Wilkens et al., 1991; Tsuji and Iturrino, 2008), the microcrack geometry in Hole U1362A appears to be similar to that of samples from Hole U1301B.

Paleomagnetism

Hole U1362A was cored with the RCB, resulting in generally small, often unoriented pieces. Measurements were made on 79 discrete pieces that were <10 cm long and on portions of 23 core sections having pieces that were >10 cm long. When measured sections contained several pieces, the data were filtered to exclude 5 cm intervals at the ends of pieces. In addition, the volume of the archive-half pieces was variable (70–210 cm^3 for individual pieces). Although irregular pieces are not often used in paleomagnetic studies, we considered these measurements worth pursuing because recovery was low and the working half was reserved for petrology, geochemistry, and physical property sampling.

Samples were demagnetized at 5 or 10 mT steps from 0 to 50 mT using the cryogenic magnetometer's in-line AF coils. The remanent magnetization direction of selected samples was determined by plotting orthogonal vector plots of demagnetization steps and using principal component analysis (Kirschvink, 1980). Intensity values range from 0.18 to 14.27 A/m (Table T10). Demagnetization results show that some samples have a steep, downward-directed overprint that is usually attributed to the isothermal remanent magnetization imparted during coring (Acton et al., 2002). This remagnetization probably affects samples with low-coercivity magnetic grains and is usually removed in the first few demagnetization steps.

Overall, our results are consistent with previous paleomagnetic investigations conducted during Expedition 301 (Expedition 301 Scientists, 2005). Most inclinations are positive (Table T10), indicating that the ocean crust formed during a normal polarity in-

terval, consistent with the 3.5 m.y. age of the Juan de Fuca plate at this location (see Fig. F11 in the "Methods" chapter). Most samples display simple magnetization behavior, with downward-directed inclinations and univectorial decay to the origin, indicating that this vector represents the characteristic remanent magnetization (ChRM) (Fig. F37). Some samples have steep downward-directed inclinations possibly influenced by an overprint imparted by the drill string (Fig. F37B). Very few samples have upward-directed inclinations (Fig. F37D). Negative inclinations cannot be entirely explained by accidentally flipping discrete samples because negative inclinations are seen for both discrete and continuous section measurements.

A more likely explanation is that these negative inclinations may represent a remagnetization of the ocean crust that occurred at a later time. Remagnetization can occur when heating or chemical changes alter the magnetic minerals in crustal basalt. Typically, the new magnetization has the same direction as the old as long as the remagnetization occurs within the same magnetic chron. Reversed magnetization could be imparted, however, if the magnetic mineral replacement occurred during a later period of time with the opposite magnetic polarity. During hydrothermal alteration, magnetic minerals such as magnetite are converted into iron sulfide minerals (Thompson and Oldfield, 1986). This is consistent with petrological and geochemical investigations in Hole U1362A that show abundant evidence of hydrothermal alteration (see **"Petrology, hard rock geochemistry, and structural geology"**), including the presence of iron sulfide minerals. A plot of intensity and inclination values versus depth shows a distinct zone of scattered inclinations around 460–470 mbsf in Unit 6 (Fig. F38). This interval corresponds to a zone with a higher frequency of veins (Fig. F30). The Hole U1301B interval that corresponds to the same depth has similarly scattered inclinations (Expedition 301 Scientists, 2005).

Downhole measurements

A wireline logging string was deployed in Hole U1362A to determine the physical and hydrological properties of upper basement rocks and to identify suitable intervals for packer placement. The logging string consisted of tools with sensors for measuring natural spectral gamma ray, bulk density, borehole fluid temperature, borehole orientation, tool motion, ultrasonic images, and hole diameter, as well as a qualitative spontaneous potential (SP). Two passes were run over the entire open hole, and a third pass was run over two intervals of particular interest.

Calipers revealed a borehole that was highly enlarged over most of the open hole section, as expected, although two notable near-gauge sections were identified as suitable packer locations.

The ultrasonic borehole images are marred by rotational and heave-induced stick-slip tool motion, and the density measurement suffered from the enlarged borehole. Where the hole condition was good, logged density compares favorably with laboratory tests of core samples from the same depths.

Some elevated gamma ray values correspond loosely with an enlarged borehole. These zones could represent areas of greater alteration and may be indicative of past hydrothermal fluid flow. However, in other intervals gamma ray values and borehole size are inversely related.

Borehole fluid temperature data were acquired while running into the hole and during the uphole logging passes. The borehole temperature gradient increases steeply at the top of the primary in-gauge interval, and a temperature anomaly was observed near the casing shoe.

Logging tool string

The 26.4 m long wireline tool string consisted (from the top down) of the logging equipment head (LEH), which contained an electrode for generating a qualitative SP curve; the Hostile Environment Natural Gamma Ray Sonde (HNGS); the Hostile Environment Litho-Density Sonde (HLDS); the Modular Temperature Tool (MTT); the General Purpose Inclinometry Tool (GPIT); and the Ultrasonic Borehole Imager (UBI). For a description of these tools, see **"Downhole measurements"** in the "Methods" chapter.

Operations

After drilling the 9⅞ inch open hole section to a total depth of 528 mbsf, the hole was cleaned and left full of seawater. After the packer BHA was made up, the drill string was run to 264 mbsf, roughly 44.5 m above the 10¾ inch casing shoe.

The wireline tool string was rigged up and run out of the drill pipe and into the 10¾ inch casing, where it was held still while the wireline heave compensator (WHC) was started. Surface heave, as measured by accelerometers near the moonpool, was observed to be ~0.9 m peak-to-trough. Downhole tool motion, as measured by the accelerometers in the wireline string, was ~180% of surface motion both before and after the WHC was started.

The wireline string was lowered into the open hole and, to avoid damaging the sensitive UBI sensor head at the bottom of the tool string, was stopped at

507 mbsf (5 m above the last known bottom fill). Borehole fluid acoustic velocity (for UBI tool calibration) and temperature were logged during the descent.

A first pass was run at 600 ft/h using low-resolution UBI settings (250 kHz, 1.0 inch vertical resolution, and 140 samples per rotation) in an attempt to acquire usable, adequate data over as much of the open hole interval as possible. We expected a small (<13 inch diameter) hole over only a few intervals, particularly across the 453.8–472 mbsf section identified via core recovery, quality, and rate of penetration. The first pass confirmed a near-gauge hole section near 447 mbsf and another near 417 mbsf. The HLDS mechanical caliper—but not the UBI ultrasonic caliper—resolved an undergauge (7.8 inch diameter) interval between 364 and 374 mbsf.

After logging up into the casing shoe, we ran back to total depth in order to conduct a second medium-resolution pass (UBI settings of 250 kHz, 0.4 inch vertical resolution, and 180 samples per rotation). We logged at 400 ft/h over the best hole section and then sped up to 800 ft/h at 414 mbsf, above which the hole was too enlarged to obtain a meaningful UBI image. We observed no diagnostic fluctuation in cable or head tension as we passed up or down through the undergauge interval identified in the first pass. Once again, the UBI caliper did not resolve the undergauge section, but the HLDS caliper saw an even tighter (5.5 inch diameter) interval, only this time it appeared to be at 376 mbsf and only 3 m thick.

After completing the second pass into casing, the tool string was run back to total depth to conduct a final high-resolution pass (UBI settings of 500 kHz, 0.2 inch vertical resolution, and 180 samples per rotation) over the good hole interval. We ran up at 400 ft/h until we passed the good hole section at 447 mbsf and then pulled up rapidly (2000 ft/h) to log the apparent tight zone. At this point the Schlumberger logging engineer experimented with the logging configuration in the hope of acquiring an accurate ultrasonic caliper over the apparent tight spot. After that reconfiguration, the UBI images became noisy and speckled, so the original settings were restored at 388 m wireline log depth below seafloor (WSF). On this third pass over the suspected tight section, the HLDS caliper saw only hole with >12 inch diameter.

The logging and operations team decided to log a fourth caliper pass through the possible tight hole interval. Just before starting the pass with the caliper extended, the winch operator lowered the tool string slightly to fix a spooling problem on the winch. Head tension dropped as the HLDS caliper took some of the tool string weight. After pulling up on the string, the Schlumberger engineer was unable to close the mechanical caliper. The caliper continued to read hole diameter, and after a brief troubleshooting period we decided to continue to log up into casing. For the rest of the pass, the caliper did not extend beyond ~14 inches, nor did it register a hole restriction at the troublesome interval. The tool string entered the casing shoe and pipe without incident. Because of the damaged caliper, the planned WHC testing period was canceled, and the tool string was pulled to the surface to complete logging operations.

Data processing

Wireline logging data were acquired by the Schlumberger acquisition system and archived in digital log interchange standard (DLIS) format. Immediately after logging, field prints of the three logging passes were generated and delivered to the operations and science teams for packer-seat identification. Simultaneously, data were transferred via satellite to the Borehole Research Group at the Lamont-Doherty Earth Observatory. There, the data were processed and transferred back to the ship for distribution and archiving in the shipboard log database. Processing details can be found in **"Downhole measurements"** in the "Methods" chapter, as well as in the processing notes found with the data in the IODP US Implementing Organization (USIO) log database.

Depth shifting

Because the principal operational objective of logging was to identify packer intervals, we used the 10¾ inch casing shoe (identified by caliper and by a step in gamma ray values) as a depth reference, rather than the seafloor (identified on the downlog by an ambiguous gamma ray response). The downlog gamma ray identified the seafloor at either 2672 or 2675 m, and the shift to the casing shoe had the effect of placing the seafloor depth at 2675.5 m. The first and third logging passes and the downlog were shifted to match the reference from the second pass, resulting in the wireline log matched depth below seafloor (WMSF) scale.

Data quality

With the exception of the HLDS caliper, measurements for all tools were highly repeatable over the notable interval described above.

An enlarged borehole over most of the open hole section affected the density measurements, which require eccentralization and good contact with the borehole wall. Similarly, the ultrasonic images and

caliper are only usable in the narrowest (less than ~13 inch) hole sections. Because wireline tools must be conveyed through drill pipe, an undersized UBI sonde head was used; the 3.56 inch OD sonde head was designed to run in holes ≤7⅝ inches. The gamma ray, temperature, and borehole orientation measurements are relatively unaffected by hole size, and it does not appear that borehole size has much influence on the SP curve.

The UBI images were severely affected by downhole tool motion despite the use of the WHC. Surface heave throughout the logging passes averaged 0.8 m peak-to-trough, with frequent excursions of >1.1 m. When logging upward, the apparent downhole heave-induced motion was reduced (compared to its motion when the tool string was held at a static depth), and downhole heave displacement averaged 0.8 m, with occasional excursions of >1.5 m. The apparent reduction in downhole heave-induced motion while logging can be a result of the HLDS caliper being extended and the tool string being pulled up at a steady speed. The third logging pass used the most ambitious UBI configuration and yielded the sharpest images over the near-gauge intervals of interest.

Preliminary results

The logging string consisted of tools with sensors for measuring SP, natural spectral gamma ray, bulk density and photoelectric effect (PEF), borehole fluid temperature, tool motion, oriented ultrasonic images, and hole diameter. Selected representative log curves from the second pass are shown in Figure F39.

Spontaneous potential

SP data from the three logging passes repeat remarkably well, exhibit little noise, and appear insensitive to hole condition. The measurement deflects noticeably at the casing shoe and then trends negatively throughout most of the open hole section. Over the 417 mbsf near-gauge interval the SP curve appears to flatten, and at the 447 mbsf near-gauge interval the SP curve reverses.

Natural gamma ray

Gamma ray measurements repeat well over the three passes. In the open hole, total gamma ray values are correlated with potassium content (Fig. F40). Values range between 2.1 and 7.4 API units, which is typical of basaltic oceanic crust (Bartetzko et al., 2001).

In a few intervals, like the one starting at 470 mbsf, an increase in gamma ray values corresponds with an increase in borehole size; intervals like these can represent zones of greater alteration and may be indicative of focused hydrothermal fluid flow through more fractured rock (Bartetzko et al., 2001; Fisher, Urabe, Klaus, and the Expedition 301 Scientists, 2005; Expedition 324 Scientists, 2010). Supporting this hypothesis, shipboard ICP-AES analyses of K_2O appear to correlate well with the HLDS caliper and with HNGS-determined potassium concentration (Fig. F41). On further inspection, however, HNGS potassium and HLDS caliper measurements correlate inversely (Fig. F42) over the bulk of the 9⅞ inch open hole section, suggesting that the apparent K_2O correlation is an artifact of sparse core sampling and the contribution from the near-gauge hole interval at 455 mbsf. Enlarged borehole size may be the primary cause of the apparent reduction in HNGS potassium concentration because of insufficient correction for borehole size during processing.

The HNGS total gamma ray curve does not correlate well with shipboard NGR analyses, the latter being both sparse and erratic (Fig. F43). The shipboard NGRL probably underestimates NGR when core samples are short and irregular in shape. For that reason, NGR measurements are highest for intact cores taken from the near-gauge hole interval starting at ~455 mbsf.

A pronounced increase in HNGS gamma ray values was observed at the casing shoe (Fig. F39), most likely indicating the presence of cement. According to the gamma ray signature, the top of cement outside the 10¾ inch casing sits at 2933 mbrf, ~47 m above the casing shoe.

Density and photoelectric effect

Wireline density and PEF measurements in Hole U1362A are impaired over most of the open hole section because of the large, washed-out borehole. Low density and PEF values correspond to intervals of enlarged borehole (Fig. F39). Where the hole is near-gauge, wireline density is consistent with MAD core sample measurements (Fig. F39). Between 417 and 428 mbsf, density values average 2.59 g/cm^3 (standard deviation = 0.31), and between 447 and 472 mbsf, where hole diameter is <12 inches, they average 2.80 g/cm^3 (standard deviation = 0.15). PEF values in the same intervals average 3.21 barns/e$^-$ (standard deviation = 0.85) and 3.96 barns/e$^-$ (standard deviation = 0.73), respectively.

Temperature

Temperature data were acquired while running into the hole and during the three uphole logging passes. The data reveal a highly repeatable borehole-fluid

temperature profile (Fig. F39). The marked gradient increase at 447 mbsf may be indicative of more conductive conditions around the massive section from 447 to 472 mbsf. The return to nearly isothermal conditions at ~475 mbsf correlates with another enlarged borehole section and lower core recovery. Successive passes hint at a slight warming trend with time, although that progression might be an artifact of the different logging speeds used at different times (where faster logging speeds promote lower measured temperatures). A short temperature anomaly (a ~0.5°C rise followed by a 0.2°C drop) was observed ~8 m below the casing shoe. The gamma ray and SP curves have too much character to offer any correlation with the temperature anomaly, which occurs in the 14¾ inch rathole section of hole that is beyond the reach of the HLDS caliper.

Ultrasonic imaging

The ultrasonic borehole images are marred by both rotational and ship heave–induced stick-slip tool motion. Postlogging processing helped mitigate tool motion effects, but they are still pronounced and visible as smears and truncations (Fig. F44). Moreover, because the UBI sonde head is undersized (see **"Data quality"**), no images can be expected where the hole is even moderately out of gauge. Where the hole is near-gauge, some centimeter- to meter-scale dipping sinusoidal features are apparent. Images from the third pass, collected using the highest-resolution UBI configuration, reveal an interval of pillow basalt lying above a zone of sheet basalt at 458 mbsf.

Caliper

The wireline logging program for Hole U1362A was intended to deliver caliper data that would help identify suitable locations for the drill string and CORK packers. Before the run, certain intervals were predicted to be near-gauge on the basis of relatively high core recovery and core quality; the most likely zone was between 454 and 472 mbsf, whereas the intervals 415–430, 390–408, and 346–380 mbsf also held promise.

The three logging passes acquired data with the HLDS mechanical caliper arm, supplemented by the UBI ultrasonic caliper. The HLDS caliper identified a remarkably consistent near-gauge interval from 447 to 472 mbsf and a second, less impressive interval from 417 to 428 mbsf (Fig. F39). These two zones correlate remarkably well with those predicted by coring. The remaining two potentially near-gauge intervals were not observed. Because the HLDS caliper has a maximum reach of ~18 inches, hole size in the 14¾ inch rathole is possibly much larger.

Ultrasonic radial measurements confirmed the intervals identified with the mechanical caliper. However, the ultrasonic caliper was highly erratic and noisy, owing, perhaps, to the high degree of downhole tool motion and to the undersized sonde head. UBI caliper measurements are not valid where hole size exceeds 13 inches. Where the ultrasonic caliper maximum and minimum values appear meaningful, they indicate a nearly circular borehole through the near-gauge sections with minor-to-major axis ratios between 0.94 and 0.97. The major axis, which represents the direction of minimum horizontal stress, lies roughly north–south.

Although the HLDS caliper measurements were generally highly repeatable, an anomalous, apparently undergauge 7.7 inch diameter interval from 363.5 to 373.5 mbsf was observed during the first pass (Fig. F45). On the second pass, the apparent tight interval had only a 5.5 inch diameter and was observed between 376 and 379 mbsf, a few meters lower than before. Two new caliper spikes were observed at 359 and 413 m WMSF. A third pass of the HLDS caliper revealed no undergauge intervals.

The mechanical caliper was damaged before a planned fourth pass could take place (see **"Operations"** in "Downhole measurements"). That failure at the end of the logging deployment is unrelated to the caliper anomalies observed during the first two passes. Even after the damage—with a known failure mode and diagnostic response at the Schlumberger surface system—the caliper still saw the entry into the casing shoe and drill pipe. It did not see the undergauge anomalies, which might represent sloughing or material working its way down the hole.

The ultrasonic caliper did not record the apparent undergauge sections shown by the HLDS caliper on the first and second passes. It is possible that the obstructions, if they existed, were dislodged before the UBI crossed the interval. It is also possible, though unlikely, that the UBI was unable to resolve diameters smaller than the expected bit size. To account for this possibility, the UBI was reconfigured midway through the third pass to measure an undergauge diameter. However, the UBI image became speckled, so the tool was reset to its original configuration.

Stratigraphy

Logging units were identified on the basis of petrophysical log response and borehole condition (Fig. F39). Logging Unit I is characterized by generally poor to moderate hole conditions and fairly stable gamma ray—except for a pronounced increase at the base of the unit—and corresponds roughly with lithologic Units 1 and 2. Logging Unit I extends from 346 mbsf (the top of the 9⅞ inch hole section) to

396 mbsf, where the gamma ray signature drops steeply.

Logging Unit II covers a zone of very poor hole condition, poor density data, and relatively low gamma ray values, all having a similar profile. As with Unit I, a gamma ray high followed by a sudden drop marks the base of the unit at 417 mbsf, as does a sharp reduction in hole size. In Unit II, which loosely matches lithologic Units 3 and 4, the SP curve exhibits step changes that are more blocky than those in Unit I.

Logging Unit III spans the interval of near-gauge hole between 417 and 428 mbsf. The unit has high density in its upper half, although surprisingly low values toward its base (considering the good hole quality). The transition from high to low density values occurs at a short zone of borehole enlargement that coincides with the base of lithologic Unit 4. The SP curve does not reflect a change in potential through logging Unit III, the very top of which also features a subtle increase in borehole fluid temperature.

Rugose, enlarged borehole is the primary feature of logging Unit IV, which is correspondingly characterized by low density readings. The SP curve begins to deflect rather sharply midway through the interval, and there is a pronounced temperature inflection toward the base of the unit. The unit ends at 447 mbsf and lies entirely within lithologic Unit 5.

Logging Unit V has generally good hole conditions (and similarly improved density measurements) and features highly variable gamma ray values. In the middle of the unit, the SP curve reverses after trending negatively since the casing shoe. The base of Unit V is marked by the apparent transition from pillow lava to sheet basalt, as observed at 458 mbsf in UBI images from the third pass, which also identifies the base of lithologic Unit 5.

The thick, consistent near-gauge hole section typifies logging Unit VI, which approximately matches lithologic Unit 6. Throughout, density values are high and correspond to those determined from core sample analyses. The SP curve increases steadily, and the gamma ray signature is remarkably low in this interval. A steep jump in gamma ray values marks the base of the unit at 470 mbsf.

Logging Unit VII extends to the base of the logged hole and is characterized by a worsening (followed by a slight improvement) of hole conditions, by a steady decrease in gamma ray values, and by a flattening and then steep inflection of both SP and temperature curves.

Hydrologic experiments

Hole U1362A

In Hole U1362A the single-element drill string packer was successfully inflated in open hole to assess the transmissivity and average permeability of the isolated zone from the packer seat at 426.5 mbsf (3098.5 mbrf) to the bottom of the hole. The packer seat was chosen primarily on the basis of caliper information from the wireline log and was also intended to be the seat for the CORK open hole packers. A depth check with the packer BHA just before packer inflation found the hole open to 519 mbsf (9 m shallower than the original drilled depth). Thus, the bottom of the test interval is uncertain and estimated to be 519–528 mbsf.

A subsequent attempt to inflate the packer in casing to estimate the transmissivity of the entire open hole interval failed because of damage to the inflation element, which was evident upon recovery of the BHA and packer. This damage may have occurred during the depth check prior to the open hole inflation or during movement of the packer following the first set of tests.

The ship's mud pump was used for all packer operations. Two Micro-Smart electronic pressure gauges (SN 40060 at 5 s sample interval and SN 4986 at 10 s sample interval) were deployed in the packer go-devil, and both worked well. The record of gauge pressure and internal temperature for the SN 40060 is shown in Figure **F46.** The packer seat was originally intended to be at 424.5 mbsf. After the go-devil landed at the intended inflation depth but before the packer was inflated, hydrostatic baseline pressure was recorded for 1 h. It was difficult to inflate the packer at the intended depth, so the packer was moved 2 m deeper, where it was successfully inflated at ~1000 psi (6.9 MPa). After inflation, the sealed-hole pressure baseline was recorded for 1 h, and then two constant-rate injection tests were conducted. Under the expectation that permeabilities in the deep basement section in Hole U1362A would be comparable to those determined during Expedition 301, deep in Hole U1301B (Becker and Fisher, 2008), similar inflation rates were used: 13 and 25 spm, or 4.4 and 8.4 L/s, respectively. Injection periods were 1 h long, and each was followed by a 1 h period of pressure recovery.

The offset between the initial hydrostatic and borehole pressure readings was expected from the effects of pumping cold, dense seawater during drilling operations, inducing a near-borehole apparent underpressure even though the natural formation state is overpressured. During both injection periods, down-

hole pressures rose in a manner consistent with the predicted response, indicating a good packer seal. Initial shipboard processing of the data from the first injection period shows a good fit to the expected linear rise of pressure versus natural log of time predicted by the Theis (1935) formulation for an injection test. The slope of the log-linear response indicates a bulk permeability for the isolated zone of ~2×10^{-12} m^2, the same as the average value reported by Becker and Fisher (2008) for a comparable section of basement in nearby Hole U1301B. This preliminary result needs to be refined with more sophisticated postcruise processing. Agreement with the value from Hole U1301B is not surprising given the similarity of the logs from the two holes. If confirmed, it would be the first direct indication of consistency of a layered hydrological structure in upper oceanic crust over lateral scales of several hundred meters.

Hole U1362B

Before installing the CORK in Hole U1362B, we ran a 24 h pumping and tracer injection experiment using a 10¾ inch casing running tool in lieu of a drill string packer to seal the hole. The configuration of shipboard systems and the preparation of tracers for this experiment are discussed in detail in **Fisher, Cowen, et al.,** but a summary of operations and results is provided herein.

A depth check following hole conditioning and prior to the start of the pumping experiment indicated that there was open hole to 353.0 mbsf (111.0 msb), meaning that the pumping test would sample conditions through 81 m of upper basement. The casing running tool was made up above a stinger comprising 3 drill collars, 25 joints of drill pipe, and a specially constructed sub containing fast-sampling OsmoSamplers and pressure gauges (the same MicroSmart tools used for packer testing). The stinger was designed and spaced out to place the pressure gauges within open hole just below the shoe of the 10¾ inch casing. The OsmoSamplers were placed above the pressure gauges but were separated from them by a solid disk of steel. The fluid samplers were housed in a chamber that connected the drill pipe above to slots in the wall of the chamber. With this design, fluids pumped down the drill pipe would wash past the fluid samplers before being jetted out into the hole, where pressure was measured.

The first attempt at running the 24 h injection experiment failed when the stinger encountered fill in the hole prior to landing the casing running tool (see **"Operations"**). After the hole was cleaned out, a reconfigured (shortened) stinger was deployed with reset OsmoSamplers and pressure gauges. We ran a circulation test with the rig pumps before reentering the hole to determine the expected response on rig gauges to various pumping rates with the mud pumps. With this test complete, the hole was reentered and the 10¾ inch casing hanger was landed in the throat of the reentry cone, creating a hydrologic seal between the ocean above and the open hole below. We waited 1 h to establish a formation baseline and then turned on the mud pumps at 20 spm, equivalent to ~6.7 L/s, approximately the same rate of fluid flow as that inferred in Hole U1301B after Expedition 301, leading to a significant pressure perturbation in Hole 1027C, 2.4 km to the north-northeast (Fisher et al., 2008). Immediately after the start of the 24 h pumping experiment, we began injecting seawater saturated with dissolved SF_6 using a manifold and automated switching valves (**Fisher, Cowen, et al.**).

The primary injectate for the Expedition 327 experiment was seawater, but after 2 h of pumping we injected freshwater ("drill water") for 1 h, and then again 17 h later. In addition, we had four brief periods during which we added salt tracers in solution to the injectate using the cement pump system: CsCl and $ErCl_3$ (salt injection 1) dissolved in seawater, CsCl and $HoCl_3$ (salt injection 2) dissolved in seawater, fluorescent microspheres in freshwater, and fluorescent-stained bacteria filtered from surface seawater and injected with seawater.

The test continued as planned for 24 h, and then the mud pump was stopped. Conditions were monitored for 1 h without moving the casing running tool to establish a final pressure baseline. The casing running tool was lifted from the casing hanger while being monitored with the VIT camera to confirm that there was no flow out of the casing, and then the pipe was retrieved to recover the fluid sampler and pressure gauges in the stinger. OsmoSampler sample coils (two of which were PTFE and two of which were copper) were extracted from the stinger and will be analyzed after the cruise to determine the composition of the injectate as it left the stinger. The pressure gauges provided a high-quality record of conditions in the hole during the experiment (Fig. **F47**).

Pressure measured at the stinger dropped by ~1.5–2 psi immediately after the casing running tool was landed in the hanger because there was a small negative pressure in the borehole created by the rapid flow of cold bottom water down the hole and into the formation. Pressure subsequently rose when pumping began, and the record became irregular when the primary injectate was switched from saltwater to freshwater. Pressure rose after the switch back to saltwater, probably coinciding with freshwa-

ter flowing out of the stinger and down the borehole. The local tidal cycle is clearly expressed during the middle two-thirds of the record, and the four periods of solute and suspended tracer injection are readily apparent as short (8–9 min) intervals of elevated pressure. The second period of freshwater injection was followed by another 1 h period of elevated pressure, again most likely caused by the pressure difference created as freshwater flowed down the borehole. The excess pressure created by pumping dropped immediately after pumping ceased, and a formation pressure baseline was reestablished. The relatively small pressure rise associated with the long period of pumping is consistent with the formation being highly permeable, but careful analysis will be required to separate the various signals that are convolved in the pressure record from this experiment.

Borehole observatories

CORK deployment operations during Expedition 327 are described in considerable detail in **"Operations,"** and CORK designs and configurations are discussed by **Fisher, Wheat, et al.** In the remainder of this section, we provide an overview of observatory operations and configurations in Holes U1362A and U1362B.

Hole U1362A

Hole U1362A was drilled to a total depth of 528.0 mbsf, equivalent to 292.0 msb (Fig. **F48;** Table **T1**). The lowermost 182.0 m of the hole was drilled with a 9⅞ inch bit, whereas the uppermost 37.5 m of open basement hole (below the 10¾ inch casing shoe) was drilled with a 14¾ inch bit. The end of the CORK installation was placed at 469.7 mbsf (233.7 msb), 58.3 m above the total depth of the hole, but a drill string depth check immediately before packer testing indicated fill at 519.0 mbsf (283.0 msb), placing 49.3 m of open hole below the base of the CORK. The base of the CORK assembly comprises (from the bottom up) a bullnose, three perforated drill collars, a section of perforated 5½ inch casing, and the deepest set of CORK casing packers (one inflatable and two swellable elements). All of the parts from the base of the inflatable packer downward are coated to reduce reactivity. The deepest set of packers separates the lower and upper monitored basement intervals (Fig. **F48**).

The CORK deployed in Hole U1362A monitors two basement intervals: a shallow interval extending from the base of the 10¾ inch casing to the top of the deepest set of swellable packers (307.5–417.5 mbsf) and a deeper interval extending from the base of the deepest inflatable packer to the bottom of the hole (429.2–528.0 mbsf). Pressure in both intervals is monitored through ¼ inch stainless steel tubing connected to miniscreens installed just below the inflatable packers at the top of the isolated intervals. A third pressure gauge is set to monitor seafloor pressure but can be switched to monitor the cased interval above the upper set of swellable packers. Pressure lines were de-aired on deployment and left open so that an installed pressure logger would record borehole and seafloor conditions immediately.

Eleven autonomous temperature probes were deployed, including two installed in OsmoSamplers (**Wheat et al.**) suspended inside perforated and coated drill collars at depth in the hole (Fig. **F48;** Table **T11**). The downhole OsmoSampler string comprises six separate instruments and a 200 lb (in water) sinker bar (Table **T12**). Three ½ inch stainless steel fluid sampling lines are configured at two depths (two sampling below packers in the upper interval and one sampling below packers in the lower interval). No wellhead OsmoSamplers were installed when the Hole U1362A CORK was deployed so that the system can remain closed during the subsequent year of pressure recovery (until a planned servicing expedition in summer 2011). One ½ inch microbiology sampling line (PTFE inner liner within a stainless steel sheath and outer plastic protective layer) ends in a titanium miniscreen that rests on perforated and coated 5½ inch casing, 7 m below the base of the deepest inflatable packer, just above the perforated collars (Table **T13**).

The CORK was deployed from the drillship and lowered to the seafloor, and the OsmoSampler and temperature logger string were installed before reentering Hole U1362A. The tapered top plug seals into the CORK wellhead with an O-ring and is held in place with a latch system. The instrument string was assembled as it was lowered into the hole, and then the top plug was attached and lowered into the wellhead. The top plug was lowered into place in the wellhead using the coring line, and latching was verified by pulling up with several hundred pounds once the plug was in position. A weakened overshot shear pin allowed release by jarring off with a single stroke.

Inspection with the VIT camera showed that at least the sinker bar and one OsmoSampler (and perhaps more than one) extended beyond the end of the CORK bullnose. A check on planned cable and CORK lengths did not explain why the instrument string was apparently too long, but this situation required recovery of the string before we could reenter Hole U1362A. We did not have a latch-release tool available on the *JOIDES Resolution*, so we had to re-

turn the CORK to the ship to remove and shorten the string. We were able to recover the CORK body and secure it above the moonpool so that the top of the wellhead extended through the rotary table. The CORK running tool was removed, and the top plug was extracted by turning release bolts on either side of the wellhead. We picked up the top plug just high enough to secure it and put sufficient slack in the cable to remove ~10 m of length. The top plug was again latched into place and the CORK was returned to the seafloor. We reentered Hole U1362A and slowly lowered the CORK into place, encountering no resistance or other difficulties as the CORK was landed in the cone.

A subsequent test of a ~25 m section of new Spectra cable using the traveling block on the drilling rig indicated that cable stretch on the order of 2% should be expected for the new Spectra cable deployed in the Expedition 327 CORKs, somewhat more than the ~1% stretch previously calculated on the basis of manufacturer specifications. The total stretch appeared to occur mostly in an initial set of ~1.5% when the Spectra cable was first loaded, with a small amount of additional stretch proportional to loads in the 500–1000 lb range. The larger overall stretch factor of 2% was used for preparation of the Hole U1362B instrument string.

The submersible/ROV platform was assembled in the moonpool and lowered onto the CORK by wireline and released. Unfortunately, the platform release system failed initially to disengage at one of three latch points, but it was eventually worked loose. However, the platform was observed to be cocked and hung up on the top of the CORK wellhead on one side. We recovered the VIT camera frame, which was attached to the platform running tool, and then returned with the camera to assess the position of the platform. We were able to land the platform by nudging it along one side with the VIT camera frame and then recovered the camera system and secured it for departure. Upon its return, the platform release system was found to have been hung up by a bolt installed on the top of the CORK wellhead that had too high a profile. A lower profile bolt was used on the Hole U1362B CORK.

Hole U1362B

Observatory installation operations in Hole U1362B were similar in some ways to those in Hole U1362A, but there were important differences. Hole U1362B was drilled through 242 m of sediment and 117 m of basement to a total depth of 359.0 mbsf (Fig. **F49;** Table **T2**). Thus, Hole U1362B had 175 m less open basement than did Hole U1362A. In addition, the basement into which Hole U1362B was drilled was restricted entirely to the rubbly and unstable part of the upper crust, meaning it was not possible to set CORK casing packers in the open hole. Thus, the Hole U1326B CORK was designed to monitor only a single interval of upper basement, with packers set in the 10¾ inch casing shoe. Hole U1362B also served as the perturbation point for the 24 h pumping and tracer injection experiment (see **"Hydrologic experiments"** and **Fisher, Cowen, et al.**), which was completed just prior to CORK installation.

The open-basement interval that was configured for monitoring with the Hole U1362B CORK extends from the base of the 10¾ inch casing shoe at 272.0 mbsf to the total depth of 359.0 mbsf. This interval includes 11.0 m of 14¾ inch hole and an additional 70.0 m of 9⅞ inch hole. The bullnose at the end of the CORK assembly was placed at 311.0 mbsf, 47.5 m above total depth and 36.5 m above the depth of fill encountered with the drill bit during a final depth check of the hole made just before assembling and running the CORK. At the base of the CORK assembly are (from the bottom up) a bullnose, three perforated drill collars, a section of perforated 5½ inch casing, and a single set of CORK casing packers (one inflatable and two swellable). All parts from the base of the inflatable packer downward are coated to reduce reactivity. The packers separate the monitored basement interval from the annular gap between the 10¾ and 16 inch casing strings (Fig. **F49**).

Pressure in the basement interval is monitored through ¼ inch stainless steel tubing connected to a miniscreen installed just below the inflatable packer near the bottom of the 10¾ inch casing shoe. A second pressure gauge in the wellhead monitors the cased annular interval that extends from above the cement around the 10¾ inch casing shoe to the 10¾ inch swellable casing packer set against the 16 inch casing near the seafloor. A third dedicated gauge in the wellhead monitors seafloor pressure. Pressure lines extending to depth were de-aired on deployment, and the valves were oriented so that the wellhead pressure logger would immediately record borehole, cased interval, and seafloor conditions.

Eight autonomous temperature probes were deployed across a range of depths, including two installed in OsmoSamplers suspended inside the perforated and coated drill collars at depth (Fig. **F49;** Table **T14**). The downhole OsmoSampler string comprises six separate instruments and a 200 lb sinker bar (Table **T15**). Three ½ inch stainless steel fluid sampling lines terminate in miniscreens installed 4 m from the base of the perforated 5½ inch casing, providing sampling redundancy. As for the Hole U1362A

CORK, no wellhead OsmoSamplers were installed on deployment so that the system could remain closed during the subsequent year of pressure recovery. A single ½ inch PTFE microbiology sampling line ends in a titanium miniscreen that rests at the base of the perforated and coated 5½ inch casing, 7 m below the base of the deepest inflatable packer, just above the perforated collars (Table T16).

The CORK was deployed from the drillship and lowered to the seafloor, and the OsmoSampler and temperature logger string were installed before reentry into Hole U1362B. The instrument string was assembled as it was lowered into the CORK, and then the top plug and latch system were lowered into place in the wellhead using the coring line. We confirmed that the string was not too long by monitoring the end of the CORK bullnose with the VIT camera during string deployment and verifying that the sinker bar did not emerge. The top plug was landed, and latching was verified by pulling up with 500–800 lb once the plug was in position; then the sinker bar was released. However, while making a pipe connection after reentering Hole U1362B but before the CORK was landed, operations personnel noted water flowing from the top of the pipe at the rig floor, suggesting that the instrument plug might not be latched into place. A sinker bar was run down the pipe on the coring line and then latched into the top plug. At that time, we could not verify that the plug was latched, and it is possible that the positive latch indication from a few hours earlier was incorrectly interpreted because of ship heave (which causes coring line tension to vary). Unfortunately, we were then unable to unlatch from the top plug, so it was brought to the surface for inspection. No problems were noted, but a different top plug was configured for deployment and the instrument string was lowered for a second time into the CORK. Once again, we were not able to verify latching, but we were able to shear off the CORK after six or seven attempts. As long as the top plug is in position, the O-ring should seal the CORK whether or not the plug is latched.

Once the CORK was landed in the reentry cone, the casing packer was inflated using the rig pumps. The inflation lines held pressure when the drill string was shut in from the ship, suggesting that the top plug was fully landed. Once the packer was inflated, we deployed the ROV platform and detached from the CORK and verified the positioning of the top plug with the VIT camera.

References

Acton, G.D., Okada, M., Clement, B.M., Lund, S.P., and Williams, T., 2002. Paleomagnetic overprints in ocean sediment cores and their relationship to shear deformation caused by piston coring. *J. Geophys. Res., [Solid Earth],* 107(B4):2067. **doi:10.1029/2001JB000518**

Banerjee, N.R., Gillis, K.M., and Muehlenbachs, K., 2000. Discovery of epidosites in a modern oceanic setting, the Tonga forearc. *Geology,* 28(2):151–154. **doi:10.1130/0091-7613(2000)28<151:DOEIAM>2.0.CO;2**

Bartetzko, A., Pezard, P., Goldberg, D., Sun, Y.-F., and Becker, K., 2001. Volcanic stratigraphy of DSDP/ODP Hole 395A: an interpretation using well-logging data. *Mar. Geophys. Res.,* 22(2):111–127. **doi:10.1023/A:1010359128574**

Becker, K., and Fisher, A.T., 2008. Borehole packer tests at multiple depths resolve distinct hydrologic intervals in 3.5-Ma upper oceanic crust on the eastern flank of Juan de Fuca Ridge. *J. Geophys. Res., [Solid Earth],* 113(B7):B07105. **doi:10.1029/2007JB005446**

Davis, E.E., Chapman, D.S., Mottl, M.J., Bentkowski, W.J., Dadey, K., Forster, C., Harris, R., Nagihara, S., Rohr, K., Wheat, G., and Whiticar, M., 1992. FlankFlux: an experiment to study the nature of hydrothermal circulation in young oceanic crust. *Can. J. Earth Sci.,* 29(5):925–952.

Davis, E.E., Fisher, A.T., Firth, J.V., et al., 1997. *Proc. ODP, Init. Repts.,* 168: College Station, TX (Ocean Drilling Program). **doi:10.2973/odp.proc.ir.168.1997**

Expedition 301 Scientists, 2005. Methods. *In* Fisher, A.T., Urabe, T., Klaus, A., and the Expedition 301 Scientists, *Proc. IODP,* 301: College Station, TX (Integrated Ocean Drilling Program Management International, Inc.). **doi:10.2204/iodp.proc.301.105.2005**

Expedition 324 Scientists, 2010. Testing plume and plate models of ocean plateau formation at Shatsky Rise, northwest Pacific Ocean. *IODP Prel. Rept.,* 324. **doi:10.2204/iodp.pr.324.2010**

Fisher, A.T., Davis, E.E., and Becker, K., 2008. Borehole-to-borehole hydrologic response across 2.4 km in the upper oceanic crust: implications for crustal-scale properties. *J. Geophys. Res., [Solid Earth],* 113(B7):B07106. **doi:10.1029/2007JB005447**

Fisher, A.T., Tsuji, T., and Gamage, K., 2010. Juan de Fuca Ridge-Flank Hydrogeology: the hydrogeologic architecture of basaltic oceanic crust: compartmentalization, anisotropy, microbiology, and crustal-scale properties on the eastern flank of Juan de Fuca Ridge, eastern Pacific Ocean. *IODP Sci. Prosp.,* 327. **doi:10.2204/iodp.sp.327.2010**

Fisher, A.T., Urabe, T., Klaus, A., and the Expedition 301 Scientists, 2005. *Proc. IODP,* 301: College Station, TX (Integrated Ocean Drilling Program Management International, Inc.). **doi:10.2204/iodp.proc.301.2005**

Hutnak, M., Fisher, A.T., Zühlsdorff, L., Spiess, V., Stauffer, P.H., and Gable, C.W., 2006. Hydrothermal recharge and discharge guided by basement outcrops on 0.7–3.6 Ma seafloor east of the Juan de Fuca Ridge: observations and numerical models. *Geochem., Geophys., Geosyst.,* 7(7):Q07O02. **doi:10.1029/2006GC001242**

Kirschvink, J.L., 1980. The least-squares line and plane and the analysis of palaeomagnetic data. *Geophys. J. R. Astron. Soc.,* 62(3):699–718. **doi:10.1111/j.1365-246X.1980.tb02601.x**

Laverne, C., Belarouchi, A., and Honnorez, J., 1996. Alteration mineralogy and chemistry of the upper oceanic crust from Hole 896A, Costa Rica rift. *In* Alt, J.C., Kinoshita, H., Stokking, L.B., and Michael, P.J. (Eds.), *Proc. ODP, Sci. Results,* 148: College Station, TX (Ocean Drilling Program), 151–170. **doi:10.2973/odp.proc.sr.148.127.1996**

Rohr, K.M.M., 1994. Increase of seismic velocities in upper oceanic crust and hydrothermal circulation in the Juan de Fuca plate. *Geophys. Res. Lett.,* 21(19):2163–2166. **doi:10.1029/94GL01913**

Shipboard Scientific Party, 1993. Site 894. *In* Gillis, K., Mével, C, Allan, J., et al., *Proc. ODP, Init. Repts.,* 147: College Station, TX (Ocean Drilling Program), 45–108. **doi:10.2973/odp.proc.ir.147.103.1993**

Shipboard Scientific Party, 1997. Rough basement transect (Sites 1026 and 1027). *In* Davis, E.E., Fisher, A.T., Firth, J.V., et al., *Proc. ODP, Init. Repts.,* 168: College Station, TX (Ocean Drilling Program), 101–160. **doi:10.2973/odp.proc.ir.168.105.1997**

Teagle, D.A.H., Alt, J.C., Bach, W., Halliday, A.N., and Erzinger, J., 1996. Alteration of upper ocean crust in a ridge-flank hydrothermal upflow zone: mineral, chemical, and isotopic constraints from Hole 896A. *In* Alt, J.C., Kinoshita, H., Stokking, L.B., and Michael, P.J. (Eds.), *Proc. ODP, Sci. Results,* 148: College Station, TX (Ocean Drilling Program), 119–150. **doi:10.2973/odp.proc.sr.148.113.1996**

Teagle, D.A.H., Alt, J.C., Umino, S., Miyashita, S., Banerjee, N.R., Wilson, D.S., and the Expedition 309/312 Scientists, 2006. *Proc. IODP,* 309/312: Washington, DC (Integrated Ocean Drilling Program Management International, Inc.). **doi:10.2204/iodp.proc.309312.2006**

Theis, C.V., 1935. The relation between the lowering of the piezometric surface and the rate and duration of discharge of a well using ground-water storage. *Trans., Am. Geophys. Union,* 16:519–564.

Thompson, R., and Oldfield, F., 1986. *Environmental Magnetism:* London (Allen and Unwin).

Tsuji, T., and Iturrino, G.J., 2008. Velocity-porosity relationships in oceanic basalt from eastern flank of the Juan de Fuca Ridge: the effect of crack closure on seismic velocity. *Explor. Geophys.,* 39(1):41–51. **doi:10.1071/EG08001**

Underwood, M.B., Hoke, K.D., Fisher, A.T., Davis, E.E., Giambalvo, E., Zühlsdorff, L., and Spinelli, G.A., 2005. Provenance, stratigraphic architecture, and hydrogeologic influence of turbidites on the mid-ocean ridge flank of northwestern Cascadia Basin, Pacific Ocean. *J. Sediment. Res.,* 75(1):149–164. **doi:10.2110/jsr.2005.012**

Wheat, C.G., Jannasch, H.W., Fisher, A.T., Becker, K., Sharkey, J., and Hulme, S., 2010. Subseafloor seawater-basalt-microbe reactions: continuous sampling of borehole fluids in a ridge flank environment. *Geochem., Geophys., Geosyst.,* 11(7):Q07011. **doi:10.1029/2010GC003057**

Wilkens, R.H., Fryer, G.J., and Karsten, J., 1991. Evolution of porosity and seismic structure of upper oceanic crust: importance of aspect ratios. *J. Geophys. Res., [Solid Earth],* 96(B11):17891–17995. **doi:10.1029/91JB01454**

Zühlsdorff, L., Hutnak, M., Fisher, A.T., Spiess, V., Davis, E.E., Nedimovic, M., Carbotte, S., Villinger, H., and Becker, K., 2005. Site surveys related to IODP Expedition 301: ImageFlux (SO149) and RetroFlux (TN116) expeditions and earlier studies. *In* Fisher, A.T., Urabe, T., Klaus, A., and the Expedition 301 Scientists, *Proc. IODP,* 301: College Station, TX (Integrated Ocean Drilling Program Management International, Inc.). **doi:10.2204/iodp.proc.301.102.2005**

Publication: 5 September 2011
MS 327-103

Figure F1. Site maps showing location of Holes U1362A and U1362B. **A.** Regional bathymetry (Davis, Fisher, Firth, et al., 1997) showing locations of ODP and IODP drill sites. Contour interval is 10 m. Solid circles are Holes U1362A and U1362B; open circles are holes drilled during earlier expeditions. Gold contours show locations of basement exposure on Baby Bare, Mama Bare, and Papa Bare outcrops. Area of dashed box is shown in B. **B.** Track chart of seismic lines around Site U1362 collected during the 2000 ImageFlux expedition (Zühlsdorff et al., 2005; Hutnak et al., 2006). Parts of seismic Lines GeoB00-482 and GeoB00-476 (thick dashed lines) are shown in Figure F2.

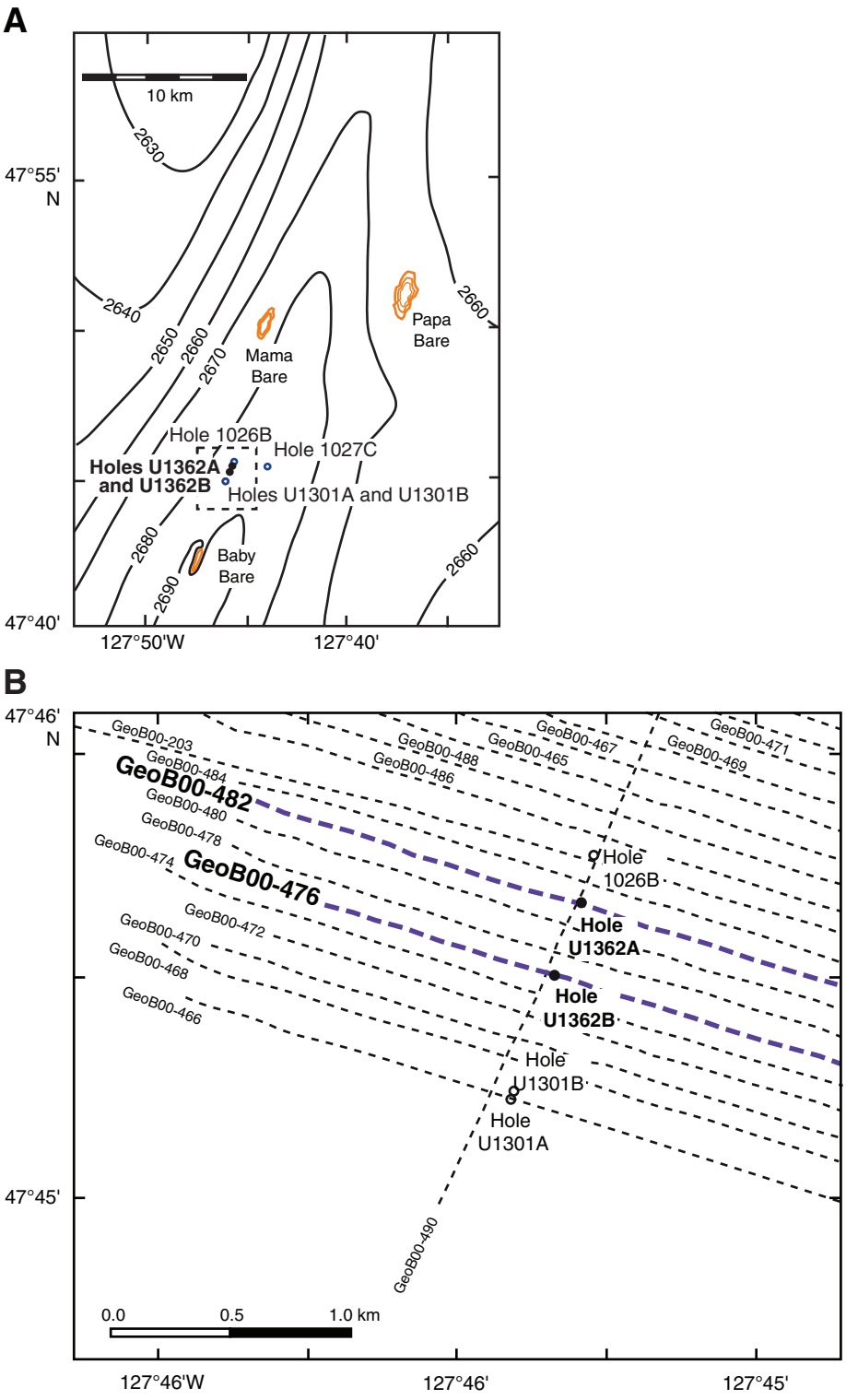

Figure F2. Seismic profiles of lines across IODP Holes U1362A and U1362B. Sediment structures and the sediment/basalt interface are clearly visible in both profiles, as are steeply dipping normal faults to the west of the holes. Both holes (indicated with vertical lines showing total depth penetration) are located over the peak of a buried basement high, near the western edge of a major distributary channel for turbidites that flowed off the North American continental shelf (Davis et al., 1992; Zühlsdorff et al., 2005; Underwood et al., 2005; Hutnak et al., 2006). **A.** Seismic Line GeoB00-482 across Hole U1362A. **B.** Seismic Line GeoB00-476 across Hole U1362B.

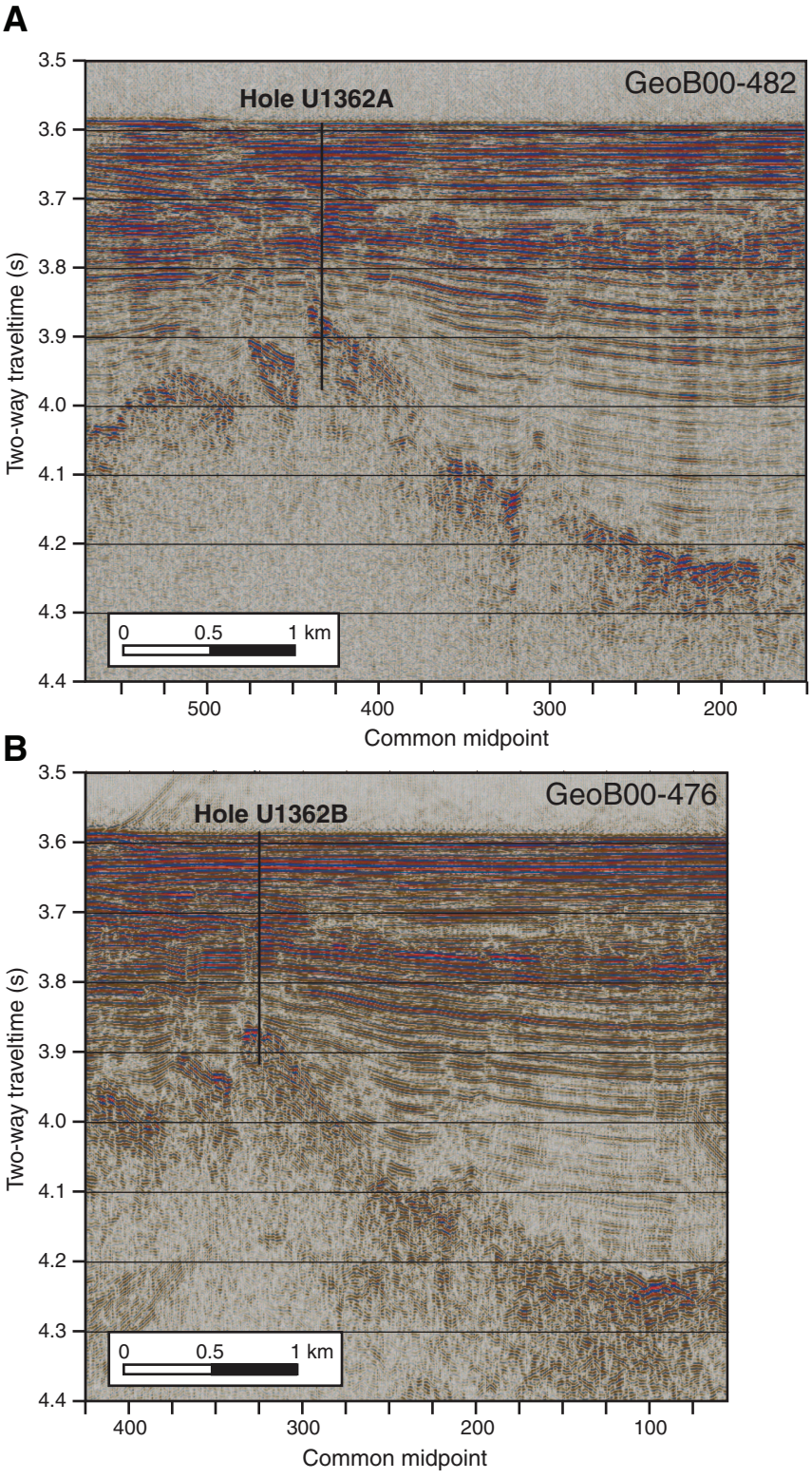

Figure F3. Schematic of Hole U1362A seafloor installation. CORK completion is shown in Figure F48.

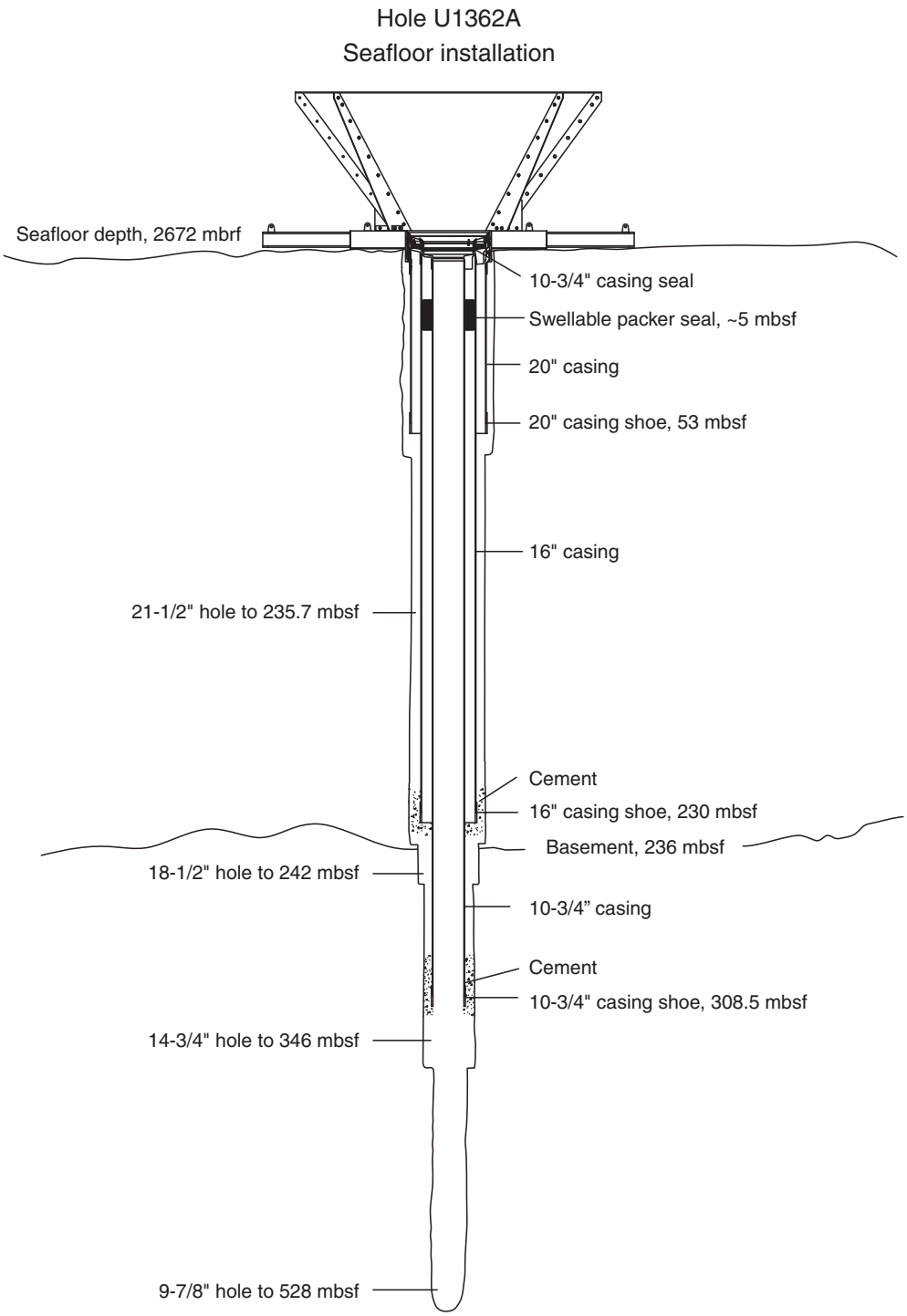

Figure F4. Schematic of Hole U1362B seafloor installation. CORK completion is shown in Figure F49.

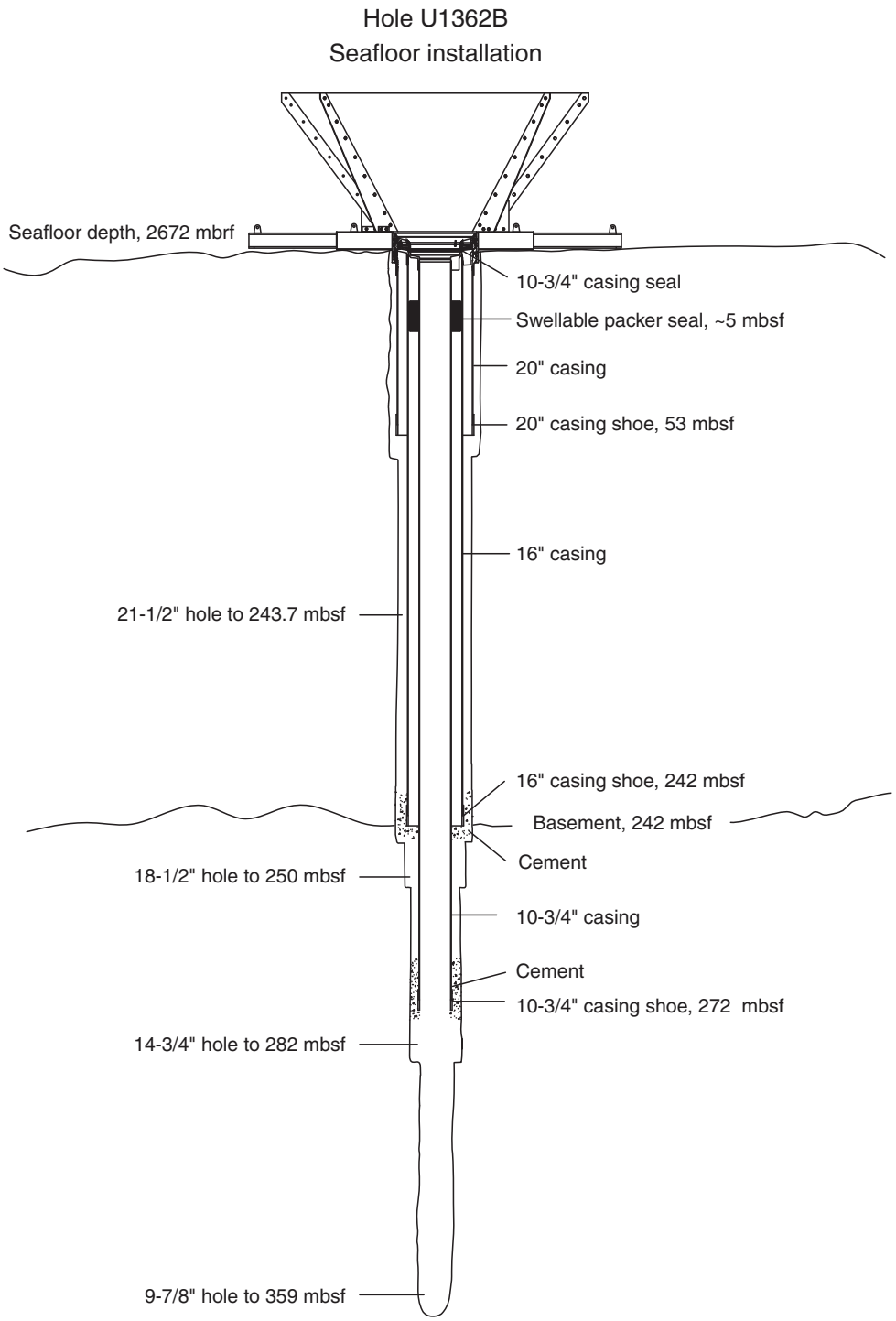

Figure F5. Lithostratigraphic log for Hole U1362A summarizing maximum groundmass grain size, phenocryst abundance and type, and degree of alteration for each unit. Plag = plagioclase, cpx = clinopyroxene, ol = olivine.

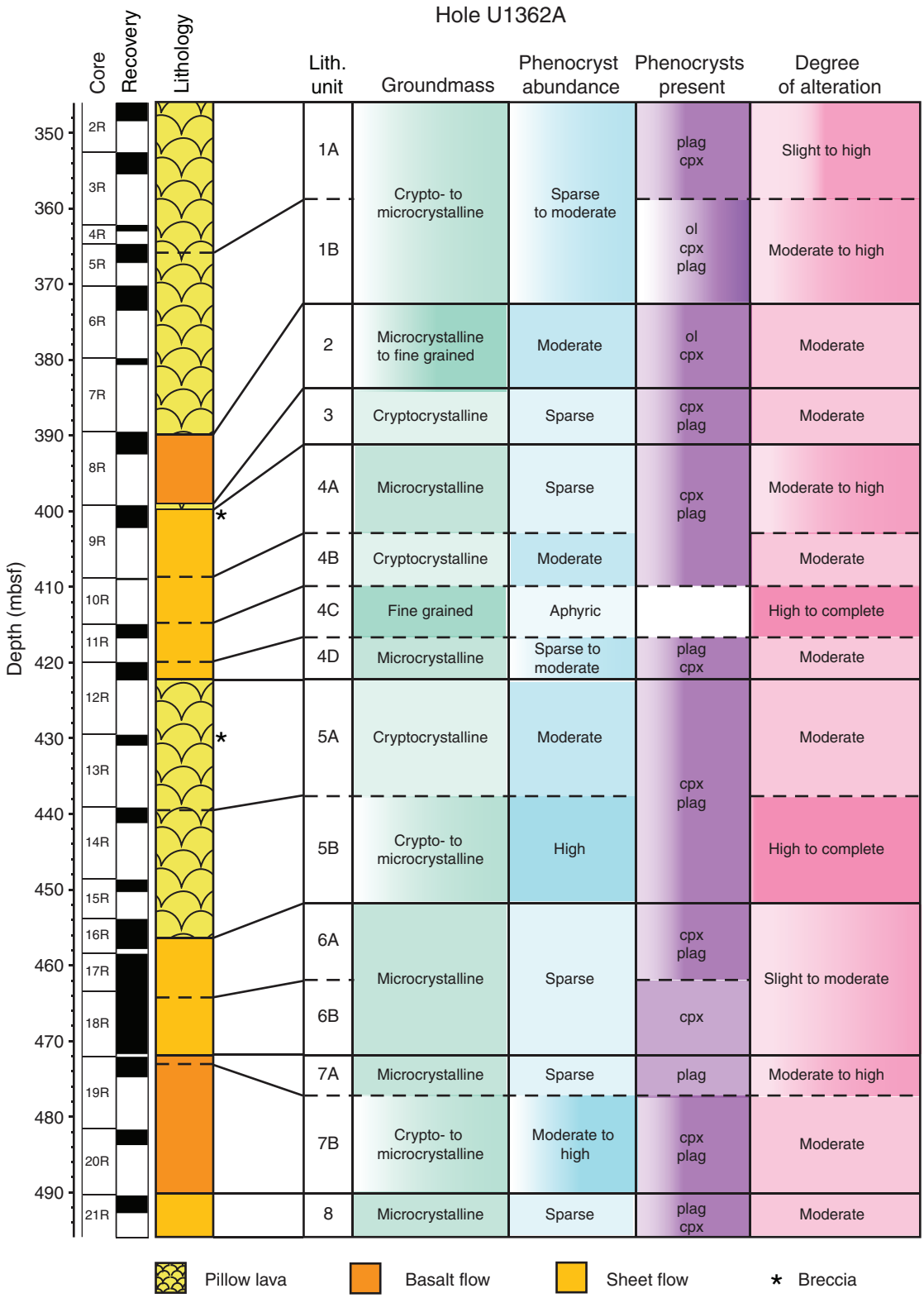

Figure F6. Photograph of curved glassy pillow fragment margin with concentric and radial cooling cracks (interval 327-U1362A-3R-1 [Piece 14, 24–37 cm]).

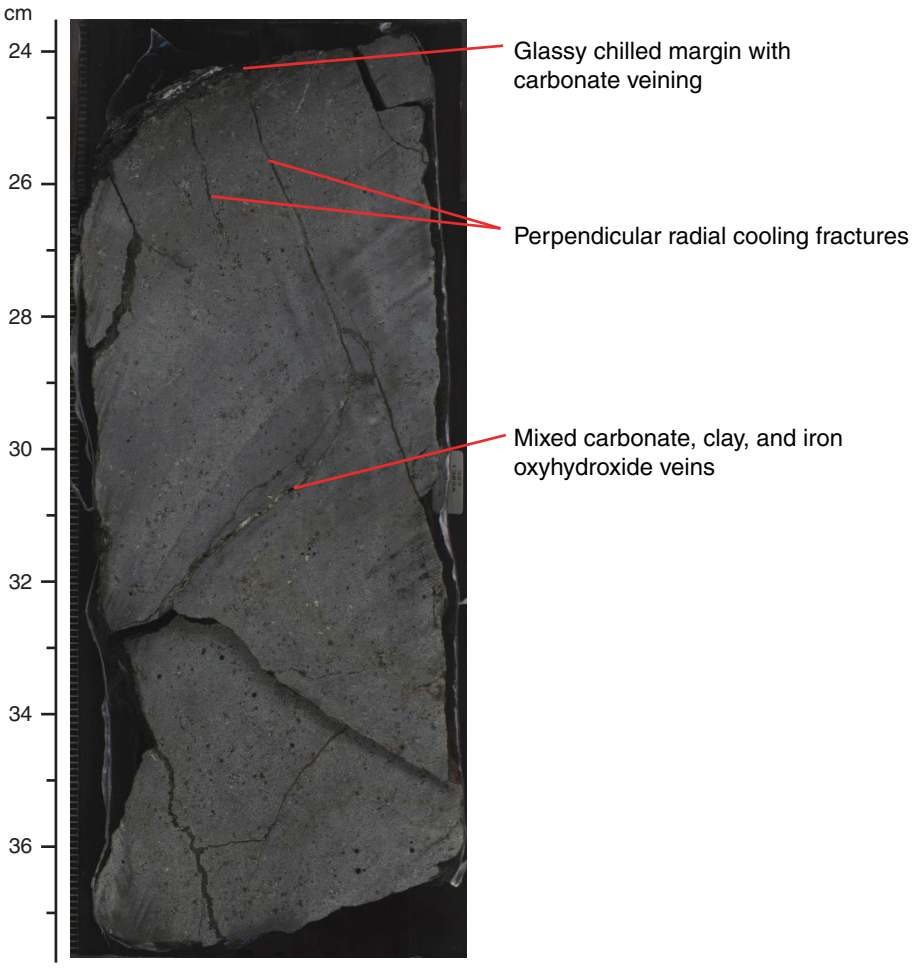

Figure F7. Photomicrograph and whole slide image of a glassy chilled pillow margin displaying a transition from holohyaline to spherulitic texture (Sample 327-U1362A-2R-2 [Piece 17, 121–126 cm]). **A.** Concentric and radial cooling cracks partially filled with saponite (thin section = 25 mm wide). **B.** Transition from fresh amber glass to glass with abundant fibrous spherulites (FOV = 4.5 mm; plane-polarized light). Orientation of the photomicrograph is shown by a red arrow.

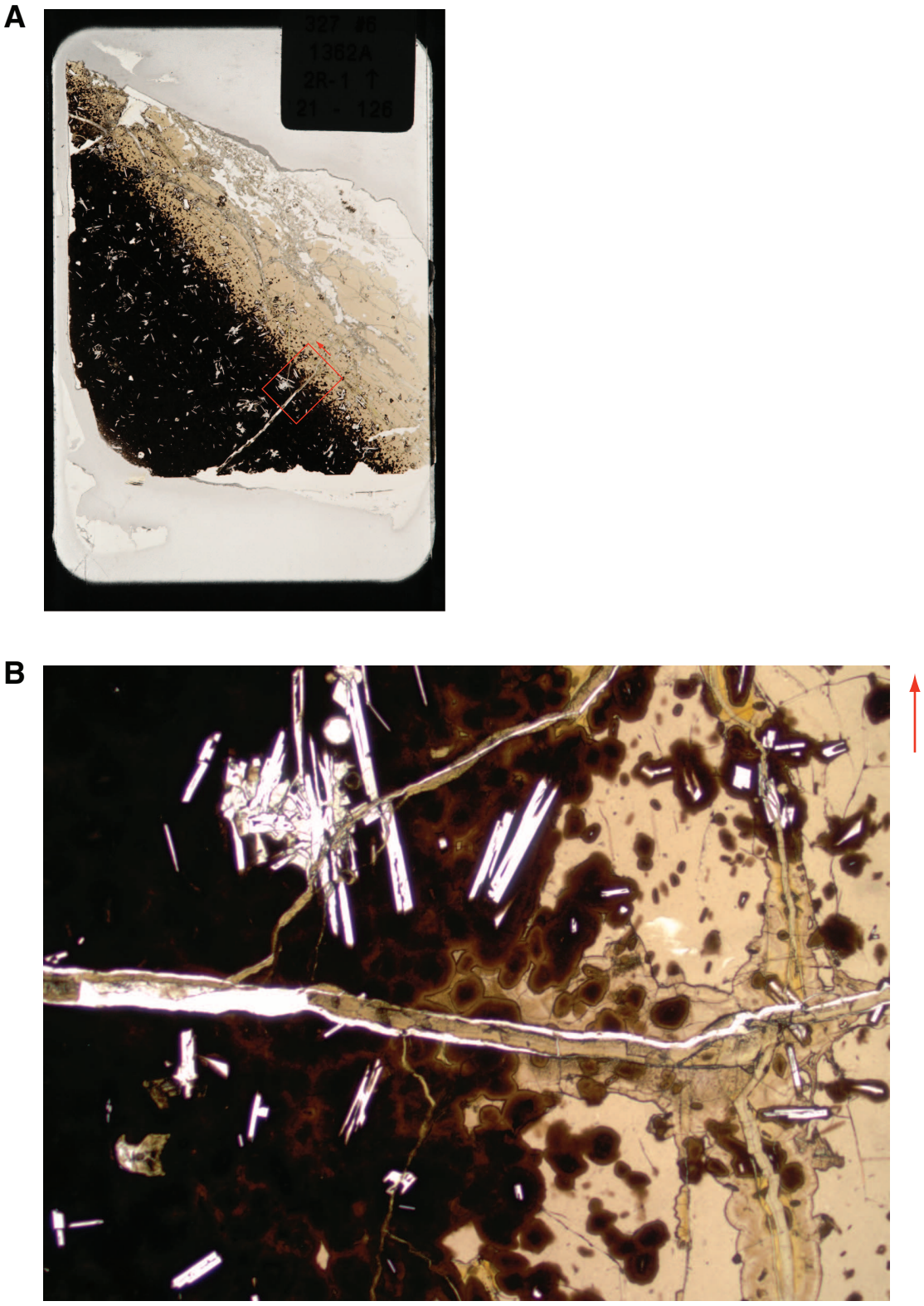

Figure F8. Photomicrographs of typical mineral assemblages, abundances, and groundmass textures within pillow lava basalt from Hole U1362A. **A.** Spherulitic groundmass (Sample 327-U1362A-2R-2 [Piece 8, 73–76 cm]) (FOV = 2.5 mm; plane-polarized light). **B.** Variolitic groundmass (Sample 327-U1362A-3R-2 [Piece 9, 79–81 cm]) (FOV = 1 mm; plane-polarized light). **C, D.** Glomeroporphyritic to subophitic clinopyroxene and plagioclase phenocrysts (Sample 327-U1362A-6R-2 [Piece 14, 74–77 cm]) (FOV = 2.5 mm) under (C) plane-polarized light and (D) cross-polarized light. **E.** Hyalophitic to intersertal groundmass (Sample 327-U1362A-13R-1 [Piece 7, 41–43 cm]) (FOV = 2.5 mm; plane-polarized light).

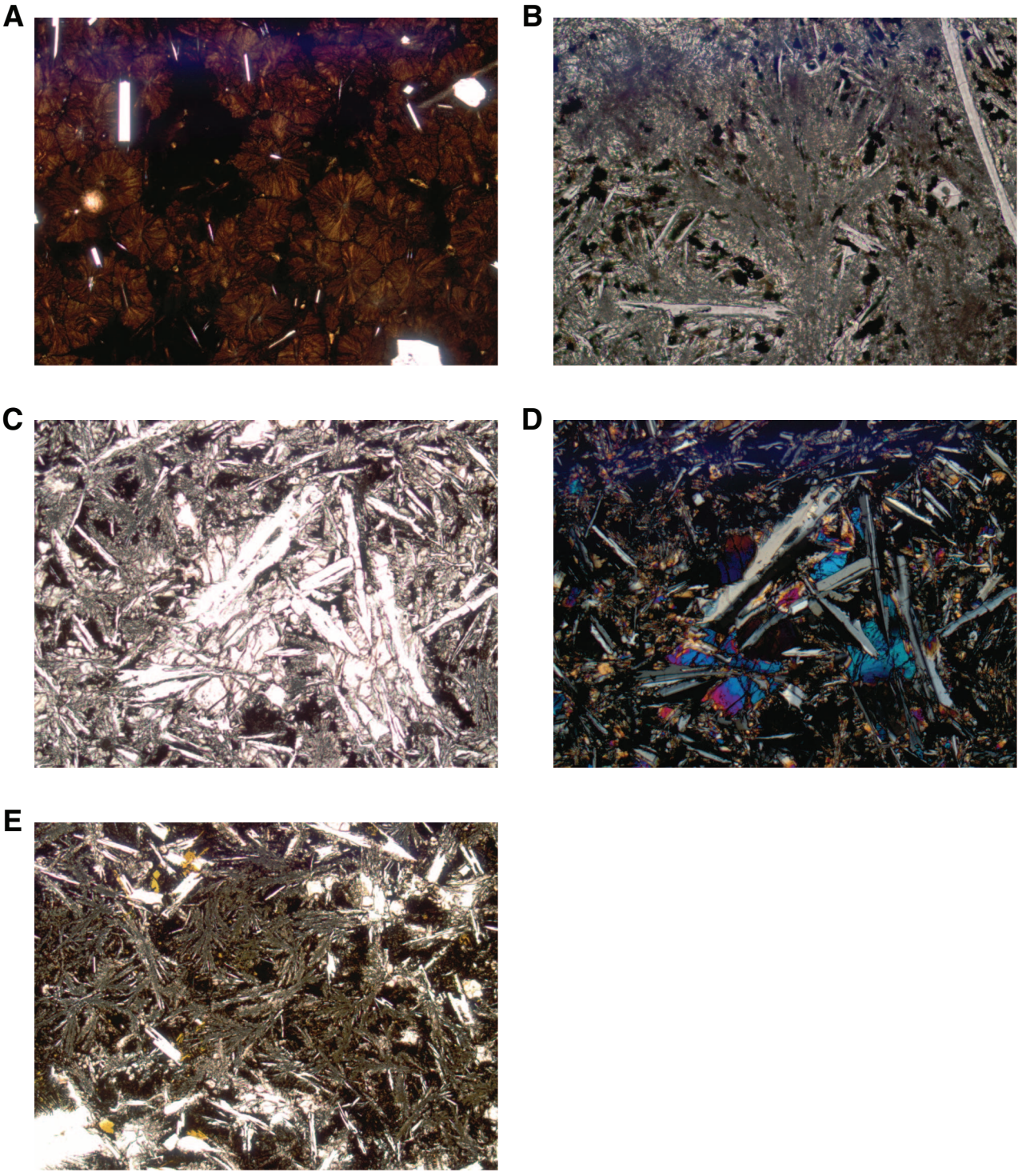

Figure F9. Photomicrographs of partially to completely replaced phenocrysts. **A.** Saponite and iron oxyhydroxide replacing plagioclase and clinopyroxene crystals along crystal edges and cracks (Sample 327-U1362A-7R-1 [Piece 5, 29–31 cm]) (FOV = 2.5 mm; plane-polarized light). **B.** Olivine pseudomorphed by bright green celadonite and pale to red-brown saponite (Sample 327-U1362A-12R-1 [Piece 10, 125–129 cm]) (FOV = 2.5 mm; plane-polarized light). **C.** Skeletal seriate olivines pseudomorphed by pale brown saponite and disseminated oxides (Sample 327-U1362A-18R-2 [Piece 3, 100–102 cm]) (FOV = 2.5 mm; plane-polarized light).

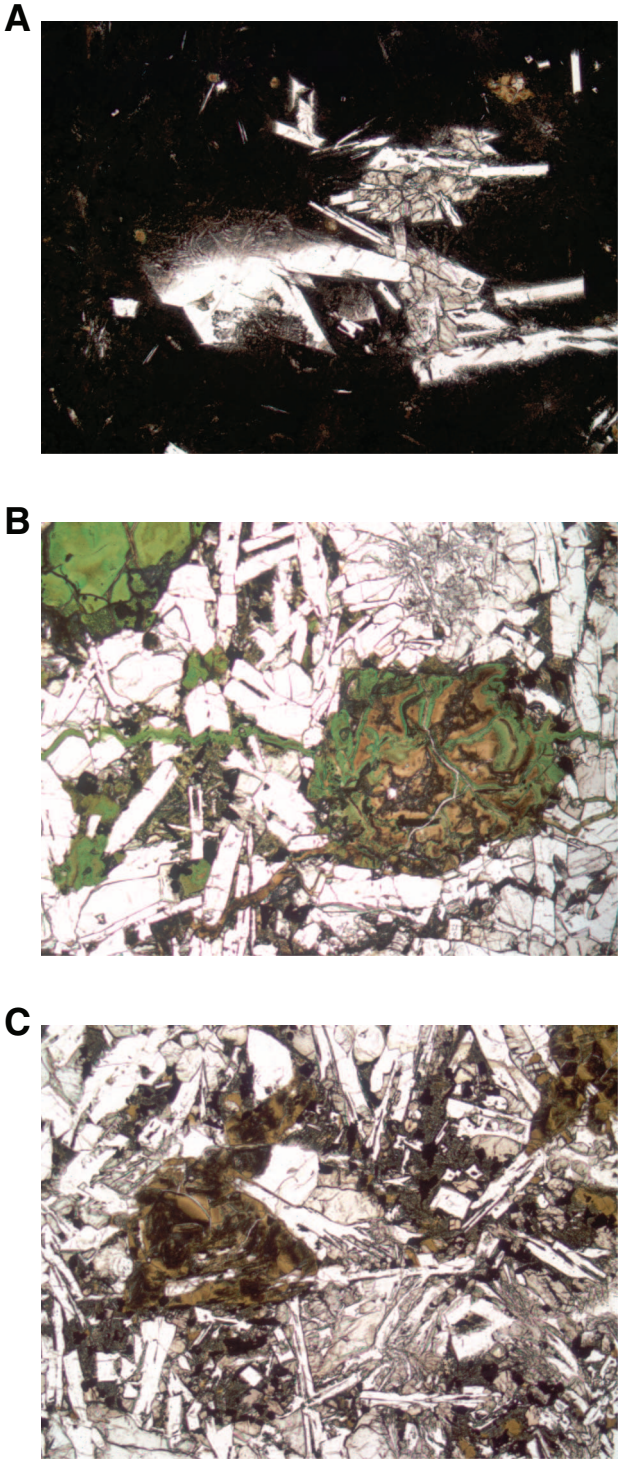

Figure F10. Photomicrographs of sheet flow textures. **A.** Subophitic to spherulitic plagioclase and clinopyroxene phenocrysts (Sample 327-U1362A-12R-1 [Piece 10, 125–129 cm]) (FOV = 4.5 mm; cross-polarized light). **B.** Subophitic plagioclase and clinopyroxene phenocrysts (Sample 327-U1362A-18R-2 [Piece 3, 100–102 cm]) (FOV = 2.5 mm; cross-polarized light).

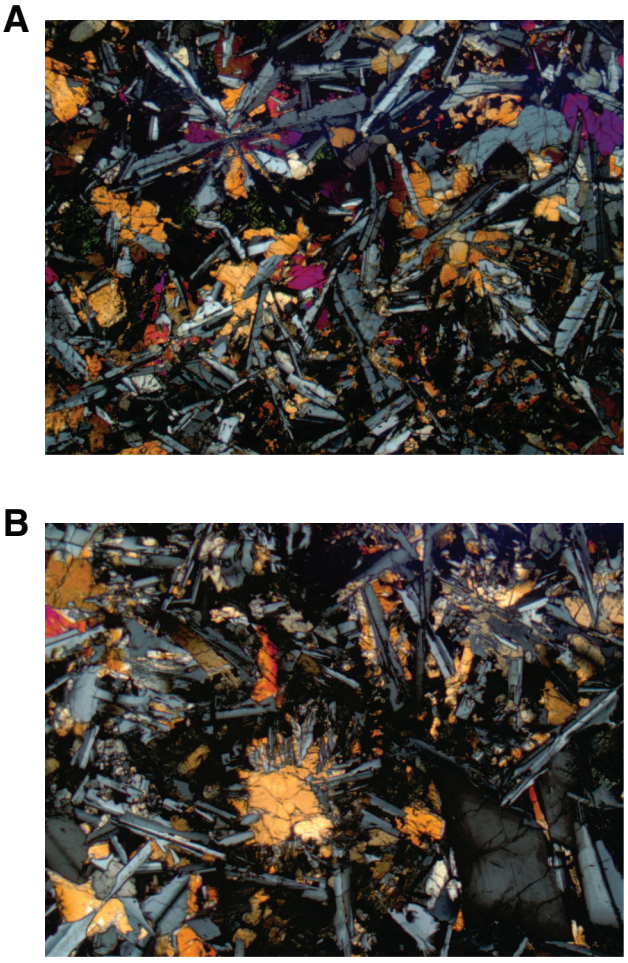

Figure F11. Photomicrograph of pale gray patchy background alteration, as observed in thin section, with discrete patches of groundmass displaying intense replacement to saponite and celadonite (Sample 327-U1362A-6R-2 [Piece 14, 74–77 cm]) (FOV = 4.5 mm; plane-polarized light).

Figure F12. Photomicrographs of saponite replacement. **A.** Intense replacement of groundmass to saponite marks a gray halo boundary (right) contrasted with low-level background alteration of groundmass (left) (Sample 327-U1362A-6R-1 [Piece 10, 39–41 cm]) (FOV = 2.5 mm; plane-polarized light). **B.** Saponite replacing mesostasis and plagioclase microcryst (center) as part of general background alteration (Sample 327-U1362A-7R-1 [Piece 5, 29–31 cm]) (FOV = 2.5 mm; cross-polarized light). **C.** Saponite-filled vein (2.5 mm wide), cross-cutting plagioclase groundmass crystals and enclosing blebs of iron oxyhydroxides (Sample 327-U1362A-8R-1 [Piece 18, 122–124 cm]) (FOV = 2.5 mm; plane-polarized light). **D.** Mesostasis and saponite-filled vesicle (Sample 327-U1362A-20R-2 [Piece 11, 70–72 cm]) (FOV = 2.5 mm; plane-polarized light). **E.** Saponite replacement destroying primary igneous texture (Sample 327-U1362A-3R-1 [Piece 17, 141–146 cm]) (FOV = 2.5 mm; plane-polarized light).

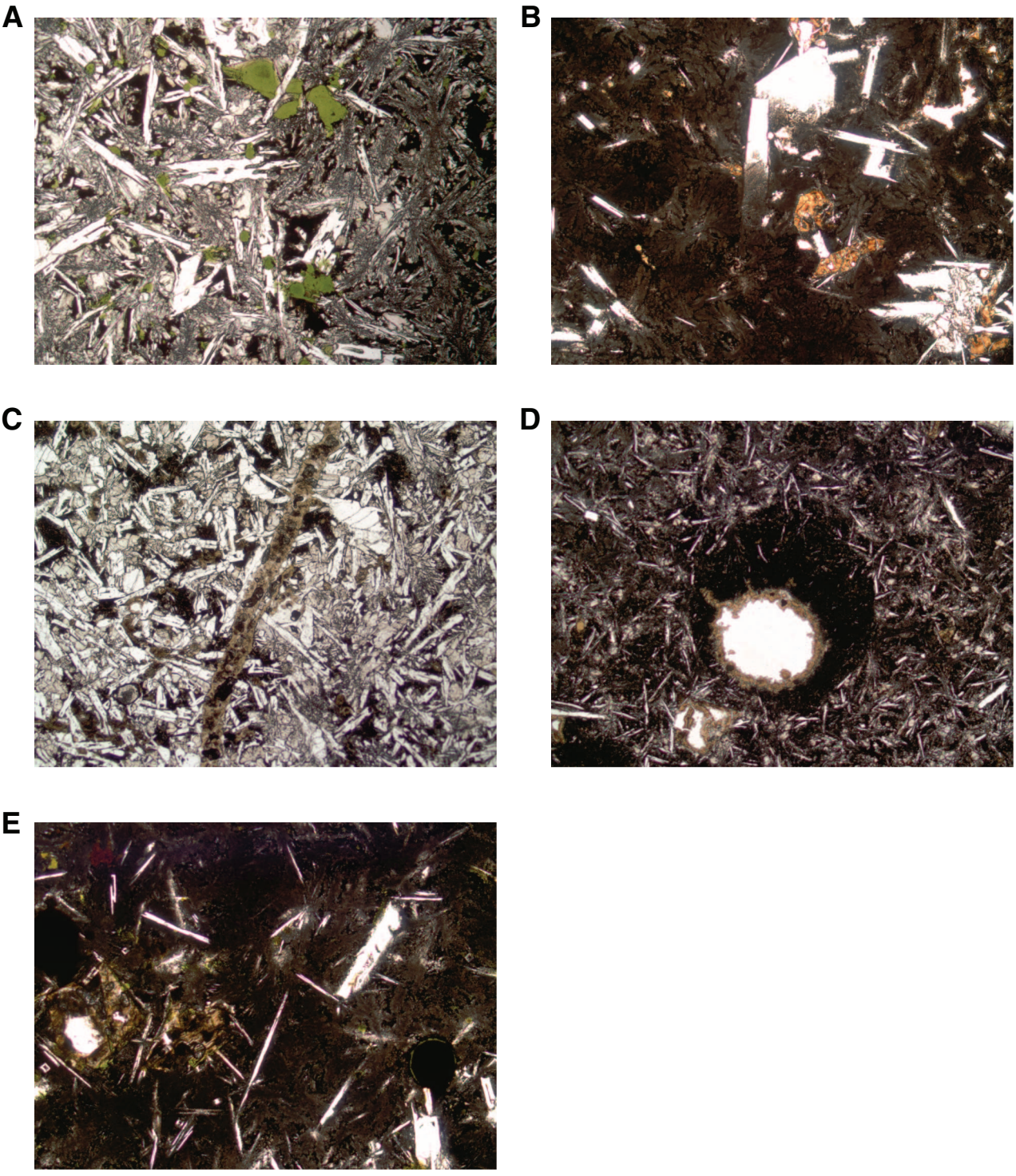

Figure F13. Photograph of basalt-hyaloclastite breccia composed of variably altered basalt clasts in a saponite and altered glass matrix (interval 327-U1362A-13R-1 [Piece 8, 48–56 cm]).

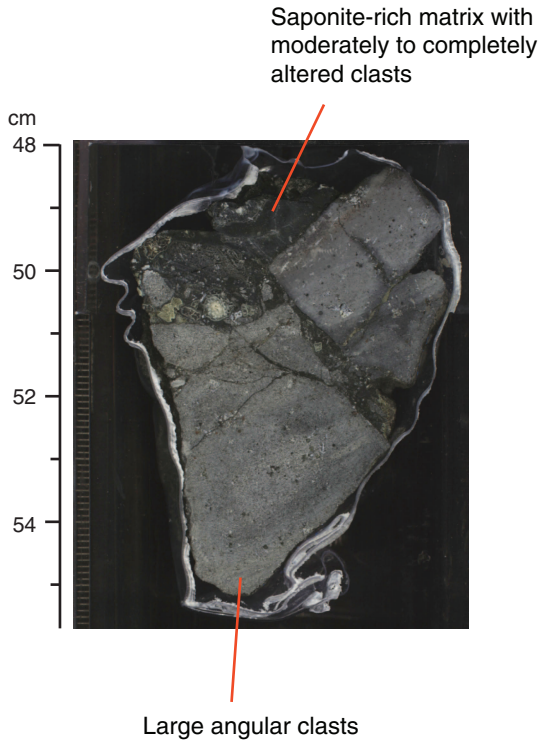

Figure F14. Photographs and sketch of cataclastic zone from Subunit 4A composed of subangular pieces of fine-grained host rock fractured in situ (interval 327-U1362A-9R-2 [Piece 10, 74–82 cm]). **A.** External view of full cataclastic zone and associated halo on whole-round piece. **B.** Cut section through cataclastic zone. **C.** Sketch illustrating orientation of subangular breccia fragments and distribution of alteration halos.

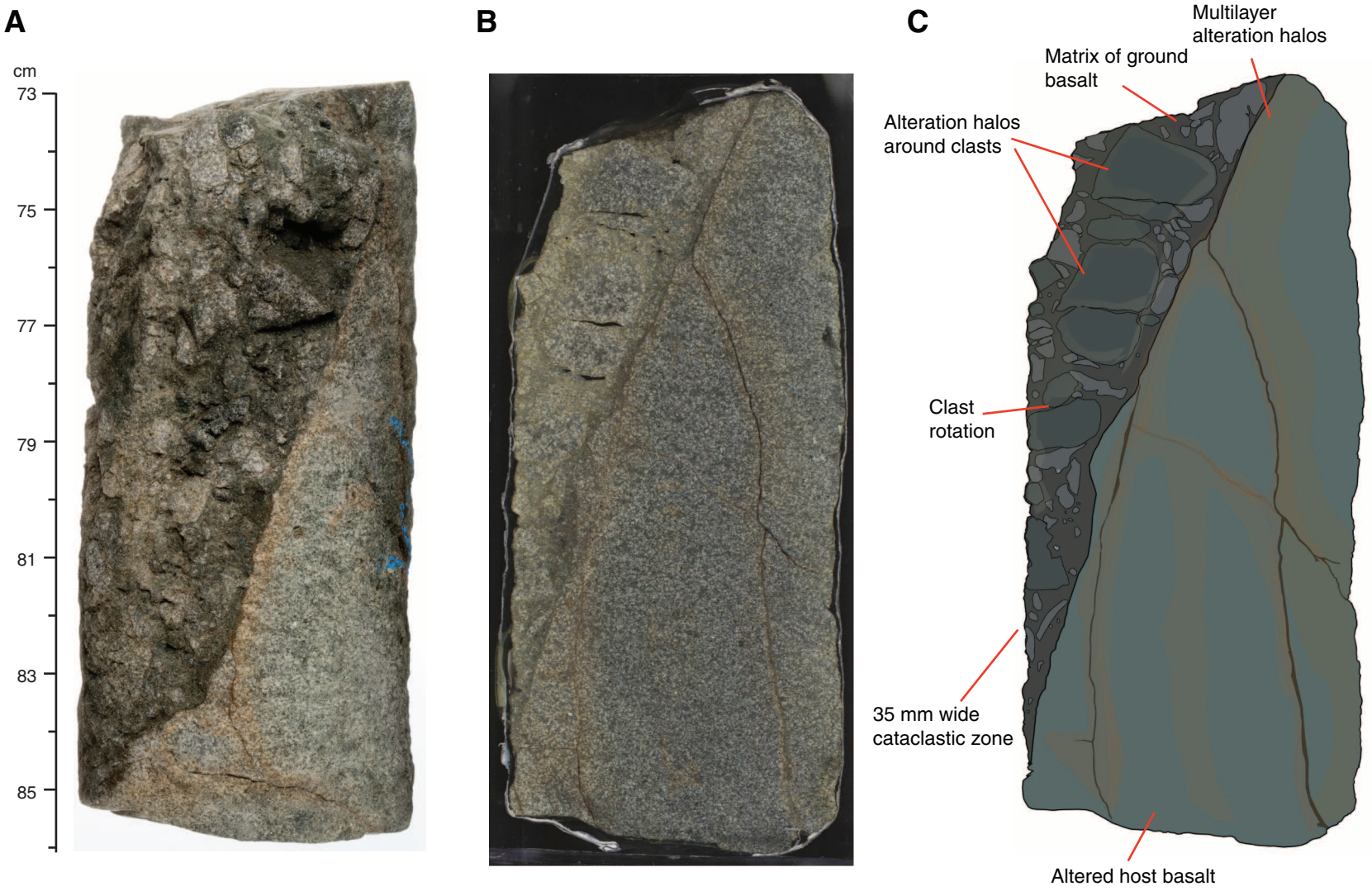

Figure F15. Photomicrographs of filled vesicles. **A.** Multilayered vesicle lined with bright orange iron oxyhydroxide followed by a saponite and iron oxyhydroxide mixed band and a deep red iron oxyhydroxide core (Sample 327-U1362A-7R-1 [Piece 5, 29–31 cm] (FOV = 2.5 mm; plane-polarized light). **B.** Vesicles filled with a mixture of saponite and celadonite with celadonite-rich rims (Sample 327-U1362A-9R-1 [Piece 20, 125–128 cm] (FOV = 4.5 mm; plane-polarized light). **C.** Vesicle with fibrous calcite lining and crystalline calcite core (Sample 327-U1362B-16R-3 [Piece 5, 89–91 cm]) (FOV = 2.5 mm; cross-polarized light). **D.** Multilayered iron oxyhydroxide and saponite-filled vesicle. Later alteration by saponite overprints initial layering to create concentric blebs of material. (Sample 327-U1367A-16R-1 [Piece 5, 89–91 cm]) (FOV = 2.5 mm; plane-polarized light).

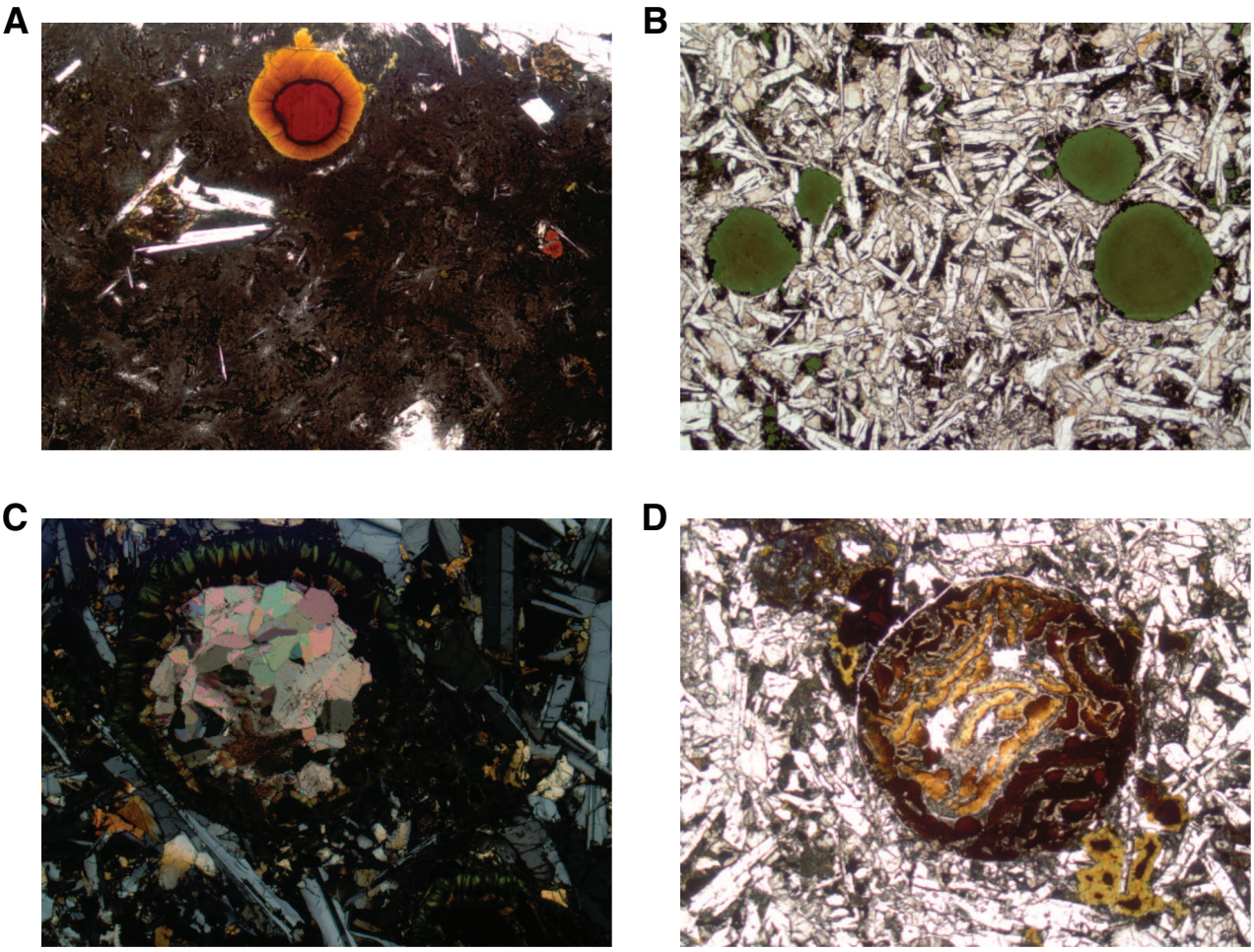

Figure F16. Photomicrograph of multilayered vesicle filled with a mixture of saponite-altered mesostasis (rim), celadonite, iron oxyhydroxide, and saponite, with celadonite in the center (Sample 327-U1362A-6R-1 [Piece 10, 39–41 cm]) (FOV = 2.5 mm; plane-polarized light).

Figure F17. Plot summarizing downhole occurrence of secondary minerals in hydrothermal veins, Hole U1362A.

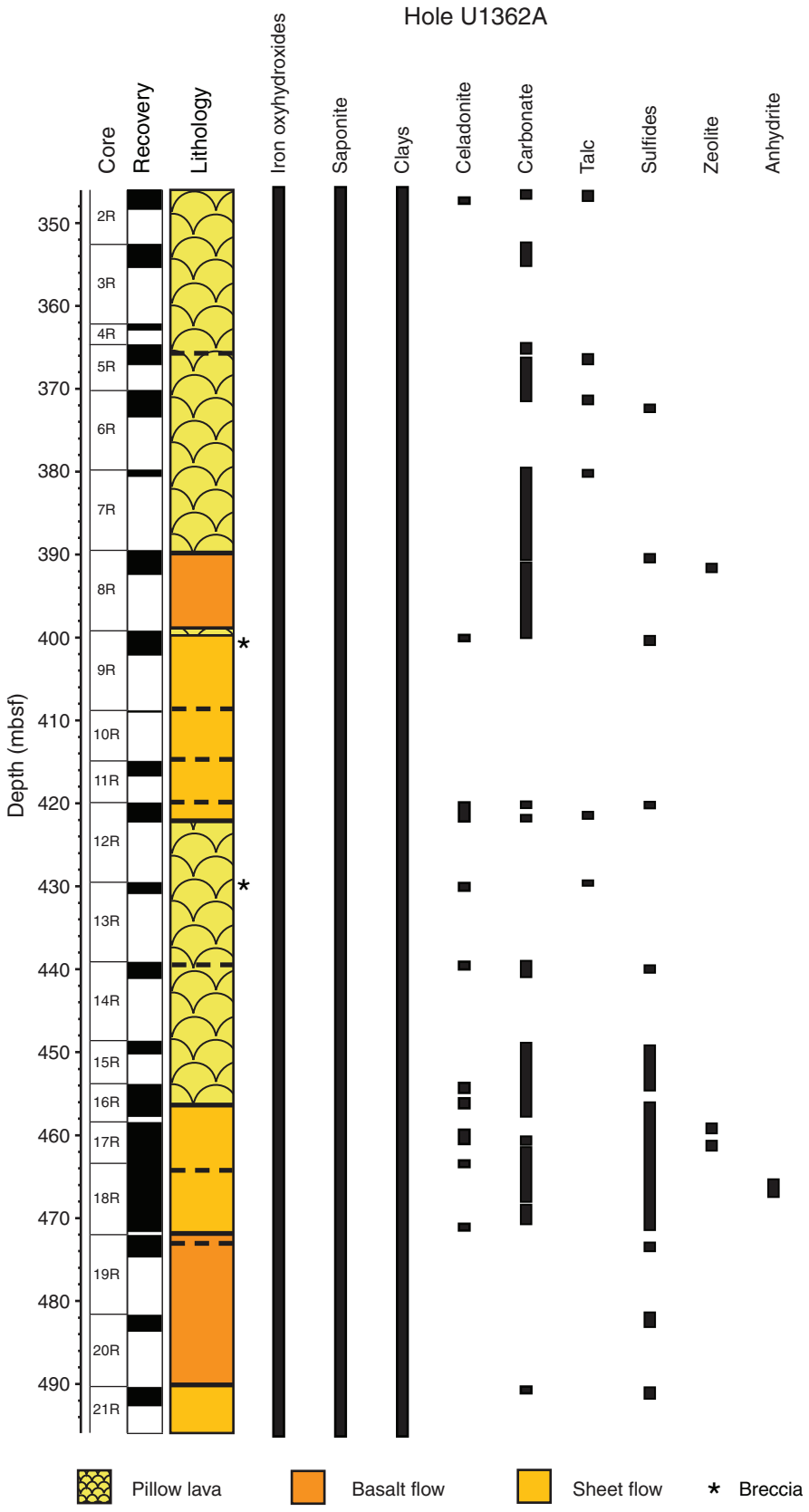

Figure F18. Photomicrographs of multifilled veins from Hole U1362A basalt. **A.** Irregular iron oxyhydroxide vein (0.2 mm), with discontinuous sections of fibrous cross-vein saponite core, cutting through plagioclase phenocrysts (Sample 327-U1367A-13R-1 [Piece 15, 41–43 cm]) (FOV = 2.5 mm; plane-polarized light). **B.** Variable microvein (<0.1 mm) composition (left to right): saponite lining, saponite with iron oxyhydroxide core, iron oxyhydroxide only, and saponite only (Sample 327-U1367A-21R-1 [Piece 16, 104–106 cm]) (FOV = 2.5 mm; plane-polarized light). **C.** Microvein of saponite lining with interchangeable iron oxyhydroxide (top right) and saponite (bottom left) cores (Sample 327-U1367A-21R-1 [Piece 16, 104–106 cm]) (FOV = 2.5 mm; plane-polarized light).

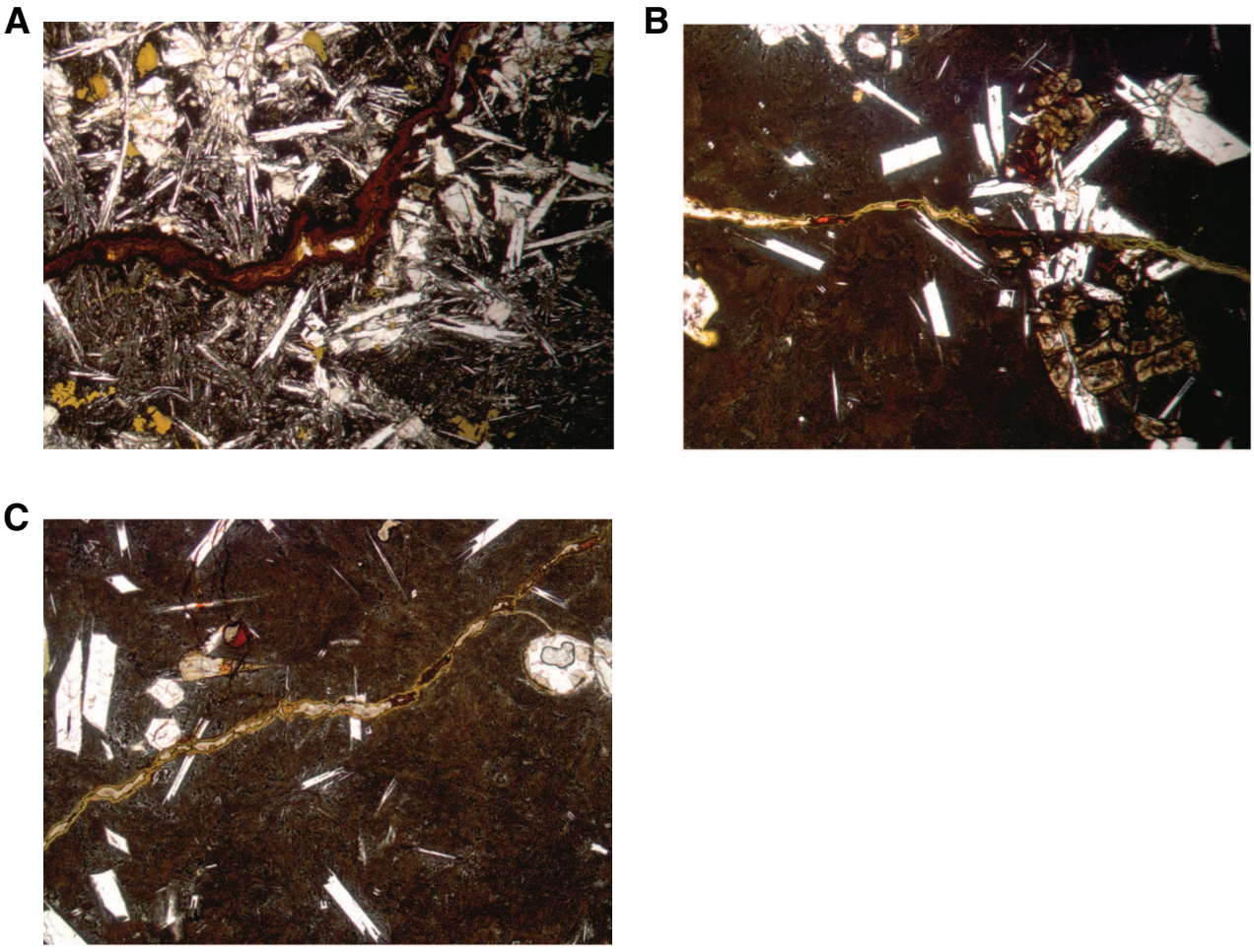

Figure F19. Photomicrographs of anhydrite present as a fibrous vein along edge of thin section (Sample 327-U1362A-18R-2 [Piece 3, 100–102 cm]). **A.** Cross-polarized light (FOV = 2.5 mm). **B.** Plane-polarized light (FOV = 2.5 mm).

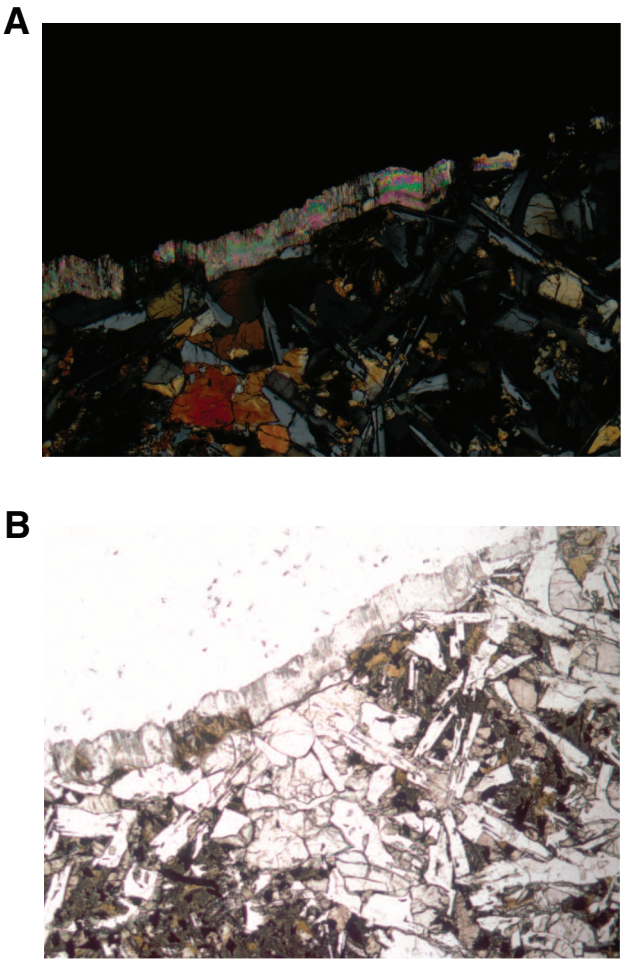

Figure F20. Photographs of gray halos. **A.** Mixed gray halo with an outer 8 mm dark gray halo and an inner 4 mm pale gray halo (interval 327-U1362A-3R-2 [Piece 8, 79–84 cm]). **B.** Dark gray rock halo as wide as 40 mm (interval 327-U1362A-14R-1 [Piece 1, 1–14 cm]).

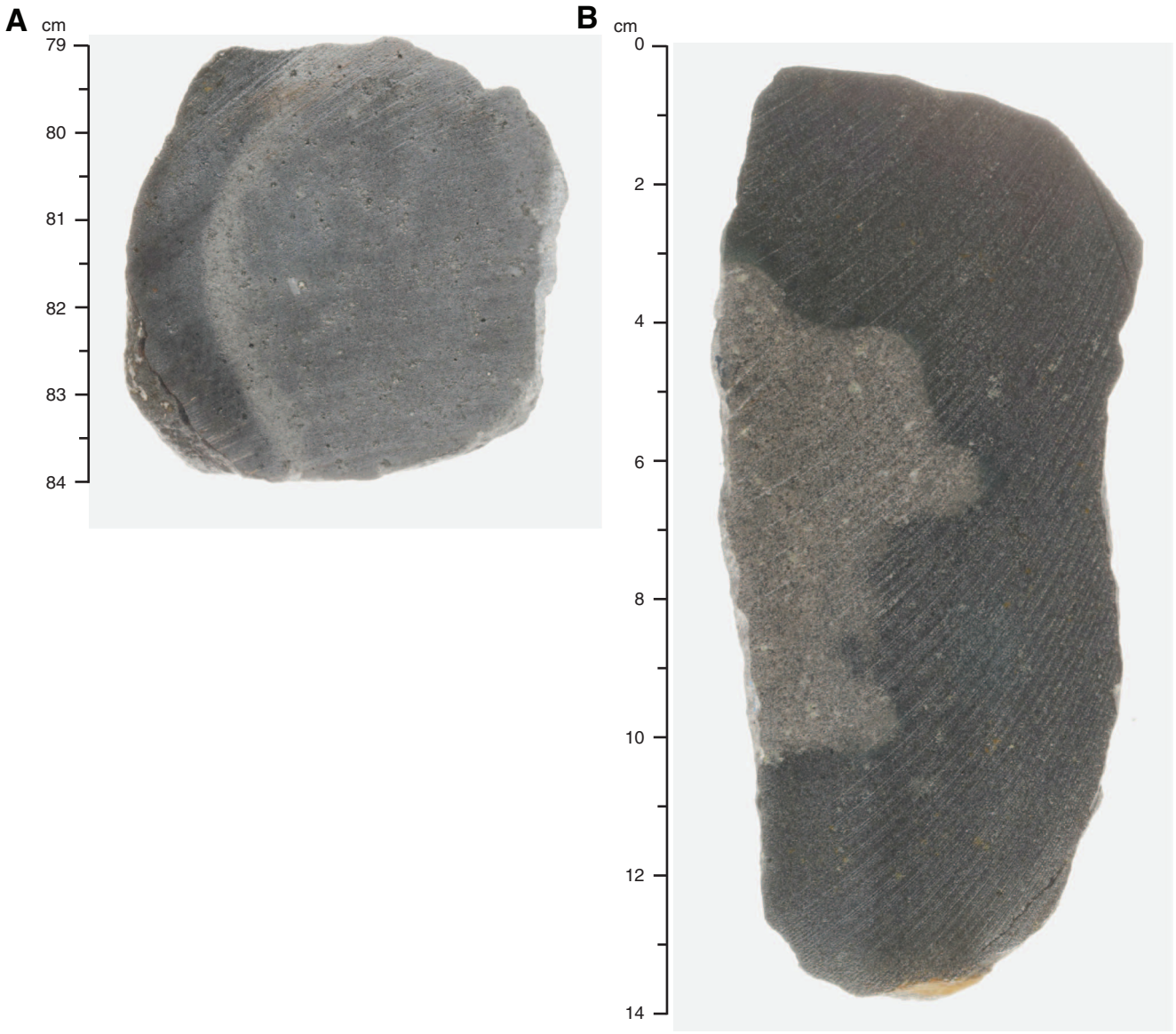

Figure F21. Photograph of rare dark green halo representing a mix of saponite and celadonite (interval 327-U1362A-13R-1 [Piece 15, 105–123 cm]).

Figure F22. Photograph of dark gray halo with orange spots (interval 327-U1362A-5R-1 [Piece 17, 88–95 cm]).

Figure F23. Photographs of multilayer halos. **A.** Pink halo (interval 327-U1362A-20R-1 [Piece 10, 70–75 cm]). **B.** Multilayered ring halo (interval 327-U1362A-11R-1 [Piece 13, 95–110 cm]). **C.** Large-scale multilayered halo (interval 327-U1362A-12R-1 [Piece 9, 95–122 cm]).

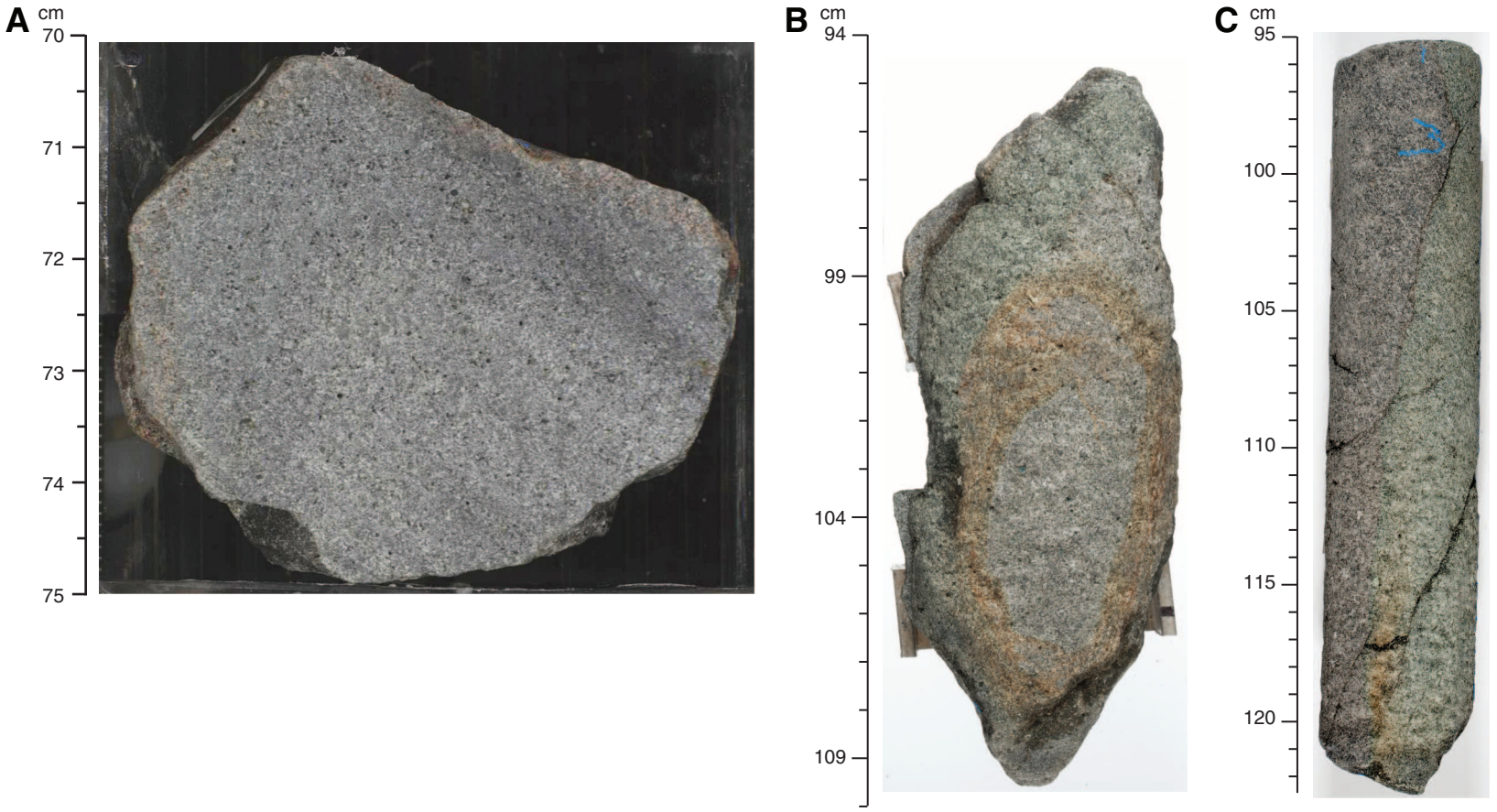

Figure F24. Photographs of alteration halo associations with host rock. **A.** Alteration halo with no association to a hydrothermal vein or structure (interval 327-U1362A-11R-1 [Piece 12, 85–95 cm]. **B.** Same as A, viewed on a cut surface. **C.** Multilayer alteration halo directly associated with a mixed saponite (dark green) and clay (pale green) vein on the exterior surface (far left) (interval 327-U1362A-9R-2 [Piece 16, 127–137 cm]).

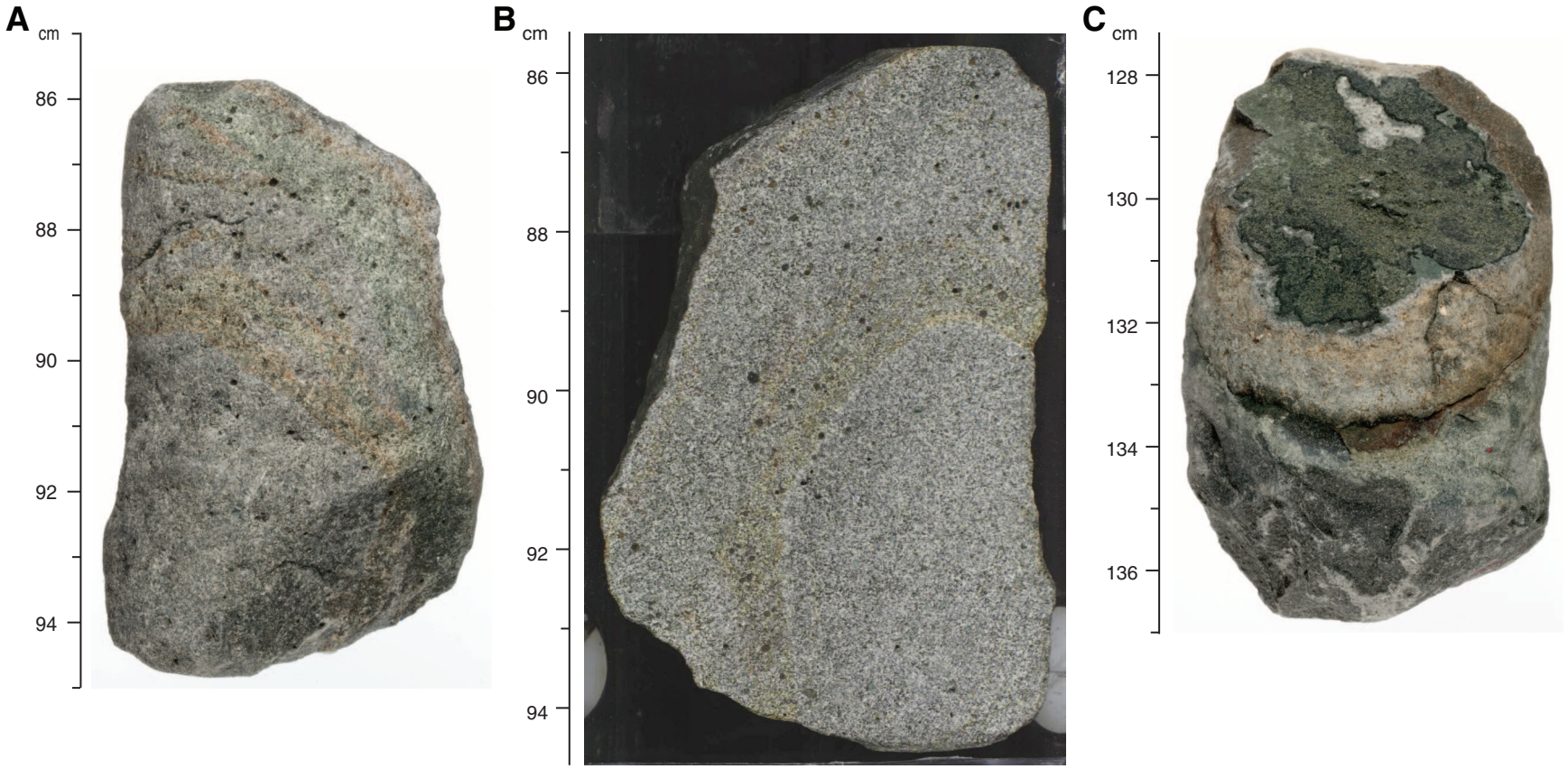

Figure F25. Plots of TiO_2 vs. Zr abundance for all ICP-AES hard rock analyses, Hole U1362A.

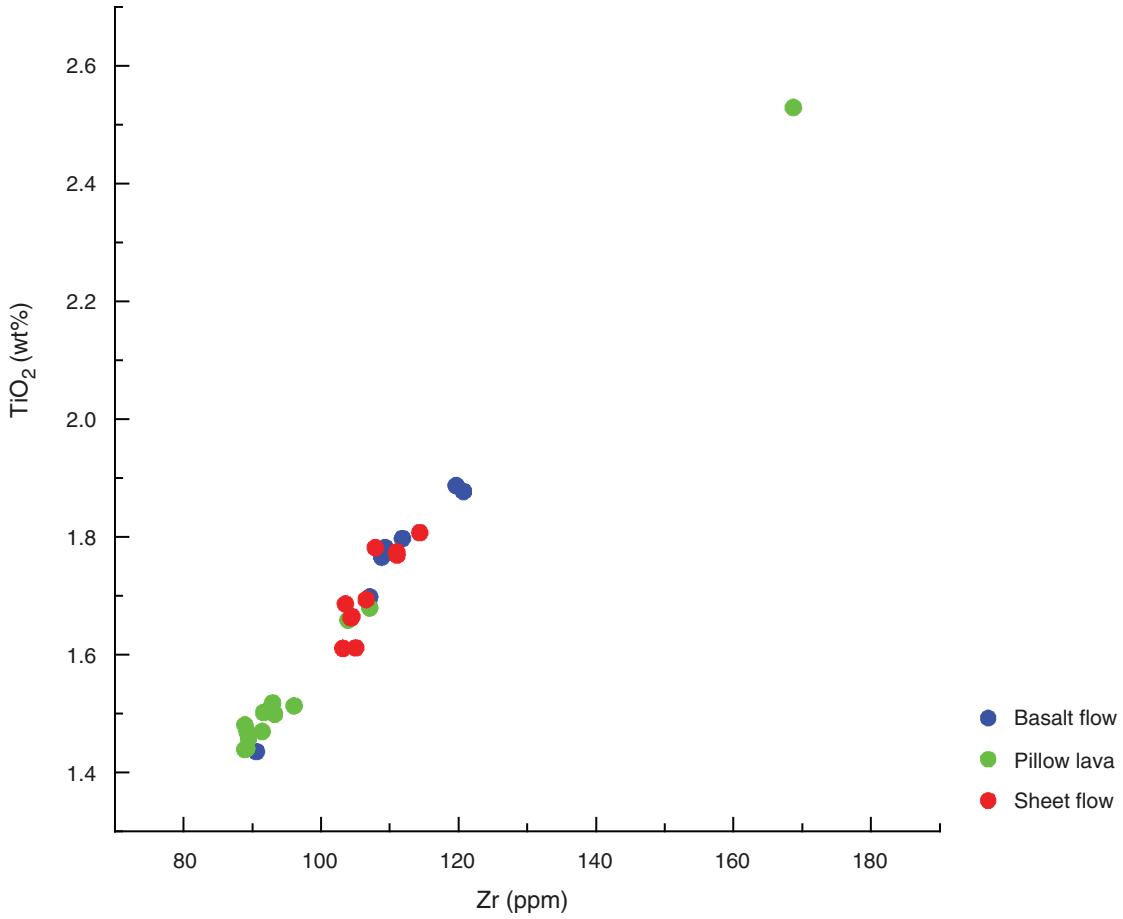

Figure F26. Plots of major element abundance vs. Mg# for all ICP-AES hard rock analyses, Hole U1362A.

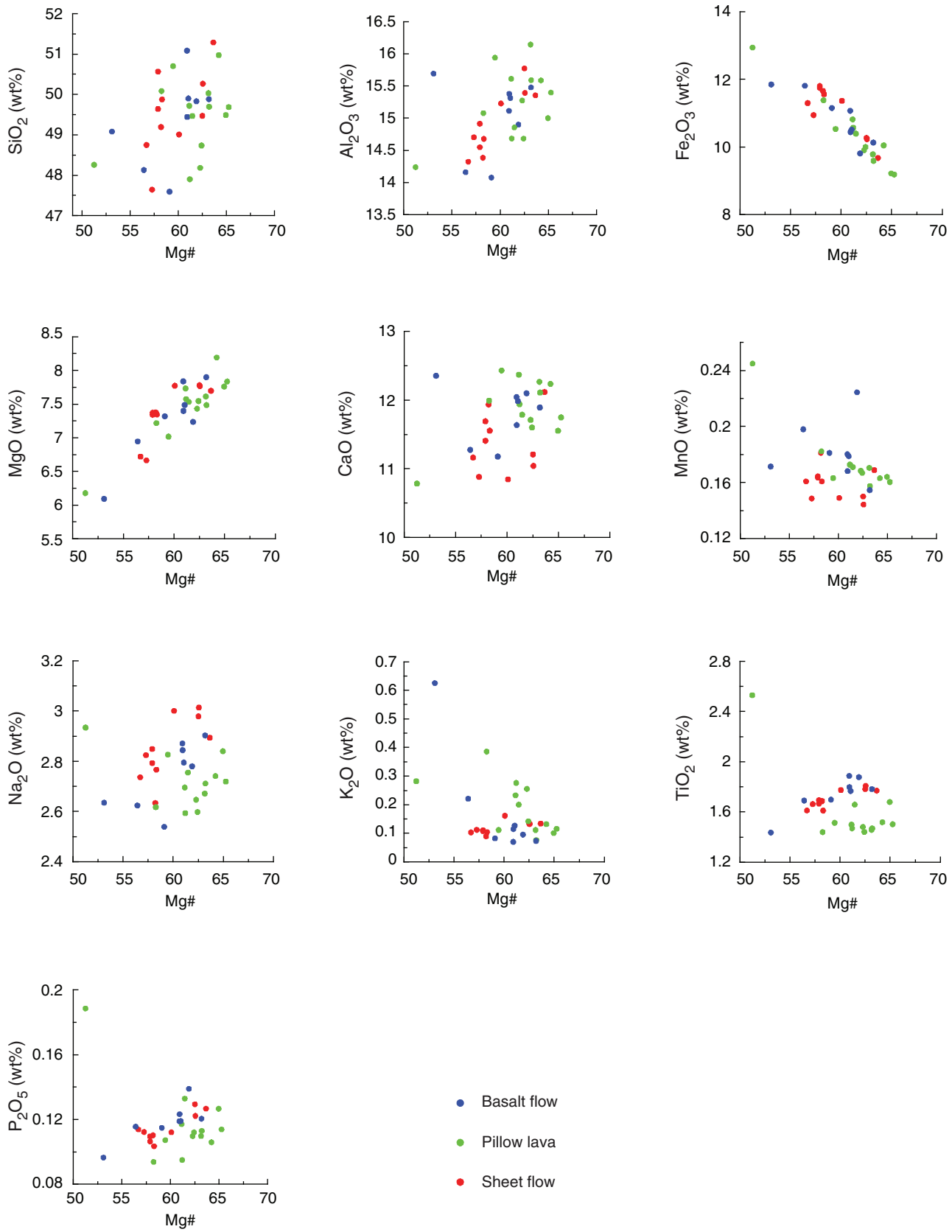

Figure F27. Plots of trace element abundances vs. Mg# for all ICP-AES hard rock analyses, Hole U1362A.

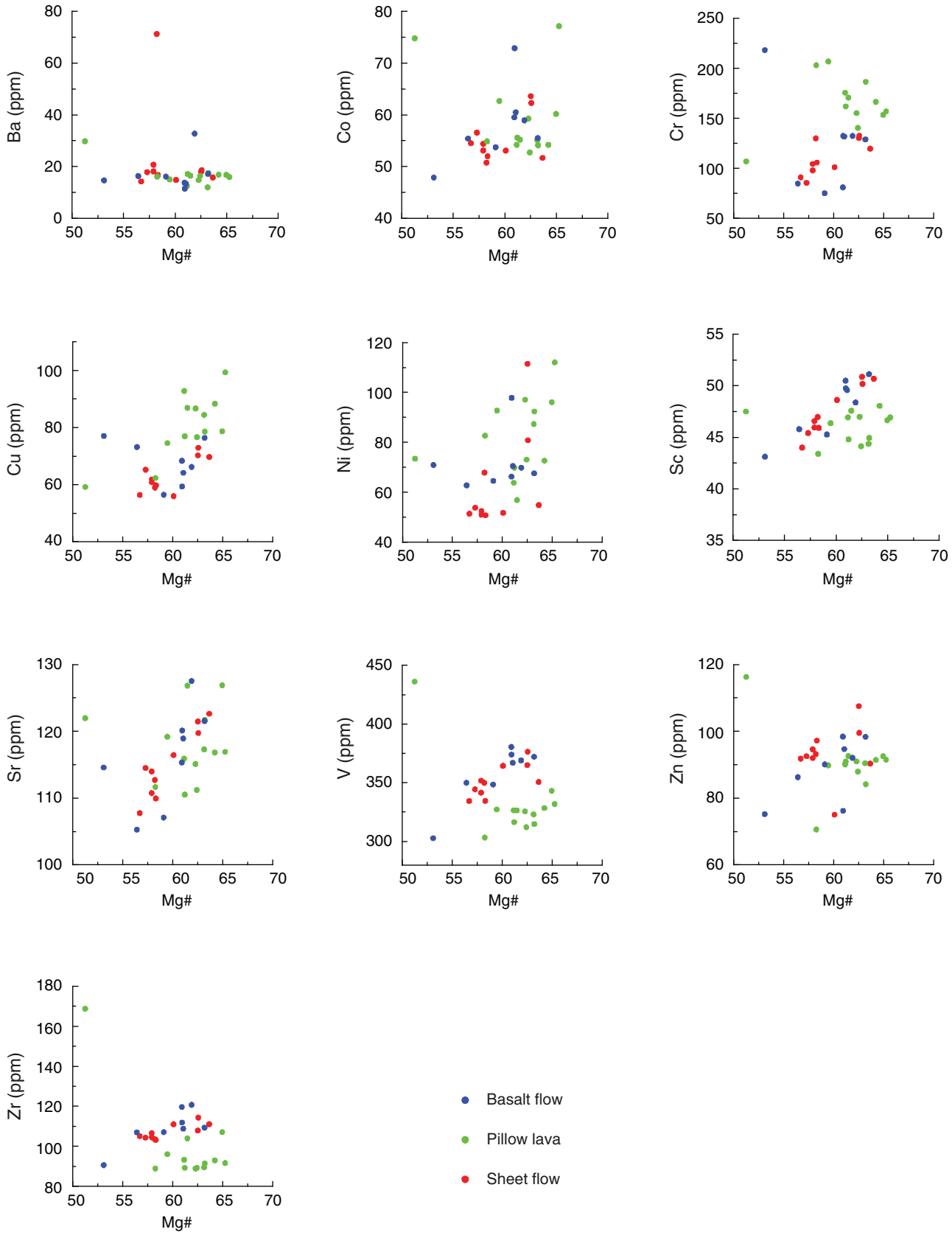

Figure F28. Plots of ICP-AES analyses vs. depth, Hole U1362A. LOI = loss on ignition. (**Continued on next page.**)

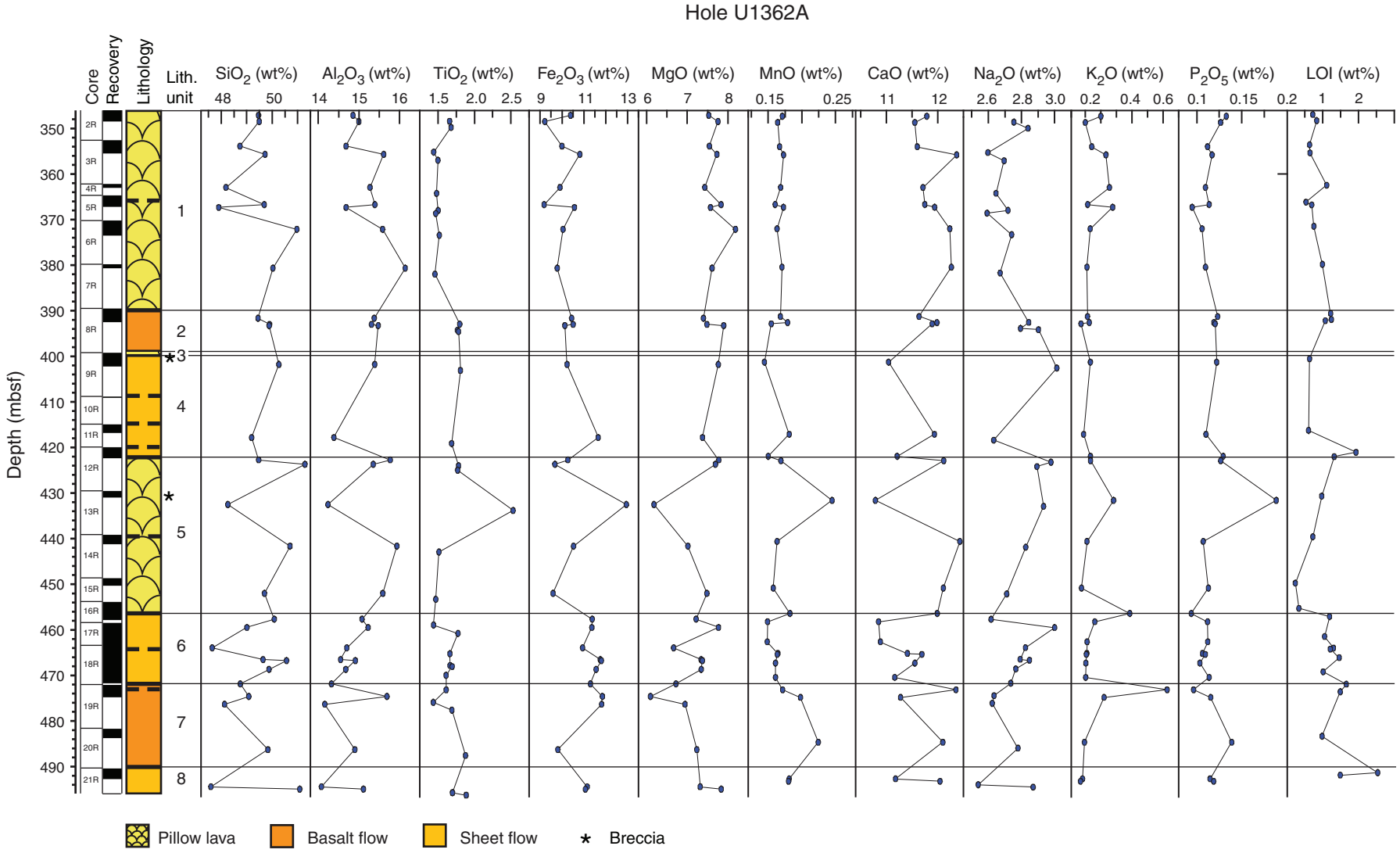

Figure F28 (continued).

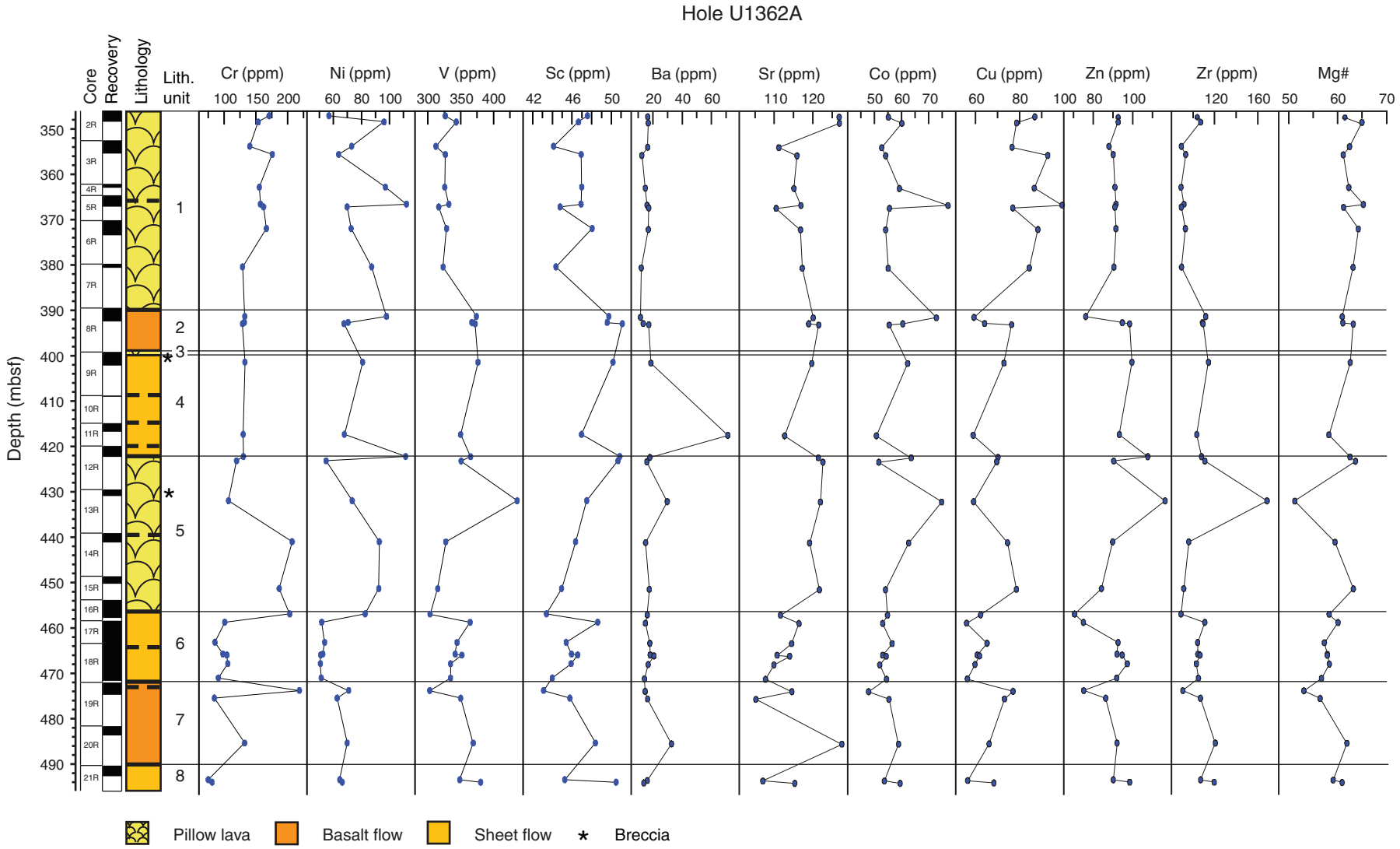

Figure F29. Plots of orientations of all measured veins and fractures in Hole U1362A rocks. **A.** Poles of veins and fractures on a lower hemisphere equal-angle projection. **B.** Distribution of true dip angles for all measured veins and fractures.

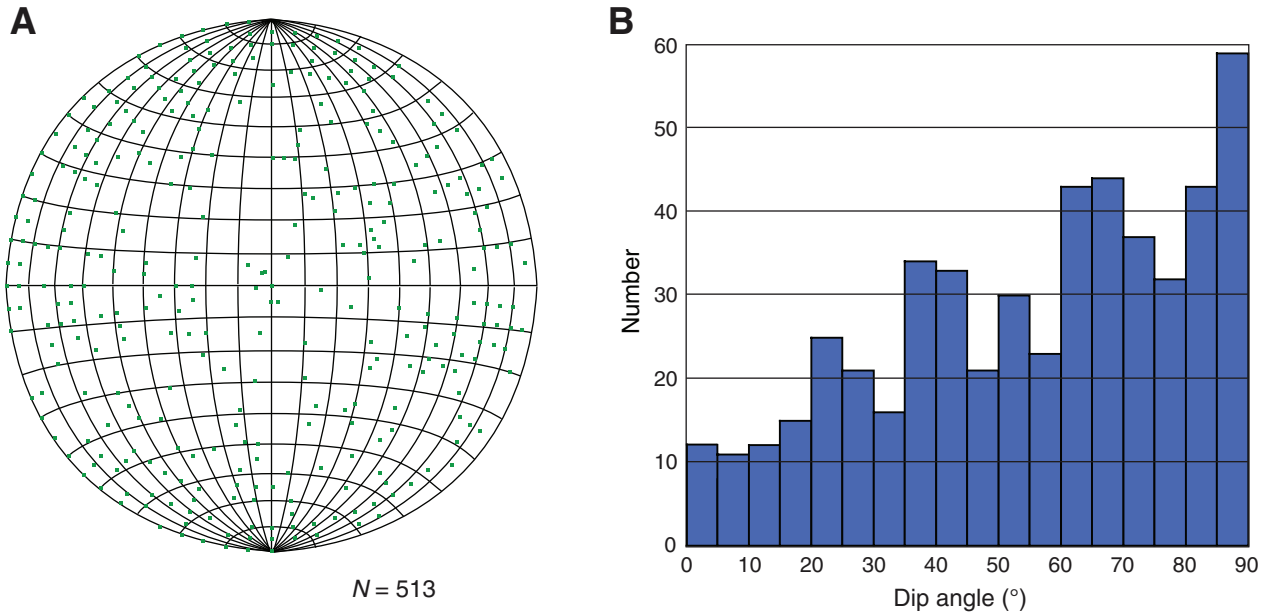

Figure F30. Distribution of true dip orientations of veins and fractures in Hole U1362A lithologic units.

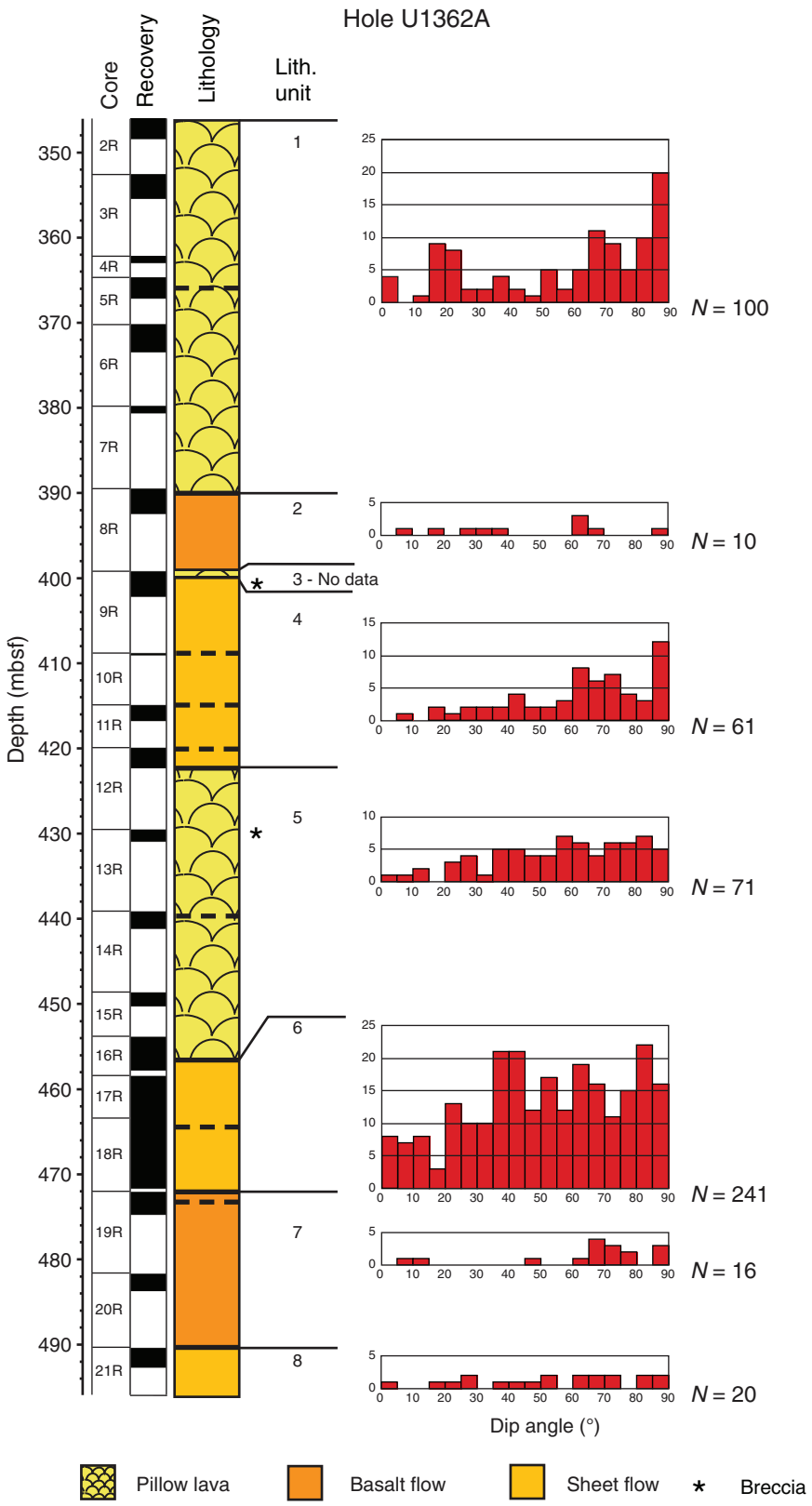

Figure F31. Comparative histograms for dip distribution of (**A**) haloed and (**B**) nonhaloed veins in all units.

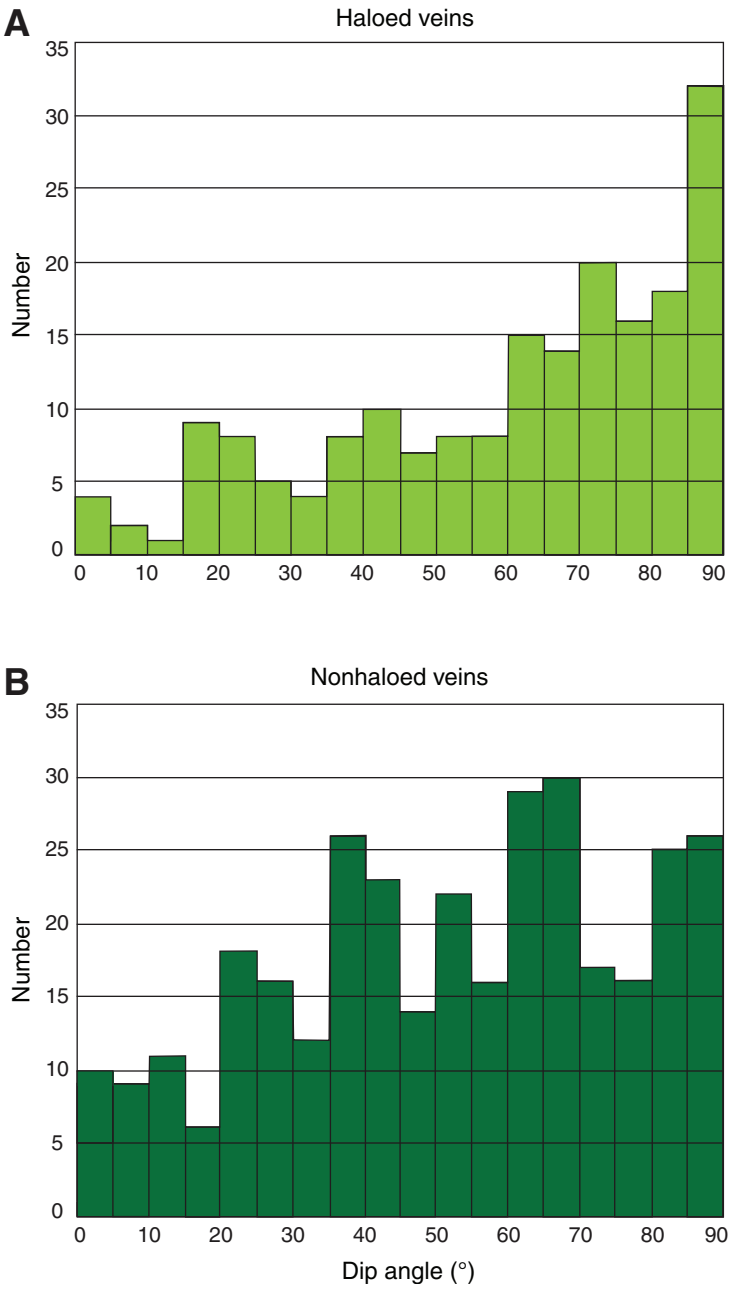

Figure F32. Composite 360° whole-round image of interval 327-U1362A-18R-1, 48–91 cm.

Figure F33. A, B. Plots of Hole U1362A *P*-wave velocities measured using manual and automated picking methods. A cubic sample has three velocities (V_{Px}, V_{Py}, and V_{Pz}), whereas a cylinder sample has one velocity (V_{Px}). **C.** Porosity from MAD measurements.

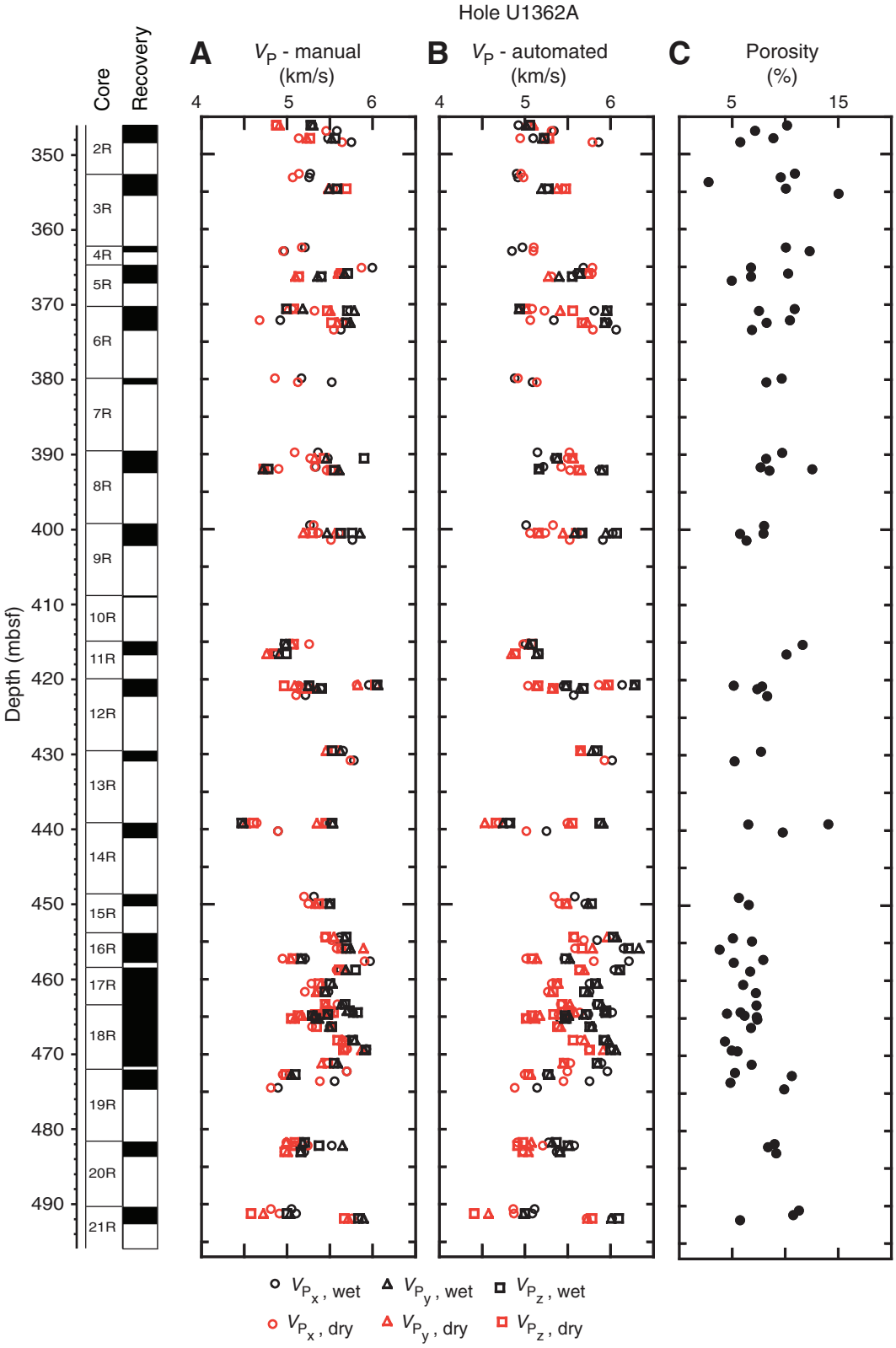

Figure F34. Plots of Hole U1362A physical properties. **A.** Gamma ray attenuation (GRA) and moisture and density (MAD) bulk densities. **B.** MAD grain density. **C.** Magnetic susceptibility from the Section Half Multisensor Logger (SHMSL) and the Whole-Round Multisensor Logger (WRMSL). **D.** Natural gamma radiation (NGR) counts per second (cps).

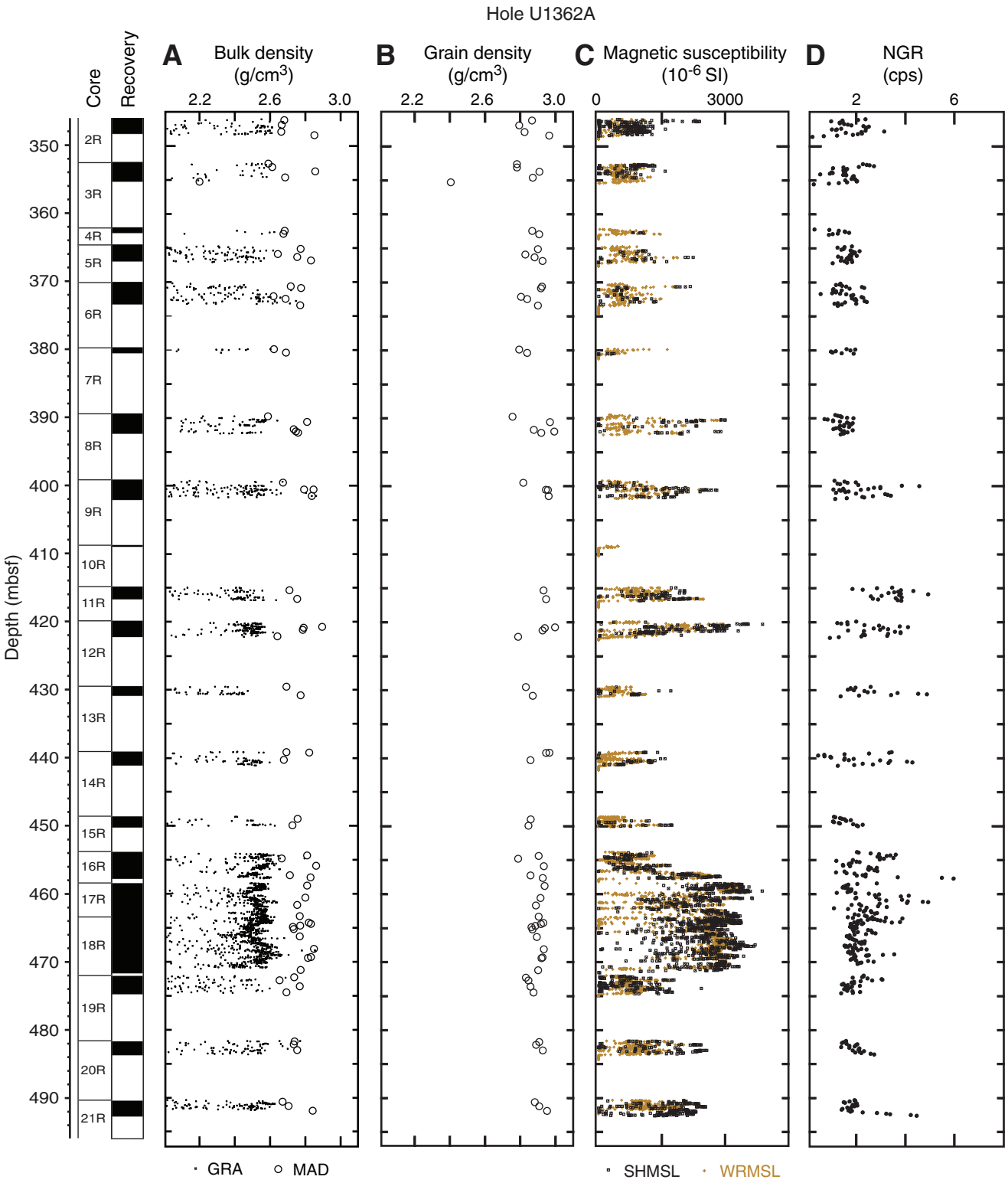

Figure F35. Plots of thermal conductivity data collected during Expeditions 327 and 301. Three values from Hole U1362A (means of multiple measurements of the same samples) are consistent with data collected from Hole U1301B during Expedition 301.

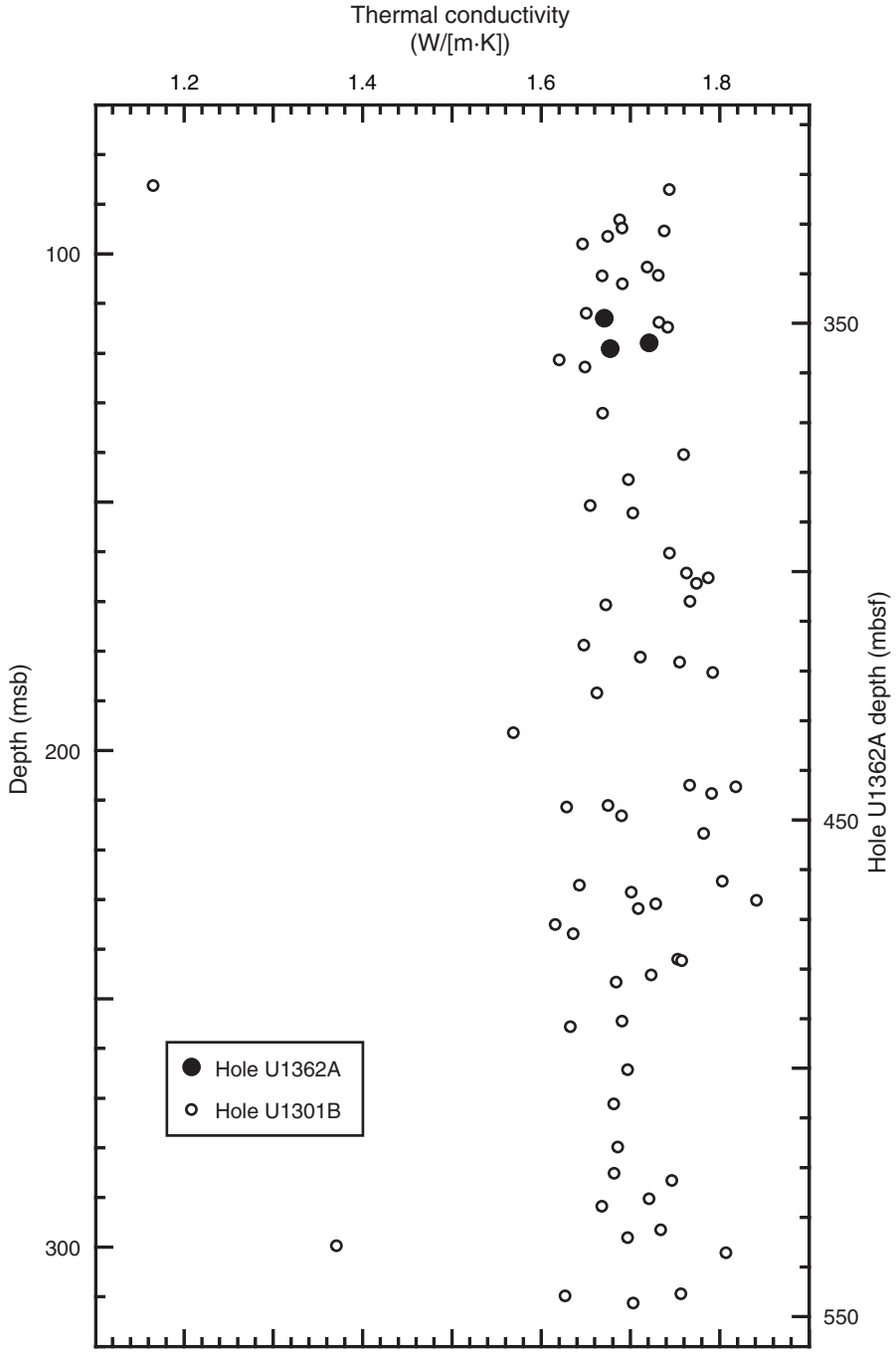

Figure F36. Plots of (**A**) automated and (**B**) manual *P*-wave velocity values vs. porosity, Hole U1362A.

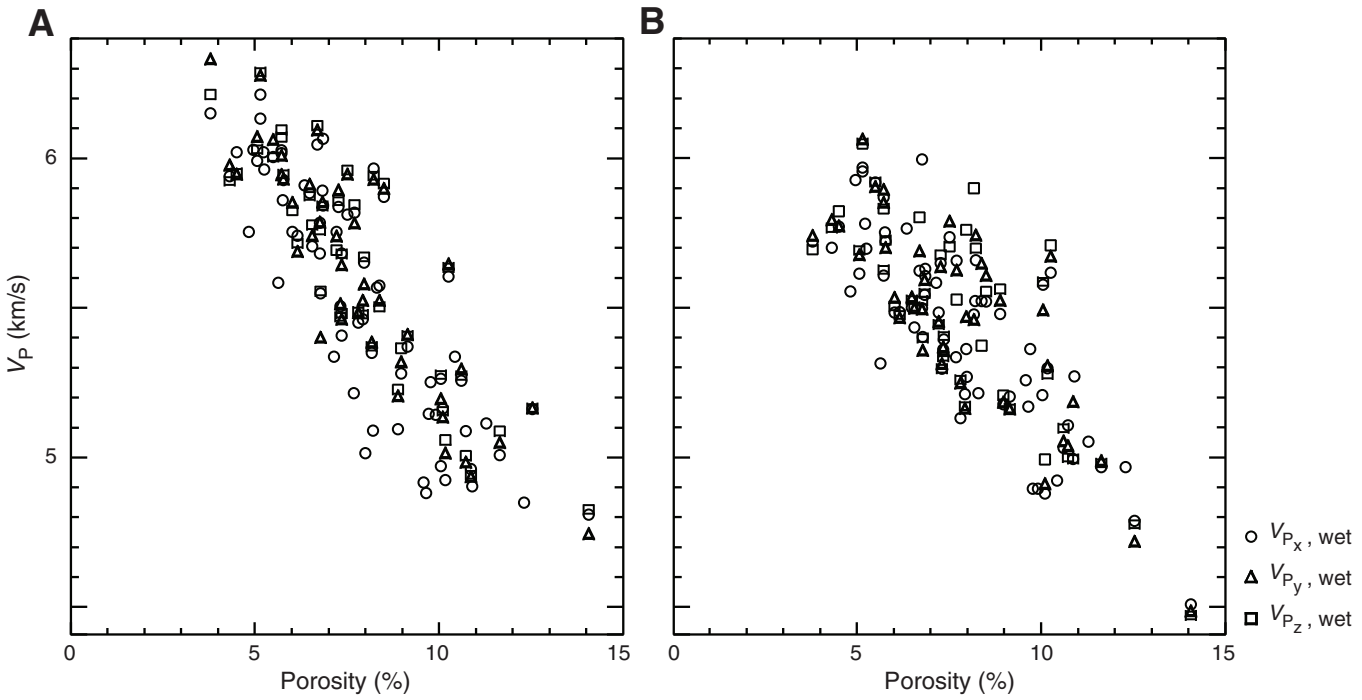

Figure F37. Demagnetization behavior of characteristic samples from Hole U1362A. **A.** Unit 1 example having an inclination value close to that expected for this location. **B.** Example of a steep inclination from Unit 4, possibly reflecting a drill string overprint. **C.** Example of inclination scatter seen in Unit 6, possibly indicating more intense alteration. **D.** Example of a rare negative inclination from Unit 8. Red squares = inclination values, blue circles = declination values. Solid lines = principal component analyses without the origin, dashed lines = principal component analyses anchored to the origin. NRM = natural remanent magnetization.

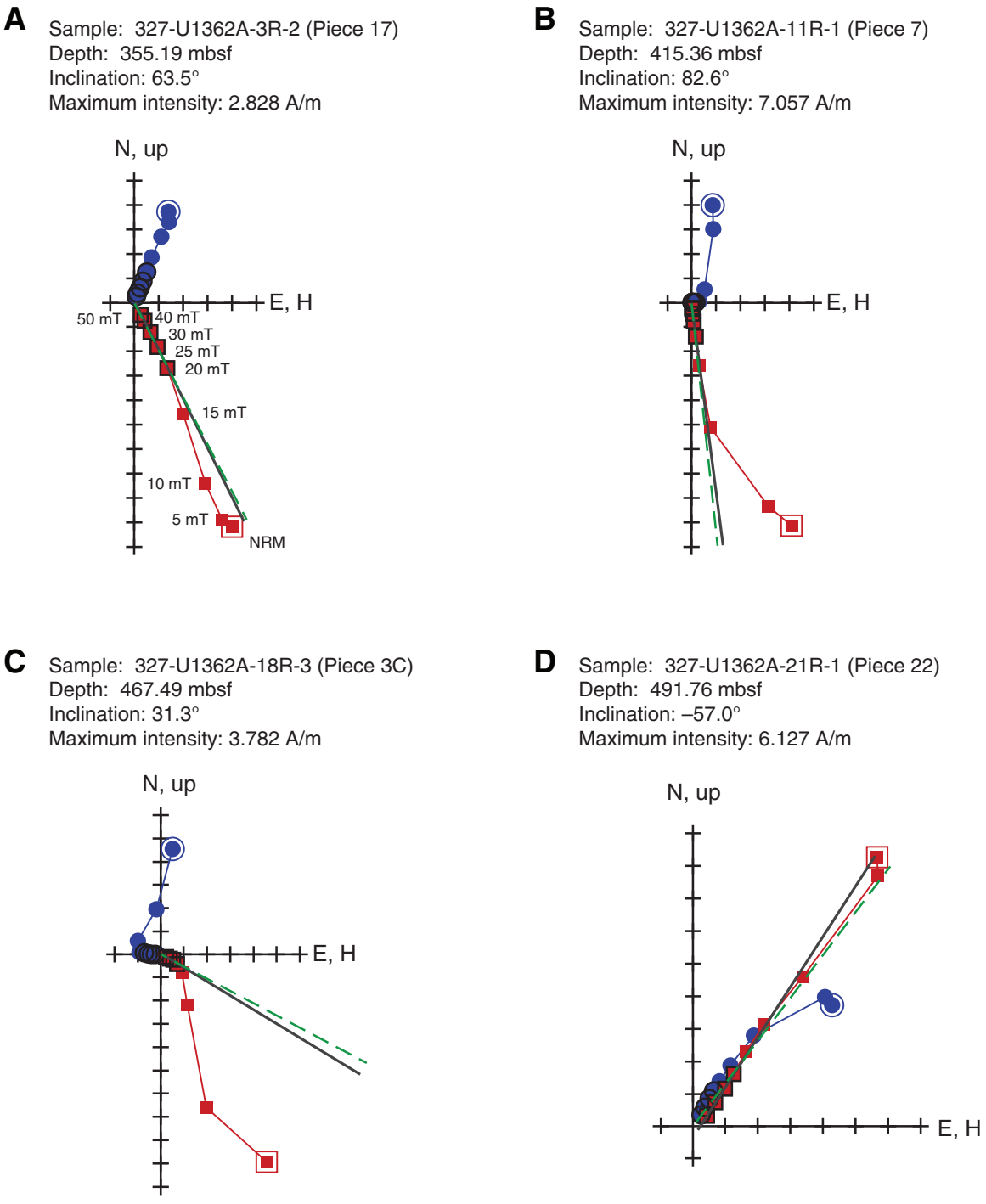

Figure F38. Plot of remanent magnetization intensity and inclination values vs. depth, Hole U1362A. Red circles = inclinations from discrete pieces at 30 mT, blue circles = inclinations from continuous sections at 30 mT, black squares = inclinations obtained from principal component analysis.

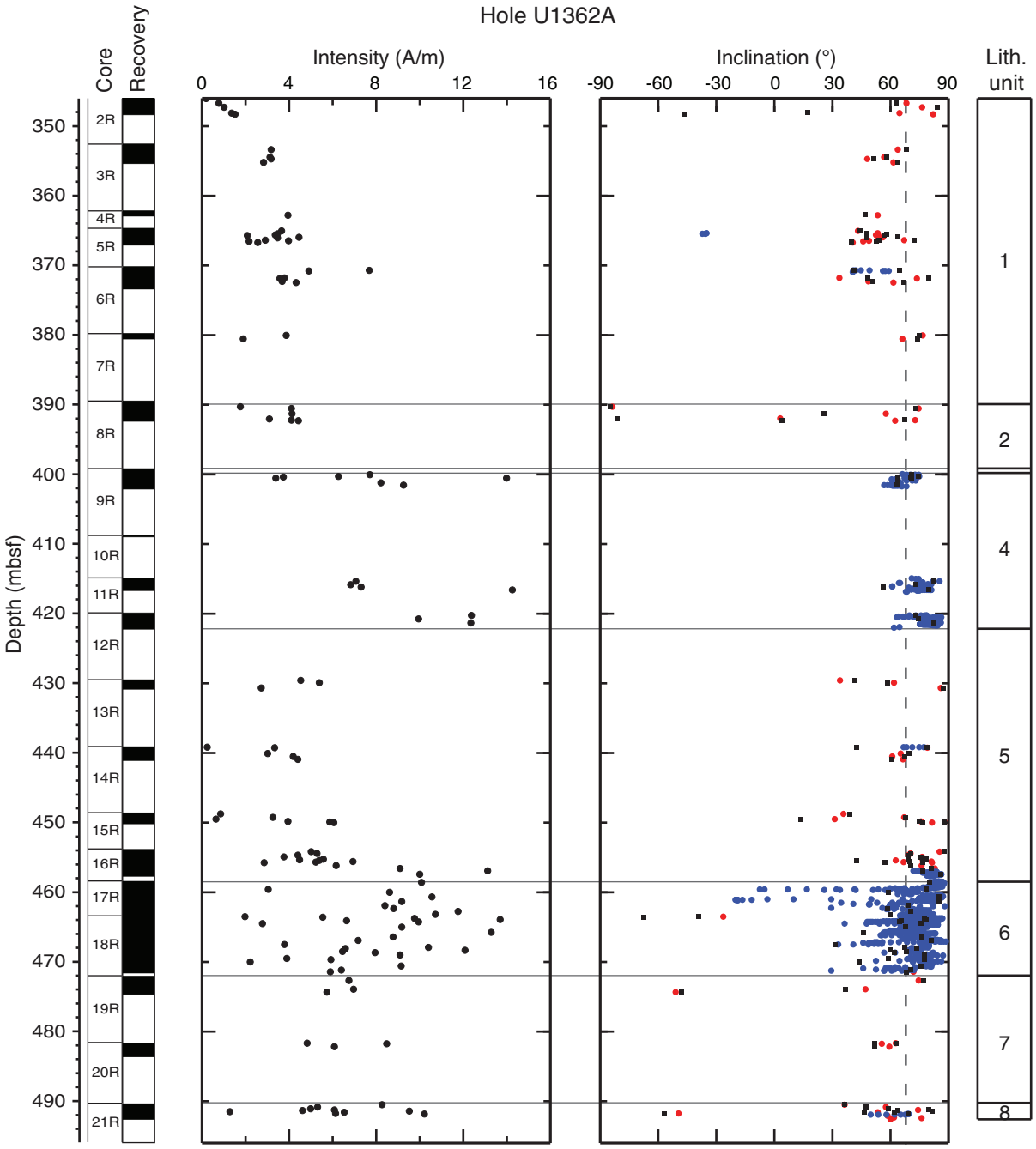

Figure F39. Plots of selected wireline logging measurements, Hole U1362A. All data are from the second logging pass. The mechanical single-arm caliper from the Hostile Environment Litho-Density Sonde (HLDS) is displayed. Total spectral gamma ray and computed potassium content are presented. Note that depth reflects the WMSF scale for logs and the CSF-A scale for core measurements. SP = spontaneous potential.

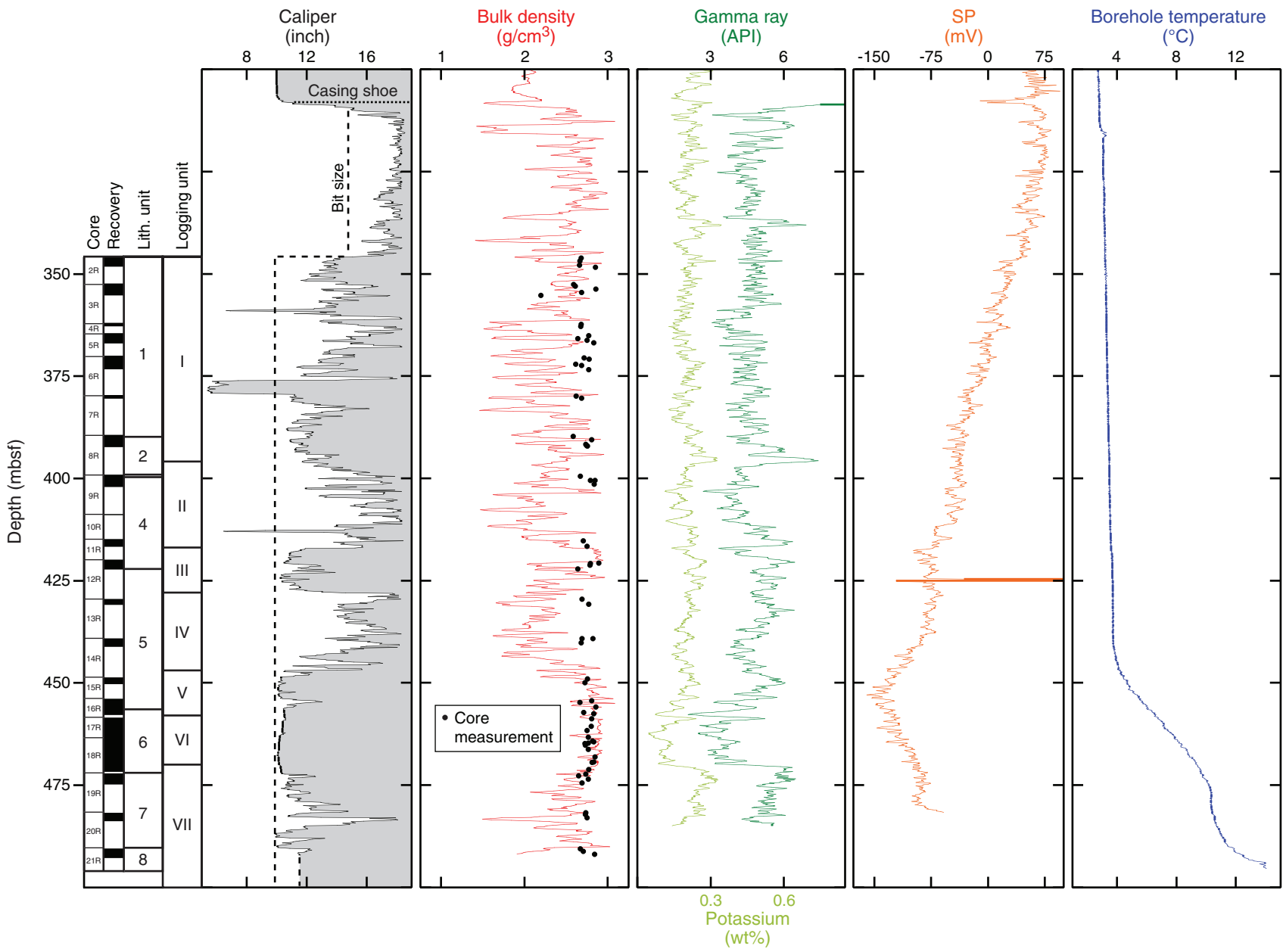

Figure F40. Plots of total gamma ray vs. potassium, thorium, and uranium. Total gamma ray in the 9⅝ inch section of Hole U1362A is strongly correlated with potassium content.

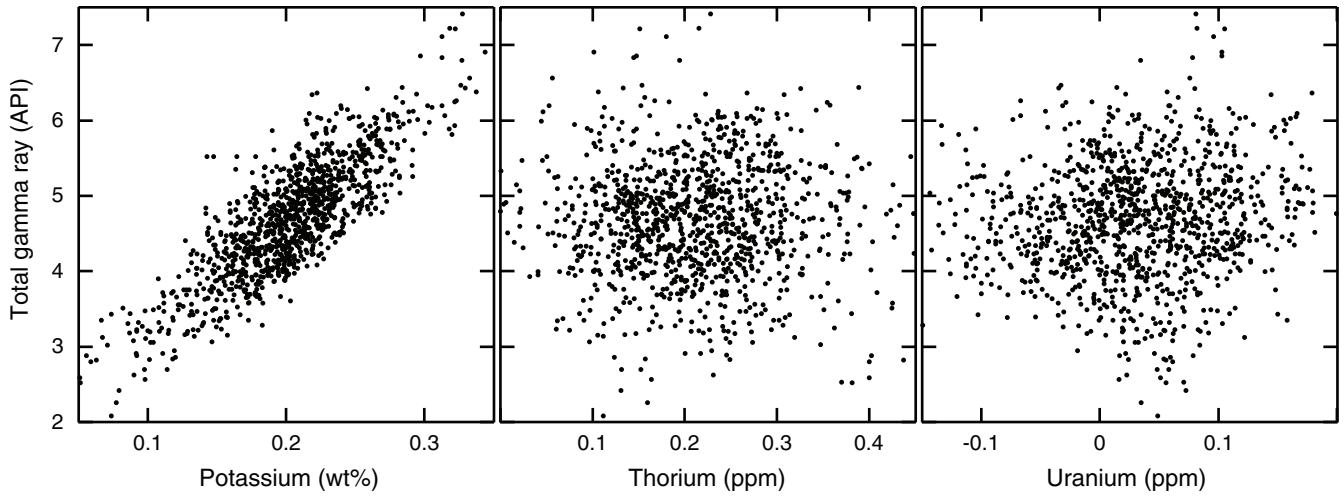

Figure F41. Plots of potassium oxide, caliper, and potassium vs. depth, Hole U1362A. Potassium oxide concentrations measured from core samples appear to loosely correspond to hole size and potassium content. ICP-AES = inductively coupled plasma–atomic emission spectroscopy, HLDS = Hostile Environment Litho-Density Sonde, HNGS = Hostile Environment Natural Gamma Ray Sonde.

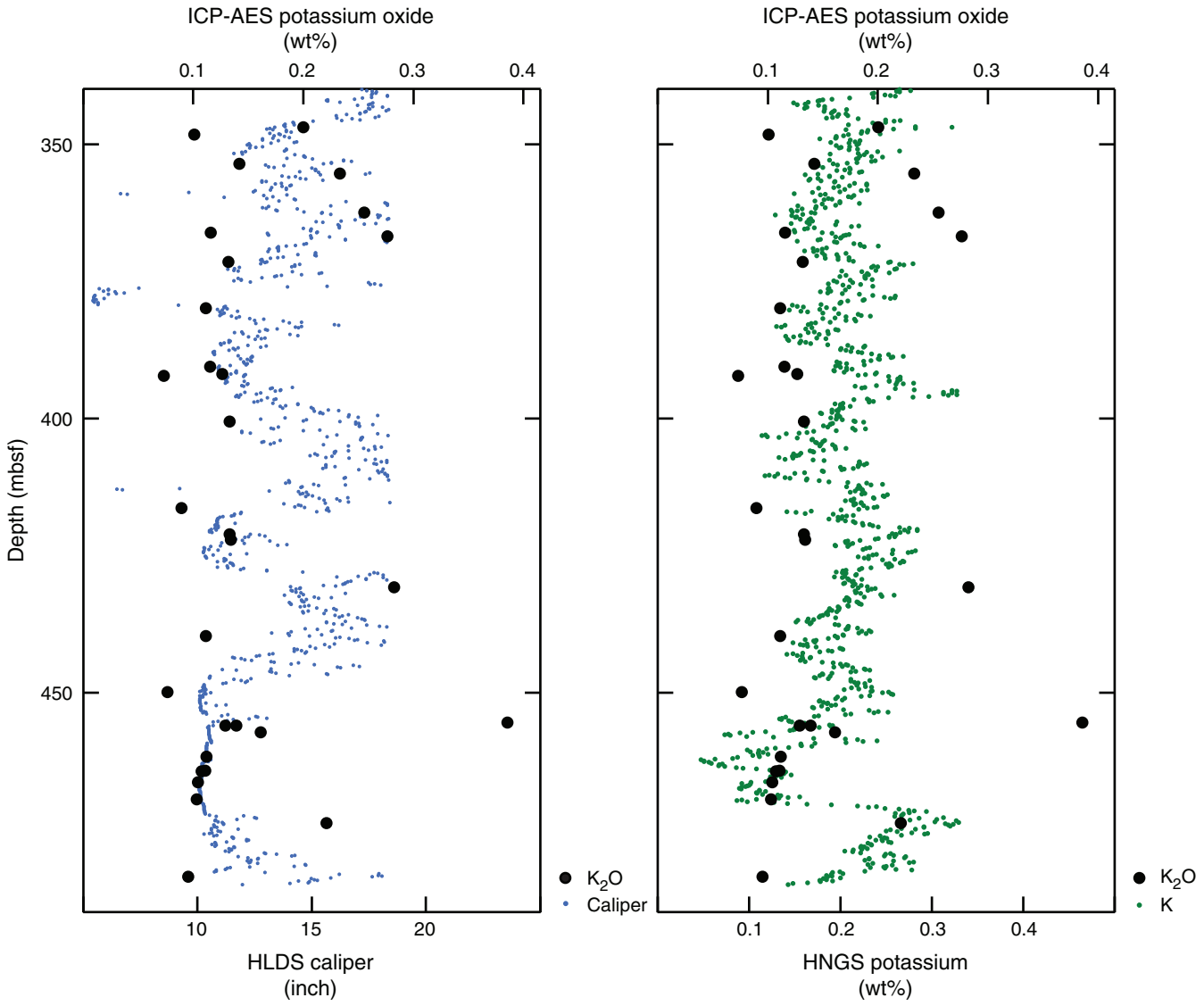

Figure F42. A. Plot of caliper and potassium vs. depth, Hole U1362A. **B.** Plot of caliper vs. potassium, Hole U1362A. Hole size and potassium content correlate poorly over the length of the 9⅞ inch section, except for the interval from 455 to 470 mbsf. HNGS = Hostile Environment Natural Gamma Ray Sonde, HLDS = Hostile Environment Litho-Density Sonde.

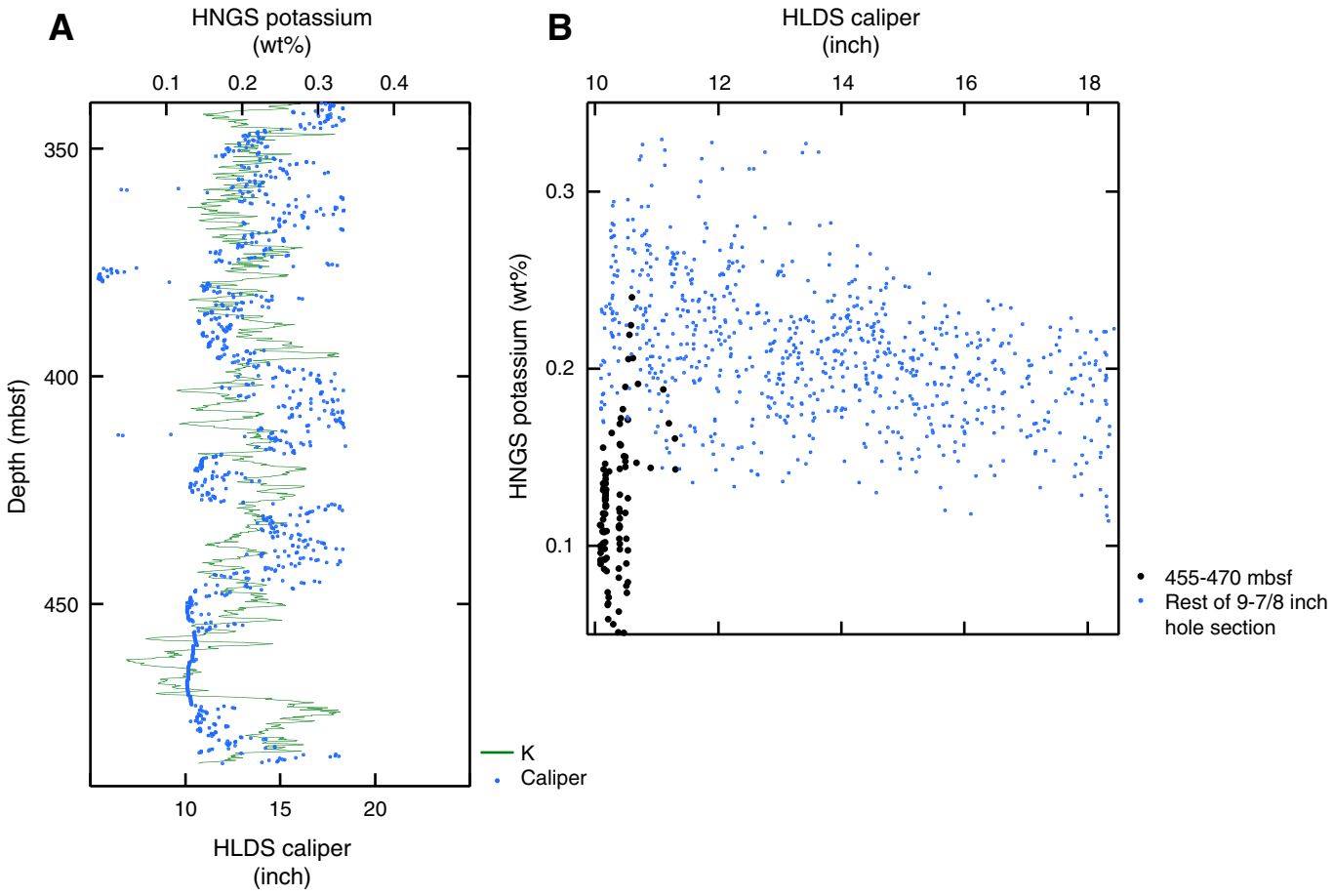

Figure F43. Plot of natural gamma radiation (NGR) core measurements and Hostile Environment Natural Gamma Ray Sonde (HNGS) gamma ray vs. depth, Hole U1362A.

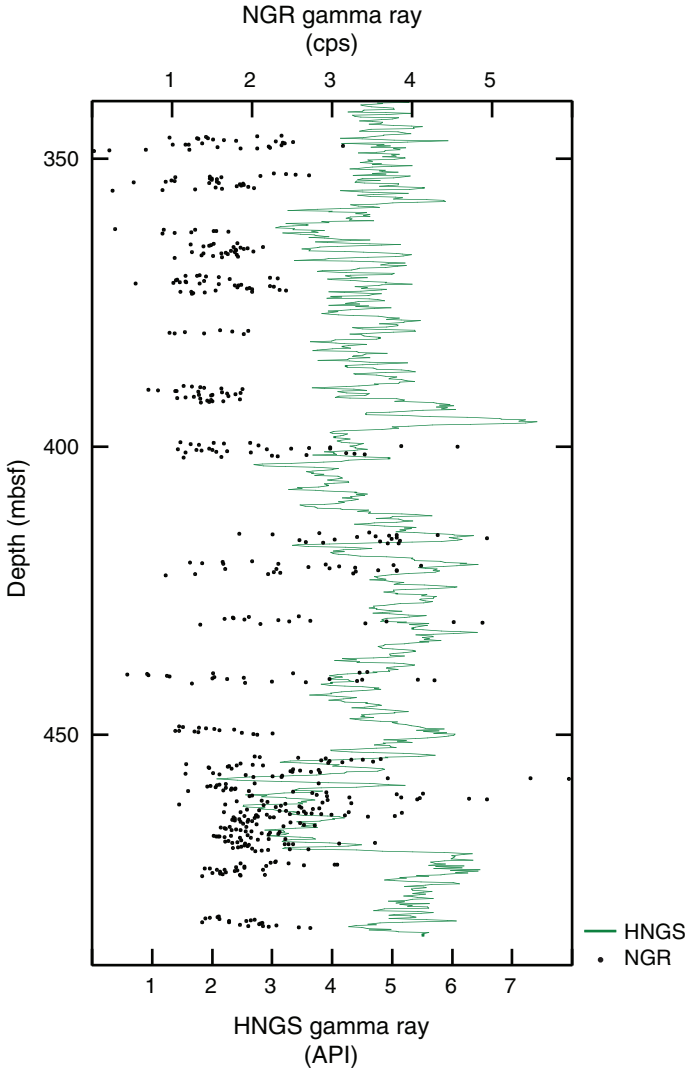

Figure F44. Selected Ultrasonic Borehole Imager (UBI) ultrasonic images from Hole U1362A. The images are displayed as unwrapped cylinders oriented to the north. Amplitude data show the amplitude of the reflected ultrasonic waveforms, whereas radius data were converted from the ultrasonic pulses' transit times. The corrected radius image virtually centers the UBI sonde within the borehole; it is apparent from the uncorrected radius image that the sound was eccentered through this interval. Dynamic normalization uses a color range for each depth interval based on maximum and minimum image values within a sliding 2 m window; static normalization establishes a range based on maximum and minimum image values over the entire imaged interval. **A.** Example of smeared interval with both vertical and rotational smearing. **B.** Example of apparently truncated image section. **C.** High-angle crosscutting feature (visible as a sinusoid) that may indicate transition from a pillow basalt interval to an underlying sheet flow.

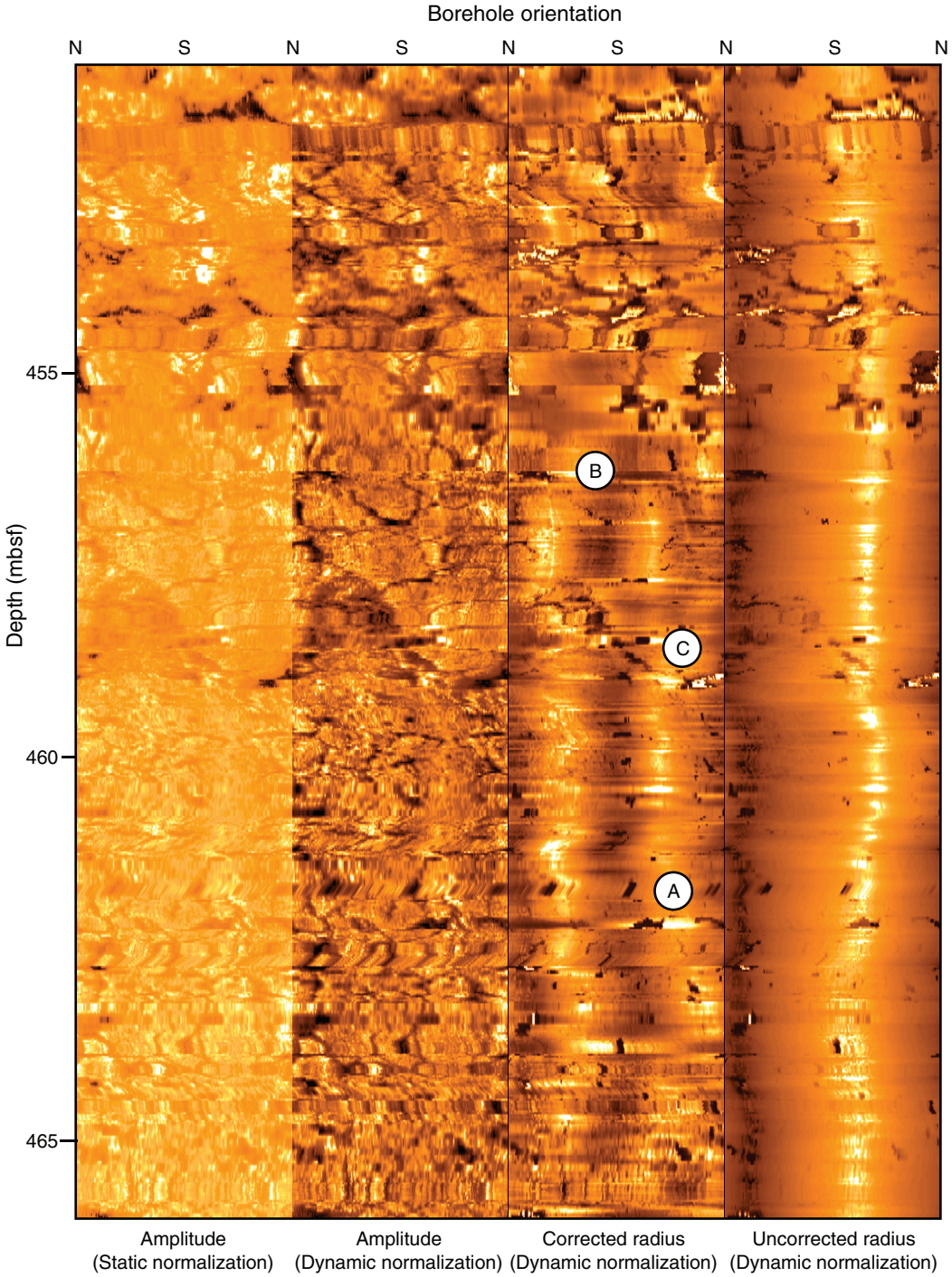

Figure F45. Plot of caliper readings from three logging passes vs. depth, Hole U1362A. The first pass shows an undergauge hole. The apparently tight interval is shorter and of smaller diameter in the second pass. No undergauge intervals are shown by the third pass. HLDS = Hostile Environment Litho-Density Sonde.

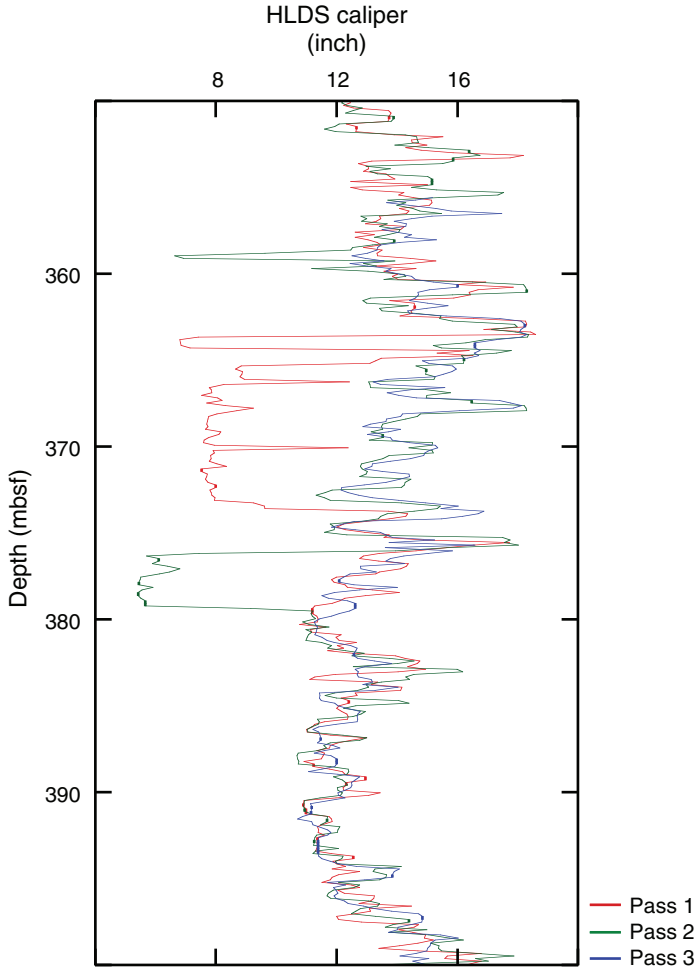

Figure F46. Pressure and temperature records collected with the Micro-Smart downhole electronic gauge during packer experiments in Hole U1362A.

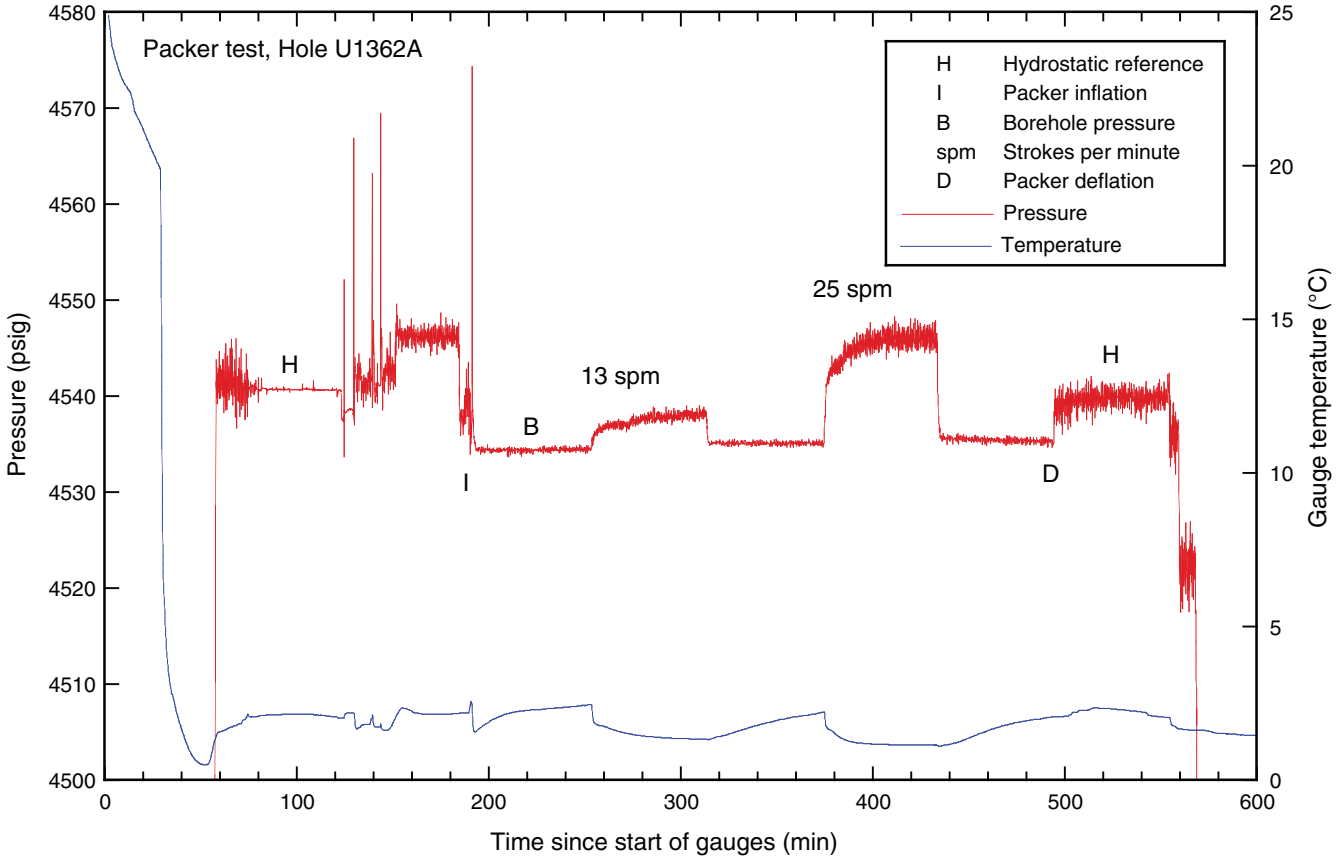

Figure F47. Pressure and temperature records collected with the Micro-Smart downhole electronic gauge during tracer injection tests in Hole U1362B. spm = strokes per minute.

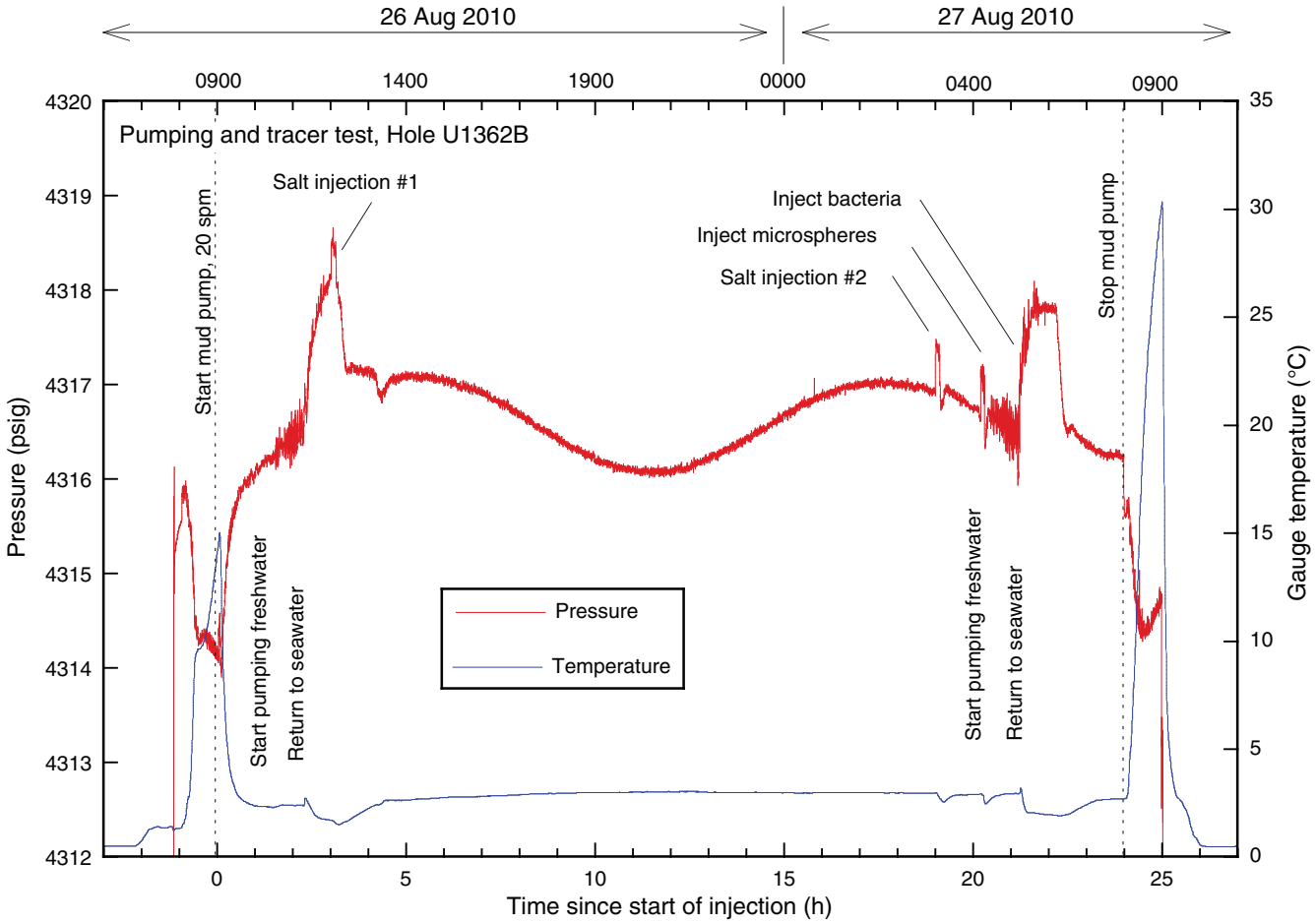

Figure F48. Diagram of Hole U1362A CORK completion. Diagram is greatly exaggerated horizontally to illustrate the geometry of the casing strings and other components, but the vertical scale is accurate.

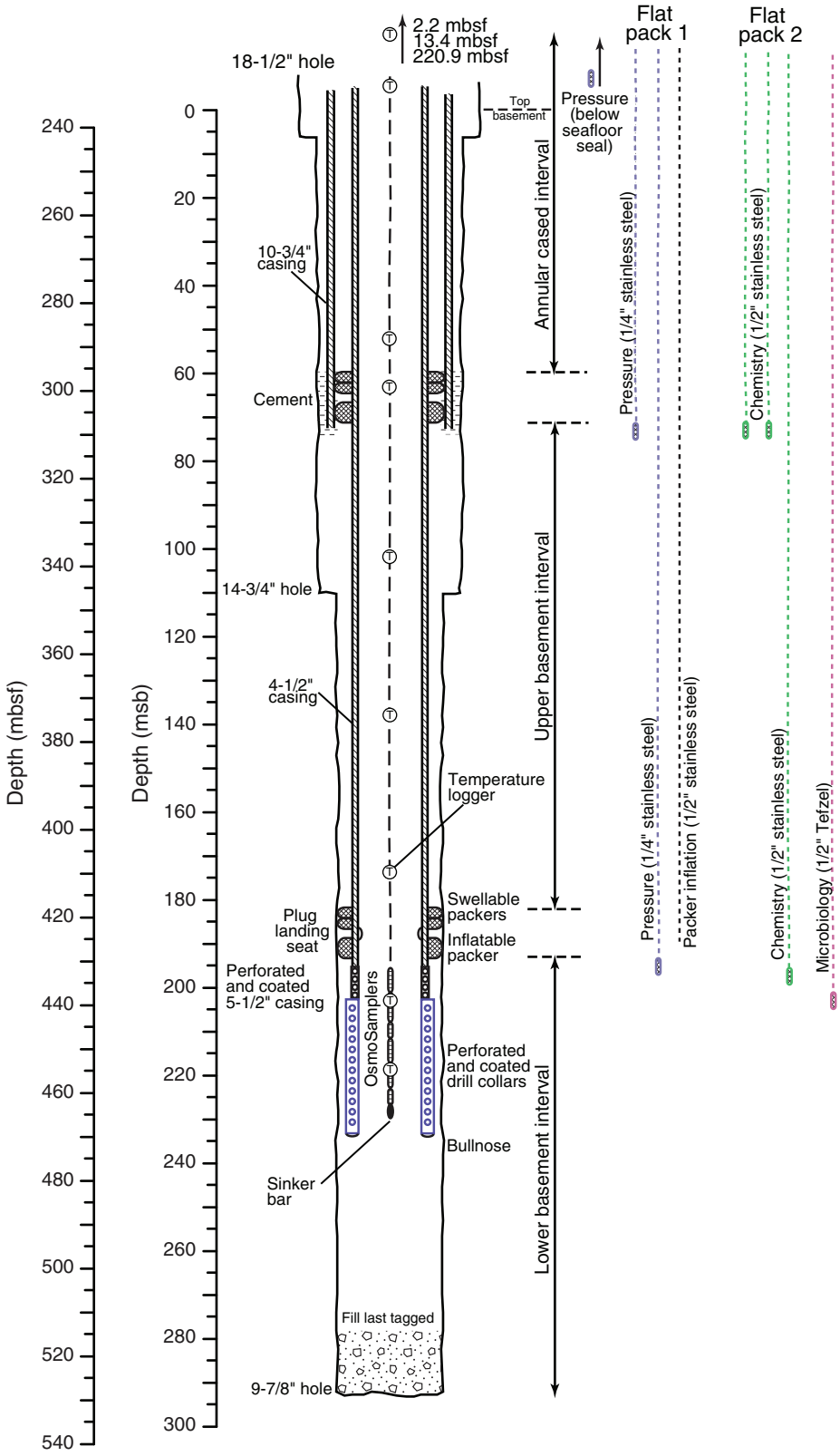

Figure F49. Diagram of Hole U1362B CORK completion. Diagram is greatly exaggerated horizontally to illustrate the geometry of the casing strings and other components, but the vertical scale is accurate.

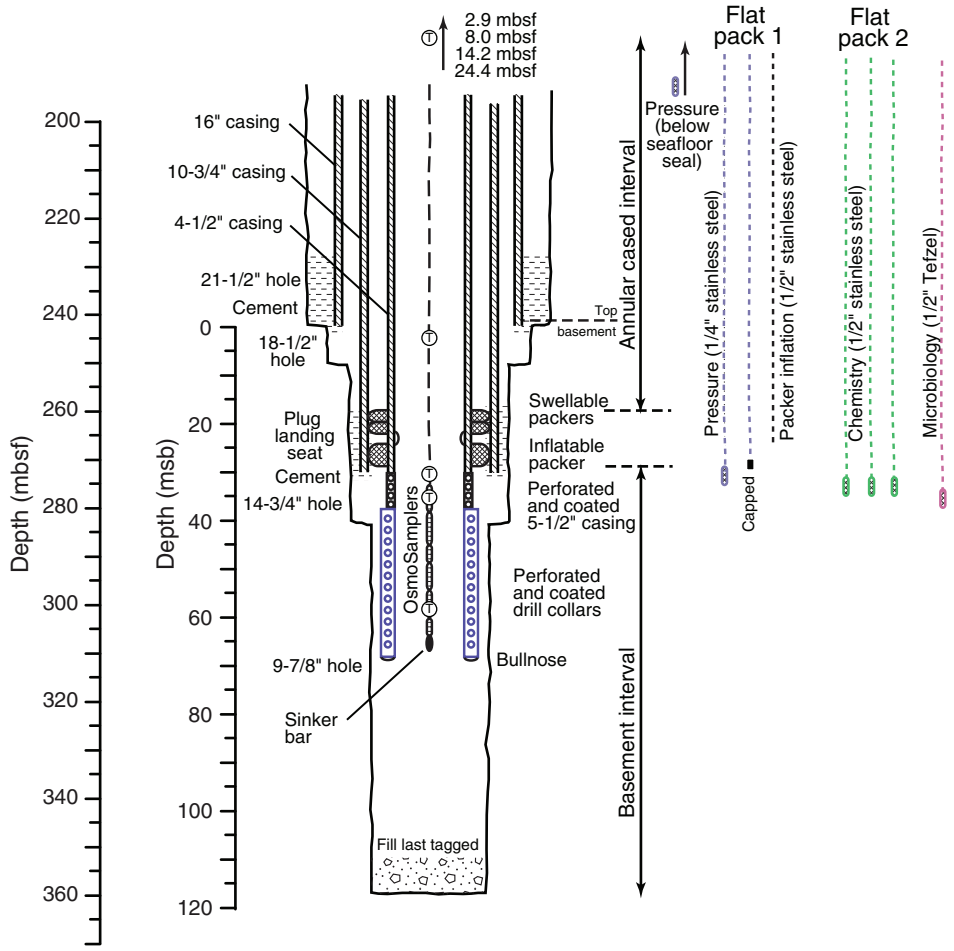

Table T1. Summary of operational depths, Hole U1362A. (See table note.)

Location	Depth			Comments
	mbrf	mbsf	msb	
Seafloor depth	2672.0	0.0	–236.0	
Basement depth	2908.0	236.0	0.0	Hard drilling, basalt chips recovered
21-1/2 inch hole	2908.0	235.7	0.0	Underreamer stopped at top of basement
18-1/2 inch hole	2914.0	242.0	6.0	Pilot bit below underreamer
14-3/4 inch hole	3018.0	346.0	110.0	Tricone bit
9-7/8 inch hole	3200.0	528.0	292.0	Tricone bits (coring, drilling)
20 inch casing shoe	2725.0	53.0	–183.0	
16 inch casing shoe	2902.0	230.0	–6.0	
10-3/4 inch casing shoe	2980.5	308.5	72.5	Shortened casing after initial attempt
CORK BHA (4-1/2 inch casing)	3141.7	469.7	233.7	End of bullnose below perforated collars
Base of cement below 10-3/4 inch casing	2981.0	309.0	73.0	Broke through when drilling out cement
Fill tagged in base of hole	3191.0	519.0	283.0	Just before packer experiments
Upper CORK packer seat top	2969.5	297.5	61.5	Element top, shallow swellable packer set
Upper CORK packer seat base	2979.3	307.3	71.3	Element base, shallow inflatable packer
Lower CORK packer seat top	3091.3	419.3	183.3	Element top, deep swellable packer set
Lower CORK packer seat base	3101.2	429.2	193.2	Element base, deep inflatable packer

Note: CORK = subseafloor borehole observatory, BHA = bottom-hole assembly.

Table T2. Summary of operational depths, Hole U1362B. (See table note.)

Location	Depth			Comments
	mbrf	mbsf	msb	
Seafloor depth	2672.0	0.0	–242.0	
Basement depth	2914.0	242.0	0.0	Hard drilling, basalt chips recovered
21-1/2 inch hole	2915.5	243.7	1.5	Underreamer slightly into basement
18-1/2 inch hole	2922.0	250.0	8.0	Pilot bit below underreamer
14-3/4 inch hole	2954.0	282.0	40.0	Tricone bit
9-7/8 inch hole	3031.0	359.0	117.0	Tricone bit
20 inch casing shoe	2725.0	53.0	–189.0	Includes tidal correction
16 inch casing shoe	2922.0	242.0	0.0	
10-3/4 inch casing shoe	2944.0	272.0	30.0	
CORK BHA (4-1/2 inch casing)	2979.9	311.0	69.0	End of bullnose below perforated collars
Base of cement below 10-3/4 inch casing	2954.0	282.0	40.0	Broke through when drilling out cement
Fill tagged in base of hole	3020.0	348.0	106.0	After injection test
Upper CORK packer seat top	2933.2	261.2	19.2	Element top, shallow swellable packer set
Upper CORK packer seat base	2943.1	271.1	29.1	Element base, shallow inflatable packer

Note: CORK = subseafloor borehole observatory, BHA = bottom-hole assembly.

Table T3. Coring summary, Site U1362. (See table notes.)

Hole U1362A
Latitude: 47°45.6628′N
Longitude: 127°45.6720′W
Time on hole (h): 719 (30 days)
Seafloor (drill pipe measurement from rig floor, m DRF): 2672
Distance between rig floor and sea level (m): 11.3
Water depth (drill pipe measurement from sea level, m): 2661.1
Total penetration (drilling depth below seafloor, m DSF): 528
Total length of cored section (m): 150
Total core recovered (m): 44.4
Core recovery (%): 30
Total number of cores: 20

Hole U1362B
Latitude: 47°45.4997′N
Longitude: 127°45.7312′W
Time on hole (h): 427 (17.8 days)
Seafloor (drill pipe measurement from rig floor, m DRF): 2672
Distance between rig floor and sea level (m): 11.3
Water depth (drill pipe measurement from sea level, m): 2661.1
Total penetration (drilling depth below seafloor, m DSF): 359
Total length of cored section (m): 0
Total core recovered (m): 0
Core recovery (%): 0
Total number of cores: 0

Core	Date (2010)	Time (UTC)	Depth DSF (m) Top of cored interval	Depth DSF (m) Bottom of cored interval	Interval advanced (m)	Length of core recovered (m)	Recovery (%)	Comments
327-U1362A-								
11	12 Jul	1800	***** Drilled from 0.0 to 53.5 m DSF *****					Drilled interval for 20 inch casing
12	14 Jul	0315	***** Drilled from 53.5 to 230.0 m DSF *****					Drilled interval for 16 inch casing
13	14 Jul	0345	***** Drilled from 230.0 to 236.0 m DSF *****					Drilled interval for 16 inch casing
14	21 Jul	1400	***** Drilled from 236.0 to 308.0 m DSF *****					Drilled interval for 10-3/4 inch casing
15	22 Jul	0930	***** Drilled from 308.0 to 346.0 m DSF *****					Drilled interval for 10-3/4 inch casing
2R	1 Aug	1235	346.0	352.6	6.6	1.99	30	
3R	1 Aug	1825	352.6	362.2	9.6	2.14	22	
4R	1 Aug	2135	362.2	364.7	2.5	0.58	23	
5R	2 Aug	0730	364.7	370.2	5.5	1.95	35	
6R	2 Aug	1600	370.2	379.8	9.6	2.42	25	
7R	3 Aug	1120	379.8	389.5	9.7	0.69	7	
8R	3 Aug	1610	389.5	399.2	9.7	2.22	23	
9R	3 Aug	2320	399.2	408.8	9.6	2.48	26	
10R	4 Aug	1030	408.8	414.9	6.1	0.24	4	
11R	4 Aug	1620	414.9	419.9	5.0	1.50	30	
12R	4 Aug	2300	419.9	429.5	9.6	2.17	23	
13R	5 Aug	0605	429.5	439.1	9.6	1.00	10	
14R	5 Aug	1230	439.1	448.6	9.5	1.62	17	
15R	7 Aug	0045	448.6	453.8	5.2	1.12	22	
16R	7 Aug	0845	453.8	458.4	4.6	3.36	73	
17R	7 Aug	1620	458.4	463.4	5.0	5.59	112	
18R	8 Aug	0045	463.4	472.0	8.6	7.50	87	
19R	8 Aug	1050	472.0	481.6	9.6	2.06	21	
20R	8 Aug	1615	481.6	490.3	8.7	1.74	20	
21R	8 Aug	1955	490.3	496.0	5.7	2.04	36	
221	10 Aug	1700	***** Drilled from 496.0 to 528.0 m DSF *****					Drilled interval for 9-7/8 inch hole
			Hole U1362A totals:		528.0	45.27	32.3	
327-U1362B-								
11	17 Jul	1700	***** Drilled from 0.0 to 53.5 m DSF *****					Drilled interval for 20 inch casing
12	18 Jul	2000	***** Drilled from 53.5 to 242.0 m DSF *****					Drilled interval for 16 inch casing
13	18 Jul	2200	***** Drilled from 242.0 to 250.0 m DSF *****					Drilled interval for 16 inch casing
14	31 Jul	2345	***** Drilled from 250.0 to 272.0 m DSF *****					Drilled interval for 10-3/4 inch casing
15	22 Aug	1910	***** Drilled from 272.0 to 339.0 m DSF *****					Drilled interval for 10-3/4 inch casing
16	25 Aug	0700	***** Drilled from 339.0 to 359.0 m DSF *****					Drilled interval for 9-7/8 inch hole
			Hole U1362B totals:		359.0	0.94	0	
			Site U1362 totals:		887.0	46.21		

Notes: DRF = drilling depth below rig floor, DSF = drilling depth below seafloor. UTC = Universal Time Coordinated. R = rotary core barrel core, numeric core type = drilled interval.

Table T4. Lithologic units, Hole U1362A.

Lith. unit	Core, section, interval (cm)	Depth (mbsf) Top	Depth (mbsf) Bottom	Unit thickness (m)	Unit lithology	Flow type
	327-U1362A-					
1A	2R-1 to 5R-1, 125	346.00	365.96	19.96	Sparsely plagioclase-clinopyroxene phyric microcrystalline basalt	Pillow
1B	5R-1, 125, to 8R-1, 46.5	365.96	389.97	24.01	Moderately olivine-clinopyroxene plagioclase phyric microcrystalline basalt	Pillow
2	8R-1, 46.5, to 8R-2	389.97	399.20	9.23	Moderately olivine-clinopyroxene phyric fine grained	Basalt flow
3	9R-1, 0–60.5	399.20	399.81	0.61	Sparsely clinopyroxene-plagioclase phyric cryptocrystalline basalt	Pillow
4A	9R-1, 60.5, through 9R-2	399.81	408.80	8.99	Sparsely (olivine) clinopyroxene-plagioclase phyric microcrystalline basalt	Sheet flow
4B	10R-1	408.80	414.90	6.10	Moderately olivine-clinopyroxene-plagioclase phyric cryptocrystalline basalt	Sheet flow
4C	11R-1 to 12R-1, 11	414.90	420.01	5.11	Aphyric fine grained	Sheet flow
4D	12R-1, 11, to 12R-2, 104	420.01	422.23	2.22	Moderately plagioclase-clinopyroxene phyric microcrystalline	Sheet flow
5A	12R-2, 104, to 14R-1, 32	422.23	439.42	17.19	Moderately clinopyroxene-plagioclase phyric cryptocrystalline basalt	Pillow
5B	14R-1, 32, to 16R-2, 120	439.42	456.50	17.08	Highly clinopyroxene-plagioclase phyric cryptocrystalline basalt	Pillow
6A	16R-2, 120, through 17R-5	456.50	464.38	7.88	Sparsely clinopyroxene-plagioclase phyric microcrystalline basalt	Sheet flow
6B	18R-1 through 18R-6	463.40	472.00	8.60	Sparsely clinopyroxene phyric microcrystalline basalt	Sheet flow
7A	19R-1, 0–121.5	472.00	473.22	1.22	Sparsely plagioclase phyric microcrystalline	Basalt flow
7B	19R-1, 121.5, through 20R-2	473.22	490.30	17.08	Highly clinopyroxene-plagioclase phyric cryptocrystalline	Basalt flow
8	21R-1 through 21R-2	490.30	496.00	5.70	Sparsely plagioclase-clinopyroxene phyric microcrystalline basalt	Sheet flow

Table T5. X-ray diffraction analyses, Hole U1362A. (See table note.)

Core, section, interval (cm)	Depth (mbsf) Top	Depth (mbsf) Bottom	Minerals
327-U1362A-			
13-1, 12–18	230.12	230.18	Pyrite, albite, gismondine
13-1, 27–34	230.27	230.34	Phillipsite, saponite, sepiolite
2R-1, 43–47	346.43	346.47	Saponite, calcite
3R-1, 22–24	352.82	352.84	Phillipsite, saponite
3R-2, 44–46	354.51	354.53	Albite, augite, sepiolite(?)
12R-1, 34–36	420.24	420.26	Albite, augite, saponite(?)
14R-2, 52–54	440.83	440.85	Montmorillonite, talc, calcite magnesian
16R-2, 56–119	455.86	456.49	Montmorillonite, talc, calcite magnesian
18R-1, 48–58	463.88	463.98	Quartz, talc(?)

Note: Sepiolite is interpreted as contamination from drilling mud.

Table T6. SEM analyses of two epidote crystals from the drill bit samples of Hole U1362A. Multiple spots within each crystal were analyzed for major oxides.

Major element oxide (wt%)	Epidote A 1	Epidote A 2	Epidote A 3	Epidote A 4	Epidote B 1	Epidote B 2	Epidote B 3
SiO_2	37.3	38.2	37.2	37.0	42.5	42.1	42.4
Al_2O_3	18.9	18.8	18.7	19.3	22.3	22.2	22.4
Fe_2O_3	17.4	17.0	17.8	17.6	11.8	12.2	12.5
MnO	0.0	0.0	0.0	0.0	0.1	0.2	0.2
MgO	0.8	0.6	0.3	0.8	0.9	1.2	0.9
CaO	24.0	24.2	24.1	23.8	20.2	19.9	20.0
Na_2O	0.1	0.1	0.3	0.4	1.0	1.2	0.7
PO_4	1.2	0.8	0.6	0.8	0.7	0.4	0.7
K_2O	0.1	0.1	0.1	0.1	0.3	0.3	0.2
TiO_2	0.1	0.1	0.5	0.2	0.1	0.3	0.0
Totals:	100.0	100.0	99.5	100.0	100.0	100.0	100.0

Table T7. ICP-AES analyses, Hole U1362A. (See table notes.) (Continued on next two pages.)

Hole:	327-U1362A-											
Core, section:	2R-1	2R-2	3R-1	3R-2	4R-1	5R-1	5R-2	6R-1	7R-1	8R-1	8R-2	8R-2
Interval (cm):	92–94	73–83	95–99	127–130	26–29	147–149	58–61	128–131	6–8	113–117	100–102	126–128
Unit/Subunit:	1A	1A	1A	1A	1A	1B	1B	1B	1B	2	2	2
Depth (mbsf):	346.93	348.28	353.57	355.355	362.475	366.18	366.795	371.495	379.87	390.65	391.98	392.24
Sample:	WDGE 2390221	WDGE 2390231	WDGE 2390251	WDGE 2390271	WDGE 2390321	WDGE 2390351	WDGE 2392651	WDGE 2392701	WDGE 2395851	WDGE 2395901	WDGE 2395951	WDGE 2395971
Major element oxide (wt%):												
SiO_2	49.46	49.49	48.73	49.72	48.18	49.69	47.90	50.97	50.03	49.44	49.90	49.88
Al_2O_3	14.85	15.00	14.68	15.61	15.27	15.40	14.68	15.59	16.14	15.38	15.31	15.48
Fe_2O_3	10.39	9.21	10.00	10.81	9.91	9.18	10.57	10.04	9.78	10.44	10.51	10.13
MnO	0.17	0.16	0.17	0.17	0.17	0.16	0.17	0.16	0.17	0.17	0.18	0.15
MgO	7.53	7.76	7.54	7.73	7.43	7.83	7.57	8.19	7.61	7.40	7.49	7.90
CaO	11.79	11.55	11.60	12.37	11.71	11.75	11.94	12.24	12.27	11.64	11.99	11.89
Na_2O	2.75	2.84	2.60	2.70	2.65	2.72	2.59	2.74	2.67	2.84	2.79	2.90
K_2O	0.20	0.10	0.14	0.23	0.26	0.12	0.28	0.13	0.11	0.11	0.13	0.07
TiO_2	1.66	1.68	1.44	1.50	1.48	1.50	1.47	1.52	1.46	1.80	1.77	1.78
P_2O_5	0.13	0.13	0.11	0.12	0.11	0.11	0.09	0.11	0.11	0.12	0.12	0.12
Totals:	98.95	97.92	97.02	100.96	97.17	98.46	97.27	101.69	100.35	99.34	100.18	100.31
Trace element (ppm):												
Ba	16	17	16	12	15	16	17	17	12	11	13	17
Co	55	60	53	54	59	77	56	54	55	73	60	55
Cr	171	153	140	176	155	157	162	166	129	132	132	129
Cu	87	79	77	93	87	99	77	88	84	59	64	76
Ni	57	96	73	64	97	112	70	73	87	98	70	68
Sc	48	47	44	47	47	47	45	48	44	50	50	51
Sr	127	127	111	116	115	117	111	117	117	120	119	122
V	326	343	312	327	326	332	316	328	323	374	367	372
Zn	93	93	88	90	91	91	91	91	90	76	95	98
Zr	104	107	89	93	89	92	89	93	89	112	109	109
LOI (wt%)	0.72	0.83	0.63	0.64	1.11	0.53	0.69	0.75	0.99	1.22	1.24	1.07
Mg#	61.47	64.96	62.42	61.15	62.28	65.25	61.21	64.22	63.15	60.94	61.06	63.19

Notes: ICP-AES = inductively coupled plasma–atomic emission spectroscopy. LOI = loss on ignition. Mg# = $(MgO/40.305)/[(MgO/40.305) + 0.9 \times 2 \times (Fe_2O_3/159.694)] \times 100$.

Table T7 (continued). (Continued on next page.)

Hole:	327-U1362A-											
Core, section:	9R-2	11R-2	12R-1	12R-2	13R-1	14R-1	15R-1	16R-2	16R-3	17R-3	17R-5	18R-1
Interval (cm):	25–27	0–23	127–129	93–95	130–132	64–66	133–135	17–20	58–60	49–51	55–57	101–103
Unit/Subunit:	4A	4C	4D	4D	5A	5B	5B	5B	6A	6A	6A	6B
Depth (mbsf):	400.623	416.36	421.18	422.13	430.81	439.75	449.94	455.485	457.29	461.68	464.22	464.42
Sample:	WDGE 2397161	WDGE 2397231	WDGE 2399041	WDGE 2399071	WDGE 2399111	WDGE 2399691	WDGE 2399741	WDGE 2399771	WDGE 2399831	WDGE 2402061	WDGE 2402071	WDGE 2402911
Major element oxide (wt%):												
SiO_2	50.26	49.19	49.47	51.29	48.26	50.70	49.70	50.08	49.01	47.64	49.64	50.57
Al_2O_3	15.39	14.38	15.77	15.35	14.24	15.94	15.59	15.08	15.23	14.70	14.55	14.91
Fe_2O_3	10.23	11.65	10.27	9.67	12.94	10.53	9.59	11.38	11.36	10.94	11.75	11.80
MnO	0.14	0.18	0.15	0.17	0.24	0.16	0.16	0.18	0.15	0.15	0.16	0.16
MgO	7.77	7.37	7.78	7.70	6.18	7.02	7.48	7.22	7.77	6.66	7.34	7.37
CaO	11.04	11.94	11.21	12.12	10.78	12.43	12.11	11.99	10.85	10.88	11.41	11.69
Na_2O	3.01	2.63	2.98	2.89	2.93	2.83	2.71	2.62	3.00	2.82	2.79	2.85
K_2O	0.13	0.09	0.13	0.13	0.28	0.11	0.08	0.39	0.16	0.11	0.11	0.11
TiO_2	1.81	1.69	1.78	1.77	2.53	1.51	1.47	1.44	1.77	1.66	1.66	1.69
P_2O_5	0.12	0.11	0.13	0.13	0.19	0.11	0.11	0.09	0.11	0.11	0.11	0.11
Totals:	99.91	99.24	99.67	101.22	98.58	101.34	98.99	100.47	99.41	95.69	99.52	101.26
Trace element (ppm):												
Ba	19	71	18	16	30	15	17	16	15	18	18	21
Co	62	51	64	52	75	63	54	55	53	57	53	54
Cr	133	130	130	119	107	207	187	203	101	85	98	104
Cu	73	59	70	70	59	75	79	62	56	65	61	62
Ni	81	68	111	55	73	93	92	83	52	54	52	51
Sc	50	47	51	51	47	46	45	43	49	45	46	47
Sr	120	113	121	123	122	119	122	112	116	115	111	114
V	376	350	365	351	436	327	315	303	364	344	342	352
Zn	100	93	108	90	116	90	84	71	75	93	92	95
Zr	114	104	108	111	169	96	91	89	111	104	104	107
LOI (wt%)	0.63	0.60	1.93	1.32	0.97	0.72	0.23	0.33	1.19	1.05	1.30	1.21
Mg#	62.56	58.21	62.52	63.65	51.25	59.46	63.21	58.26	60.09	57.28	57.90	57.90

Table T7 (continued).

Hole:	327-U1362A-						
Core, section:	18R-3	18R-5	19R-1	19R-2	20R-2	21R-1	21R-2
Interval (cm):	8–10	58–60	13–17	31–34	70–72	130–132	32–35
Unit/Subunit:	6B	6B	7A	7B	7B	8	8
Depth (mbsf):	466.32	469.44	472.15	473.825	483.6	491.61	492.135
Sample:	WDGE 2402971	WDGE 2403021	WDGE 2402671	WDGE 2402721	WDGE 2402791	WDGE 2402831	WDGE 2402851
Major element oxide (wt%):							
SiO_2	49.88	48.75	49.08	48.13	49.83	47.59	51.08
Al_2O_3	14.68	14.32	15.69	14.16	14.90	14.08	15.11
Fe_2O_3	11.56	11.30	11.85	11.81	9.81	11.15	11.07
MnO	0.16	0.16	0.17	0.20	0.22	0.18	0.18
MgO	7.34	6.72	6.09	6.95	7.24	7.32	7.84
CaO	11.55	11.16	12.36	11.28	12.10	11.18	12.05
Na_2O	2.77	2.74	2.63	2.62	2.78	2.54	2.87
K_2O	0.10	0.10	0.62	0.22	0.10	0.08	0.07
TiO_2	1.61	1.61	1.44	1.69	1.88	1.70	1.89
P_2O_5	0.10	0.11	0.10	0.12	0.14	0.11	0.12
Totals:	99.75	96.97	100.03	97.16	98.99	95.93	102.27
Trace element (ppm):							
Ba	17	14	15	16	33	16	14
Co	52	54	48	55	59	54	60
Cr	106	91	218	84	132	75	81
Cu	60	56	77	73	66	56	68
Ni	51	51	71	63	70	64	66
Sc	46	44	43	46	48	45	50
Sr	110	108	115	105	128	107	115
V	334	334	303	350	369	348	380
Zn	97	92	75	86	92	90	98
Zr	103	105	91	107	121	107	120
LOI (wt%)	1.46	1.01	1.66	1.49	0.98	2.54	1.49
Mg#	58.32	56.70	53.10	56.42	61.89	59.10	60.92

Table T8. Microsphere density in microbiology samples, Hole U1362A.

Core, section, interval (cm)	Depth (mbsf)	Description	Microspheres/g
327-U1362A-			
2R-1, 23	346.23	Pillow basalt with chilled margin, outer surface scraping without flame sterilization	49
2R-2, 37	347.87	Fractured pillow basalt with green alteration crust, exterior	45
2R-2, 37	347.87	Fractured pillow basalt with green alteration crust, interior	0
3R-1, 60	353.20	Fractured pillow basalt with green and brown alteration crust, interior	0
3R-2, 90	354.97	Fractured pillow basalt with rust-colored alteration crust, exterior	22
4R-1, 0	362.20	Fractured basalt with chilled margin, white and green alteration crusts, exterior crust	4,800
5R-1, 19	364.89	Fractured basalt with chilled margin, green alteration crusts, exterior glass and crust	734
6R-1, 84	371.04	Fractured basalt, green alteration crusts, exterior crust	0
6R-1, 84	371.04	Fractured basalt, green alteration crusts, exterior crust	67
6R-1, 84	371.04	Fractured basalt, green alteration crusts, exterior crust	395
7R-1, 73	380.53	Unfractured basalt, turquoise alteration crust, recovered from core catcher, exterior crust	0
7R-1, 73	380.53	Unfractured basalt, turquoise alteration crust, recovered from core catcher, exterior crust and interior rock	129
8R-1, 56	390.06	Massive basalt with fractures, brown/black/white/green alteration crusts, interior crust	0
11R-1, 23	415.12	Massive basalt with vesicles and partial chilled margin, green and yellow alteration halo, pink/green/brown/black crust at end, exterior crust	272
11R-1, 23	415.12	Massive basalt with vesicles and partial chilled margin, green and yellow alteration halo, pink/green/brown/black crust at end, exterior crust and interior rock	98
12R-1, 66	420.56	Small massive basalts, green and orange alteration crust	0
13R-1, 32	429.82	Fractured basalt with green/brown alteration crust	209
14R-1, 38	439.48	Fractured basalt with green/black/orange/brown alteration crust and partial chilled margin, exterior green crust	941
14R-1, 38	439.48	Fractured basalt with green/black/orange/brown alteration crust and partial chilled margin, exterior glassy margin	353
15R-1, 68	449.28	Fractured basalt with green alteration crust, exterior green crust	1,600
15R-1, 68	449.28	Fractured basalt with green alteration crust, interior rock	0
16R-1, 125	455.05	Fractured basalt with altered glassy margin, 1 mm thick flaky reddish-brown alteration crust in fractures, glass	0
16R-1, 125	455.05	Fractured basalt with altered glassy margin, 1 mm thick flaky reddish-brown alteration crust in fractures, crust	1,600
16R-1, 125	455.05	Fractured basalt with altered glassy margin, 1 mm thick flaky reddish-brown alteration crust in fractures, glass	0
16R-1, 125	455.05	Fractured basalt with altered glassy margin, 1 mm thick flaky reddish-brown alteration crust in fractures, crust	889
16R-2, 130	456.60	Fractured basalt with crossing fractures and green alteration halo around center vein, orange/green/black alteration crust in veins, exterior crust	0
16R-2, 130	456.60	Fractured basalt with crossing fractures and green alteration halo around center vein, orange/green/black alteration crust in veins, interior crust	0
17R-3, 89	462.07	Massive basalt with green halo around veins, sulfides on one end, flaky white/brown alteration crust, scraping on sulfides	10,700
18R-1, 37	463.77	Massive basalt with white alteration crust on side and sulfides on top, side crust	0
18R-1, 37	463.77	Massive basalt with white alteration crust on side and sulfides on top, top crust	271
18R-1, 37	463.77	Massive basalt with white and green alteration, rock	0
18R-2, 62	465.52	Massive basalt with fractures, brown/white/green alteration crust, crust	0
19R-2, 51	474.01	Massive basalt with light green, red and dark green alteration crusts, green crust	0
20R-1, 90	482.50	Fractured basalt with partial chilled margin, red and green alteration, sulfides, glassy margin	100
21R-2, 42	491.26	Massive basalt, rust-red alteration crusts, exterior	0
21R-1, 109	491.39	Fractured basalt with altered partial chilled margin, rust-red alteration crusts, exterior glassy margin	79

Table T9. Physical property data, Hole U1362A. (Continued on next page.)

Core, section, interval (cm)	Top depth (mbsf)	Uncorrected velocity, wet (m/s)			Corrected velocity, wet (m/s)			Density (g/cm^3)		Porosity (%)	Thermal conductivity (W/[m·K])
		x-axis	*y*-axis	*z*-axis	*x*-axis	*y*-axis	*z*-axis	Bulk	Grain		
327-U1362A-											
2R-1, 17–19	346.17	4923	5014	5058	5297	5306	5277	2.68	2.87	10.17	
2R-1, 92–96	346.92	5336			5584			2.67	2.79	7.15	
2R-2, 40–42	347.90	5095	5204	5226	5479	5524	5561	2.66	2.82	8.89	
2R-2, 73–84	348.96										1.67
2R-2, 90–92	348.40	5859			5752			2.85	2.96	5.76	
3R-1, 1–4	352.61	4904			5271			2.59	2.78	10.90	
3R-1, 50–52	353.10	4916			5258			2.61	2.78	9.58	
3R-1, 66–77	353.92										1.72
3R-1, 113–115	353.73							2.86	2.91	2.76	
3R-2, 52–61	355.11										1.68
3R-2, 54–56	354.61	5262	5196	5275	5577	5492	5587	2.69	2.87	10.05	
3R-2, 120–123	355.27							2.20	2.41	15.01	
4R-1, 23–25	362.43	4971			5208			2.68	2.87	10.04	
4R-1, 71–73	362.91	4848			4966			2.68	2.91	12.31	
5R-1, 43–45	365.13	5681			5996			2.77	2.90	6.77	
5R-1, 120–122	365.90	5604	5646	5636	5617	5671	5709	2.64	2.83	10.26	
5R-2, 11–13	366.31	5548	5400	5554	5402	5357	5399	2.76	2.88	6.78	
5R-2, 66–68	366.86							2.83	2.93	4.96	
6R-1, 41–43	370.61	4961	4935	4941	4995	5185	4994	2.72	2.92	10.87	
6R-1, 69–71	370.89	5812	5947	5958	5735	5788	5705	2.78	2.92	7.51	
6R-2, 48–51	372.14	5337			4922			2.62	2.80	10.43	
6R-2, 82–84	372.48	5966	5929	5941	5659	5742	5696	2.69	2.84	8.23	
6R-3, 25–27	373.41	6065			5630			2.77	2.90	6.85	
7R-1, 9–11	379.89	4880			5169			2.62	2.79	9.64	
7R-1, 59–62	380.39	5089			5522			2.69	2.84	8.21	
8R-1, 27–29	389.77	5145			5362			2.59	2.76	9.71	
8R-1, 107–109	390.57	5349	5385	5370	5477	5460	5899	2.81	2.97	8.18	
8R-2, 71–73	391.68	5215			5335			2.73	2.88	7.69	
8R-2, 100–102	391.97	5162	5164	5164	4788	4719	4777	2.75	2.99	12.54	
8R-2, 118–120	392.15	5870	5899	5915	5522	5608	5552	2.76	2.92	8.50	
9R-1, 29–31	399.49	5013			5269			2.67	2.82	7.99	
9R-1, 130–132	400.50	5651	5579	5669	5363	5469	5760	2.79	2.94	7.96	
9R-2, 19–21	400.55	6026	5945	6072	5608	5852	5627	2.85	2.96	5.73	
9R-2, 109–111	401.45	5910			5764			2.84	2.96	6.35	
11R-1, 44–46	415.34	5007	5049	5086	4967	4989	4981	2.71	2.93	11.64	
11R-2, 26–28	416.61	5163	5135	5155	4880	4911	4993	2.75	2.95	10.10	
12R-1, 87–89	420.77	6133	6277	6287	5955	6063	6050	2.90	3.00	5.14	
12R-1, 97–99	420.87	5450	5484	5488	5131	5248	5259	2.79	2.94	7.81	
12R-2, 3–5	421.22	5681	5642	5680	5394	5355	5405	2.79	2.93	7.36	
12R-2, 96–98	422.15	5569			5214			2.64	2.79	8.30	
13R-1, 5–7	429.55	5819	5783	5844	5656	5626	5527	2.69	2.83	7.70	
13R-1, 133–135	430.83	6020			5780			2.77	2.87	5.23	
14R-1, 8–10	439.18	4809	4745	4825	4508	4486	4472	2.69	2.97	14.06	
14R-1, 11–13	439.21	5884	5913	5874	5499	5535	5525	2.82	2.95	6.49	
14R-1, 117–119	440.27	5251			4894			2.68	2.86	9.77	
15R-1, 40–44	449.00	5584			5313			2.76	2.86	5.64	
15R-1, 133–135	449.93	5705	5741	5776	5435	5499	5503	2.73	2.85	6.55	
16R-1, 58–60	454.38	5992	6072	6029	5614	5676	5693	2.81	2.91	5.07	
16R-1, 100–102	454.80	5842			5606			2.67	2.79	6.86	
16R-2, 59–61	455.89	6151	6332	6212	5721	5740	5695	2.86	2.93	3.80	
16R-3, 55–57	457.25	5462	5524	5477	5211	5163	5171	2.71	2.86	7.92	
16R-3, 91–93	457.61	6212			5969			2.83	2.93	5.16	
17R-1, 38–40	458.78	6046	6093	6109	5624	5689	5801	2.81	2.94	6.69	
17R-2, 74–76	460.58	5754	5851	5825	5484	5534	5505	2.80	2.92	6.02	
17R-3, 49–51	461.67	5753	5739	5693	5483	5453	5444	2.75	2.89	7.21	
17R-4, 65–67	463.33	5837	5893	5856	5649	5636	5677	2.77	2.90	7.27	
17R-5, 55–57	464.21	5927	5930	5947	5722	5701	5726	2.82	2.93	5.77	
18R-1, 101–103	464.41	6020	5946	5951	5771	5773	5822	2.83	2.92	4.50	
18R-1, 129–131	464.69	5740	5688	5715	5486	5465	5476	2.77	2.88	6.15	
18R-2, 8–10	464.85	5505	5514	5471	5296	5312	5296	2.73	2.86	7.31	
18R-2, 45–47	465.22	5408	5462	5482	5360	5369	5336	2.73	2.87	7.35	
18R-3, 8–10	466.31	5784	5785	5758	5498	5496	5524	2.77	2.89	6.77	
18R-4, 56–58	468.12	5940	5977	5924	5701	5793	5767	2.85	2.93	4.32	
18R-5, 46–48	469.31	6028			5927			2.83	2.93	4.96	
18R-5, 58–60	469.43	6003	6061	6003	5919	5904	5920	2.82	2.92	5.50	
18R-6, 108–110	471.20	5892	5854	5840	5544	5593	5548	2.77	2.90	6.83	
19R-1, 27–29	472.27	5962			5698			2.74	2.83	5.25	

Table T9 (continued).

Core, section, interval (cm)	Top depth (mbsf)	Uncorrected velocity, wet (m/s)			Corrected velocity, wet (m/s)			Density (g/cm^3)		Porosity (%)	Thermal conductivity (W/[m·K])
		x-axis	*y*-axis	*z*-axis	*x*-axis	*y*-axis	*z*-axis	Bulk	Grain		
19R-1, 71–73	472.71	5256	5294	5272	5031	5054	5096	2.65	2.85	10.61	
19R-2, 11–13	473.61	5754			5555			2.77	2.86	4.83	
19R-2, 98–100	474.48	5142			4894			2.69	2.88	9.91	
20R-1, 15–17	481.75	5280	5318	5366	5177	5184	5207	2.74	2.91	8.98	
20R-1, 58–60	482.18	5575	5524	5504	5523	5647	5374	2.73	2.89	8.38	
20R-2, 11–13	483.00	5371	5411	5406	5202	5162	5163	2.75	2.93	9.14	
21R-1, 32–34	490.62	5114			5053			2.67	2.88	11.29	
21R-1, 93–95	491.23	5087	4984	5004	5107	5037	5000	2.71	2.91	10.74	
21R-2, 9–11	491.89	6017	6008	6094	5868	5894	5832	2.84	2.95	5.73	

Table T10. Remanent magnetization intensity and inclination values, Hole U1362A. (See table notes.) (Continued on next page.)

Core, section	Depth (mbsf)	Treatment	Intensity (A/m)	Inclination (°)	PCA (*N*)	MAD (°)	Lith. unit
327-U1362A-							
2R-1 (Piece 1)	346.04	AF d	0.177	–70.6	4	4.74	1A
2R-1 (Piece 9)	346.65	AF d	0.767	63.1	4	7.98	1A
2R-1 (Piece 17)	347.28	AF d	1.012	84.2	4	3.25	1A
2R-2 (Piece 6)	348.08	AF d	1.364	17.5	4	8.59	1A
2R-2 (Piece 8)	348.28	AF d	1.509	–46.7	4	13.24	1A
3R-1 (Piece 8)	353.32	AF d	3.163	68.0	4	1.6	1A
3R-2 (Piece 5)	354.41	AF d	3.120	58.3	5	1.01	1A
3R-2 (Piece 8)	354.64	AF d	3.161	51.2	5	1.29	1A
3R-2 (Piece 17)	355.19	AF d	2.828	63.5	5	1.17	1A
4R-1 (Piece 8)	362.71	AF d	3.960	46.8	4	3.07	1A
5R-1 (Piece 6)	364.96	AF d	3.665	44.3	4	1.53	1A
5R-1 (Piece 13)	365.38	AF d	3.472	47.6	4	0.58	1A
5R-1 (Piece 17)	365.62	AF d	3.369	58.1	4	1.37	1A
5R-1 (Piece 18)	365.70	AF d	2.093	56.8	4	1.48	1A
5R-1 (Piece 22)	365.92	AF d	4.444	63.7	4	1.78	1A
5R-1 (Piece 24)	366.02	AF d	3.472	47.6	4	0.58	1B
5R-2 (Piece 2)	366.31	AF d	2.908	72.3	4	2.07	1B
5R-2 (Piece 3)	366.41	AF d	3.985	53.9	4	2.46	1B
5R-2 (Piece 5)	366.54	AF d	2.170	52.6	4	3.47	1B
5R-2 (Piece 7)	366.68	AF d	2.564	39.9	4	1.95	1B
6R-1 (Piece 10)	370.65	AF s	7.670	41.1	4	3.08	1B
6R-1 (Piece 11)	370.76	AF s	4.899	64.5	4	2.82	1B
6R-2 (Piece 3)	371.79	AF d	3.784	48.3	4	2.48	1B
6R-2 (Piece 4)	371.87	AF d	3.585	79.7	4	2.2	1B
6R-2 (Piece 11)	372.23	AF d	3.689	50.9	4	1.1	1B
6R-2 (Piece 14)	372.44	AF d	4.322	66.9	4	1.91	1B
7R-1 (Piece 4)	380.01	AF d	3.875	74.7	5	0.95	1B
7R-1 (Piece 13)	380.48	AF d	1.884	73.9	4	1.35	1B
8R-1 (Piece 14)	390.28	AF d	1.753	–84.6	4	0.28	2
8R-1 (Piece 16)	390.53	AF d	4.115	73.1	4	1.78	2
8R-2 (Piece 3)	391.24	AF d	4.131	25.7	4	8.72	2
8R-2 (Piece 16)	391.96	AF d	3.090	–81.3	4	1.21	2
8R-2 (Piece 18)	392.15	AF d	4.112	67.5	4	1.98	2
8R-2 (Piece 19)	392.26	AF d	4.436	3.8	4	13.25	2
9R-1 (Piece 14)	399.97	AF s	7.713	70.7	4	0.96	4A
9R-1 (Piece 17)	400.24	AF s	6.255	74.5	4	3.61	4A
9R-1 (Piece 18)	400.34	AF d	3.728	70.6	4	0.89	4A
9R-1 (Piece 21)	400.54	AF d	3.381	70.8	4	1.89	4A
9R-2 (Piece 3)	400.54	AF s	14.000	63.8	4	0.99	4A
9R-2 (Piece 10)	401.19	AF s	8.209	64.0	4	1.05	4A
9R-2 (Piece 15)	401.48	AF s	9.242	63.2	4	2.72	4A
11R-1 (Piece 7)	415.36	AF s	7.057	82.6	5	0.53	4c
11R-1 (Piece 12)	415.82	AF s	6.816	72.8	5	0.41	4C
11R-1 (Piece 15)	416.14	AF s	7.313	56.2	4	1.57	4C
11R-2 (Piece 1)	416.55	AF s	14.270	79.7	4	0.92	4C
12R-1 (Piece 7)	420.29	AF s	12.360	73.0	4	1.95	4D
12R-1 (Piece 8)	420.74	AF s	9.947	74.3	4	2.57	4D
12R-2 (Piece 1a)	421.33	AF s	12.340	82.2	5	1.27	4D
13R-1 (Piece 1)	429.55	AF d	4.532	41.6	5	1.4	5A
13R-1 (Piece 7)	429.94	AF d	5.387	58.5	4	0.63	5A
13R-1 (Piece 15)	430.64	AF d	2.725	87.4	4	1.14	5A
14R-1 (Piece 1)	439.13	AF s	0.251	42.3	4	13.29	5A/5B
14R-1 (Piece 2)	439.28	AF d	3.328	78.8	5	1.32	5B
14R-1 (Piece 14)	440.08	AF d	3.005	69.6	4	1.16	5B
14R-2 (Piece 1)	440.54	AF d	4.177	67.3	5	1.24	5B
14R-2 (Piece 3)	440.93	AF d	4.408	60.7	4	2.2	5B
15R-1 (Piece 3)	448.74	AF d	0.865	38.9	4	8.98	5B
15R-1 (Piece 12)	449.22	AF d	3.260	67.8	4	1.5	5B
15R-1 (Piece 15)	449.46	AF d	0.636	13.9	4	2.2	5B
15R-1 (Piece 19)	449.83	AF d	3.943	74.7	5	0.45	5B
15R-1 (Piece 20)	449.93	AF d	5.870	87.5	4	0.66	5B
15R-1 (Piece 21)	450.00	AF d	6.056	76.7	5	1.08	5B
16R-1 (Piece 5)	454.16	AF d	5.008	88.0	4	0.89	5B
16R-1 (Piece 6)	454.38	AF d	5.270	70.4	5	1.28	5B
16R-1 (Piece 8)	454.67	AF d	4.401	69.1	4	1.2	5B
16R-1 (Piece 10)	454.93	AF d	3.759	75.5	4	0.54	5B

Table T10 (continued).

Core, section	Depth (mbsf)	Treatment	Intensity (A/m)	Inclination (°)	PCA (*N*)	MAD (°)	Lith. unit
16R-1 (Piece 14)	455.24	AF d	5.573	78.5	4	0.59	5B
16R-2 (Piece 1)	455.34	AF d	4.488	68.9	4	1.74	5B
16R-2 (Piece 2)	455.42	AF d	5.399	42.2	4	1.06	5B
16R-2 (Piece 4)	455.56	AF d	6.928	70.1	4	2.24	5B
16R-2 (Piece 5)	455.66	AF d	5.234	57.4	4	0.84	5B
16R-2 (Piece 6)	455.79	AF s	2.855	76.9	4	1.04	5B
16R-2 (Piece 7)	456.18	AF s	6.159	70.6	5	1.04	5B
16R-2 (Piece 8)	456.55	AF d	9.094	81.0	5	1.04	6A
16R-3 (Piece 3)	456.95	AF s	13.130	76.4	4	1.14	6A
16R-3 (Piece 5)	457.43	AF s	9.994	86.1	4	2.31	6A
17R-1 (Piece 1a)	458.55	AF s	10.090	80.2	4	1.42	6A
17R-1 (Piece 1f)	459.62	AF s	3.041	78.5	4	4.5	6A
17R-2 (Piece 1)	459.99	AF s	8.619	58.8	4	4.5	6A
17R-2 (Piece 7a)	460.70	AF s	10.560	84.9	4	3.91	6A
17R-3 (Piece 1)	461.30	AF s	9.163	84.8	4	0.77	6A
17R-3 (Piece 5)	461.91	AF s	8.406	69	4	1.39	6A
17R-3 (Piece 7)	462.32	AF s	8.813	58.4	4	1.53	6A
17R-4 (Piece 1a)	462.77	AF s	11.750	70.5	5	0.7	6A
17R-4 (Piece 2b)	463.17	AF s	10.720	60.1	4	10.77	6A
17R-4 (Piece 3)	463.56	AF s	5.543	–67.4	4	9.51	6A
17R-5 (Piece 1b)	463.91	AF s	13.710	78.2	5	0.81	6A
17R-5 (Piece 1f)	464.22	AF s	9.949	64.5	4	1.92	6A
18R-1 (Piece 3)	463.52	AF d	1.967	–39.0	4	10.61	6B
18R-1 (Piece 5a)	463.76	AF s	9.767	77.3	5	1.2	6B
18R-1 (Piece 6b)	464.06	AF s	6.633	65.5	5	1.4	6B
18R-1 (Piece 7b)	464.54	AF s	2.767	75.9	4	1.96	6B
18R-2 (Piece 1b)	465.00	AF s	9.185	67.9	4	0.93	6B
18R-2 (Piece 3c)	465.79	AF s	13.280	46.2	4	18.94	6B
18R-3 (Piece 1a)	466.38	AF s	8.784	76.1	4	1.18	6B
18R-3 (Piece 2b)	466.89	AF s	7.181	81.4	4	1.46	6B
18R-3 (Piece 3c)	467.49	AF s	3.782	31.3	4	6.42	6B
18R-4 (Piece 1d)	467.89	AF s	10.390	67.3	4	1.2	6B
18R-4 (Piece 2)	468.10	AF d	6.587	73.6	4	0.64	6B
18R-4 (Piece 3)	468.33	AF s	12.090	59.8	4	4.07	6B
18R-4 (Piece 4)	468.50	AF d	6.442	68.4	4	1.78	6B
18R-4 (Piece 5b)	468.67	AF s	7.941	62.0	4	2.3	6B
18R-5 (Piece 1)	468.98	AF s	9.086	77.4	5	1.14	6B
18R-5 (Piece 3)	469.54	AF s	3.885	58.7	4	2.52	6B
18R-5 (Piece 4)	469.68	AF d	5.908	77.8	5	0.62	6B
18R-5 (Piece 5c)	470.00	AF s	2.217	43.8	4	6.36	6B
18R-6 (Piece 1)	470.59	AF s	9.153	76	5	0.91	6B
18R-6 (Piece 3)	471.13	AF s	6.409	70.5	4	3.24	6B
18R-6 (Piece 4)	471.44	AF d	5.902	68.1	5	1.36	6B
19R-1 (Piece 11)	472.63	AF d	6.742	77.2	4	1.15	7A
19R-2 (Piece 9)	473.95	AF d	6.965	36.8	4	1.94	7B
19R-2 (Piece 16)	474.35	AF d	5.738	–48.0	4	2.48	7B
20R-1 (Piece 1)	481.65	AF d	4.828	63.1	4	3.82	7B
20R-1 (Piece 2)	481.74	AF d	8.467	51.9	4	4.43	7B
20R-1 (Piece 9a)	482.20	AF d	6.067	52.0	4	2.1	7B
21R-1 (Piece 4)	490.52	AF d	8.274	36.4	4	4.09	8
21R-1 (Piece 8)	490.80	AF d	5.301	47.5	4	1.99	8
21R-1 (Piece 15)	491.28	AF d	6.074	79.7	4	1.15	8
21R-1 (Piece 18)	491.54	AF d	1.277	46.4	4	2.13	8
21R-1 (Piece 22)	491.76	AF d	6.127	–57.0	4	1.06	8
21R-2 (Piece 1)	491.87	AF s	10.220	69.0	4	2.98	8
21R-2 (Piece 3)	491.10	AF d	4.981	58.8	4	2.41	8
21R-2 (Piece 6)	491.34	AF d	4.608	63.7	4	2.39	8
21R-2 (Piece 7)	491.45	AF d	9.514	81.5	4	1.86	8
21R-2 (Piece 8b)	491.56	AF d	6.526	61.8	4	1.16	8

Notes: Depth = midpoint of discrete piece or depth in section. AF = alternating field, AF d = discrete piece, AF s = continuous section. PCA = principal component analysis. MAD = maximum angular deviation; smaller values indicate more reliable samples.

Table T11. Temperature logger depths, Hole U1362A CORK. (See table notes.)

Manufacturer (serial number)	Depth		
	msd	mbsf	msb
Onset (768608)	8.4	2.2	–233.8
Onset (768609)	19.7	13.4	–222.6
Antares (1857021)	227.2	220.9	–15.1
Antares (1857022)	237.4	231.2	–4.8
Antares (1857023)	294.9	288.6	52.6
Antares (1857024)	305.1	298.8	62.8
Antares (1857027)	344.1	337.9	101.9
Antares (1857028)	380.0	373.8	137.8
Antares (1857031)	415.9	409.7	173.7
End of Spectra cable	438.8	432.6	196.6
Antares (1857025)	NA	438.6	202.6
Antares (1857026)	NA	454.1	218.1
End of sinker bar	NA	466.2	230.2

Notes: msd = meters Spectra depth (distance from top of cable, terminated at top plug). All depths are corrected for Spectra cable shortening, including updated accounting for cable stretch, as described in text. Depths in units of msd are not applicable (NA) for two deepest Antares tools deployed inside OsmoSamplers or the end of the sinker bar.

Table T12. OsmoSampler types and depths (instrument bottom), Hole U1362A CORK. (See table notes.)

Type	Depth	
	mbsf	msb
OsmoSampler, acid addition	438.0	202.0
OsmoSampler, microbiology*	444.8	208.8
OsmoSampler, standard	448.2	212.2
OsmoSampler, enrichment	453.6	217.6
OsmoSampler, BOSS*	459.1	223.1
OsmoSampler, copper	462.5	226.5
Sinker bar, 200 lb, coated	466.2	230.2

Notes: All depths are corrected for Spectra cable shortening, including an updated accounting for cable stretch, as described in the text. * = contains autonomous temperature probe 0.56 m from top of sampler (see depths in Table T11). BOSS = BioOsmoSampling System.

Table T13. Fluid sampling intake depths, Hole U1362A CORK. (See table notes.)

Screen/point type	Material	Depth	
		mbsf	msb
Pressure (cased interval)*	NA	0.1	NA
Pressure (shallow basement)	Stainless steel	307.8	71.8
Pressure (deep basement)	Stainless steel	430.1	194.1
Geochemistry (shallow basement)	Stainless steel	309.3	73.3
Geochemistry (shallow basement)	Stainless steel	309.3	73.3
Geochemistry (deep basement)	Stainless steel	434.2	198.2
Microbiology (deep basement)	Titanium	439.8	203.8

Notes: * = no screen is attached immediately below seafloor CORK seal for pressure monitoring of cased interval. NA = not applicable.

Table T14. Temperature logger depths, Hole U1362B CORK. (See table notes.)

Manufacturer (serial number)	Depth		
	msd	mbsf	msb
Antares (1857034)	9.0	2.9	–239.1
Antares (1857038)	14.0	8.0	–234.0
Antares (1857039)	20.0	14.2	–227.8
Antares (1857040)	30.0	24.4	–217.6
Onset (768607)	246.3	245.0	3.0
Onset (768610)	273.8	273.0	31.0
End of Spectra cable	282.6	276.3	34.3
Antares (1857035)	NA	276.9	34.9
Antares (1857037)	NA	301.4	59.4
End of sinker bar	NA	310.0	68.0

Notes: msd = meters Spectra depth (distance from top of cable, terminated at top plug). All depths account for Spectra cable stretch, as described in the text. Depths in units of msd are not applicable (NA) for two deepest Antares tools deployed inside OsmoSamplers.

Table T15. OsmoSampler types and depths (instrument bottom), Hole U1362B CORK. (See table notes.)

Type	Depth	
	mbsf	msb
OsmoSampler, standard*	279.9	37.9
OsmoSampler, microbiology	286.6	44.6
OsmoSampler, acid addition	292.0	50.0
OsmoSampler, enrichment	297.5	55.5
OsmoSampler, copper	300.9	58.9
OsmoSampler, BOSS*	306.4	64.4
Sinker bar, 200 lb, coated	310.0	68.0

Notes: All depths are corrected for Spectra cable shortening, including an updated accounting for cable stretch, as described in the text. * = contains autonomous temperature probe 0.56 m from top of sampler (see depths in Table T14). BOSS = BioOsmoSampling System.

Table T16. Fluid sampling intake depths, Hole U1362B CORK. (See table notes.)

Screen/point type	Material	Depth	
		mbsf	msb
Pressure (cased interval)*	NA	0.1	NA
Pressure (open basement)	Stainless steel	272.0	30.0
Geochemistry (shallow basement)	Stainless steel	278.8	36.8
Geochemistry (shallow basement)	Stainless steel	278.8	36.8
Geochemistry (deep basement)	Stainless steel	278.8	36.8
Microbiology (deep basement)	Titanium	281.7	39.7

Notes: * = no screen is attached immediately below seafloor CORK seal for pressure monitoring of cased interval. NA = not applicable.